UNIVERSITÉ DE MONTRÉAL

METHANOL-TO-OLEFINS IN A FLUIDIZED BED: EXPERIMENTAL AND MODELLING STUDY

MADS KAARSHOLM

DÉPARTEMENT DE GÉNIE CHIMIQUE

ÉCOLE POLYTECHNIQUE DE MONTRÉAL

THÉSE PRÉSENTÉE EN VUE DE L'OBTENTION

DU DIPLÔME DE PHILOSOPHIAE DOCTOR

(GÉNIE CHIMIQUE)

MARS 2009

© Mads Kaarsholm, 2009.

Library and Archives Canada

Published Heritage Branch

395 Wellington Street
Ottawa ON K1A 0N4
Canada

Bibliothèque et Archives Canada

Direction du Patrimoine de l'édition

395, rue Wellington
Ottawa ON K1A 0N4
Canada

Your file Votre référence
ISBN: 978-0-494-49419-6
Our file Notre référence
ISBN: 978-0-494-49419-6

NOTICE:
The author has granted a non-exclusive license allowing Library and Archives Canada to reproduce, publish, archive, preserve, conserve, communicate to the public by telecommunication or on the Internet, loan, distribute and sell theses worldwide, for commercial or non-commercial purposes, in microform, paper, electronic and/or any other formats.

The author retains copyright ownership and moral rights in this thesis. Neither the thesis nor substantial extracts from it may be printed or otherwise reproduced without the author's permission.

AVIS:
L'auteur a accordé une licence non exclusive permettant à la Bibliothèque et Archives Canada de reproduire, publier, archiver, sauvegarder, conserver, transmettre au public par télécommunication ou par l'Internet, prêter, distribuer et vendre des thèses partout dans le monde, à des fins commerciales ou autres, sur support microforme, papier, électronique et/ou autres formats.

L'auteur conserve la propriété du droit d'auteur et des droits moraux qui protège cette thèse. Ni la thèse ni des extraits substantiels de celle-ci ne doivent être imprimés ou autrement reproduits sans son autorisation.

In compliance with the Canadian Privacy Act some supporting forms may have been removed from this thesis.

While these forms may be included in the document page count, their removal does not represent any loss of content from the thesis.

Conformément à la loi canadienne sur la protection de la vie privée, quelques formulaires secondaires ont été enlevés de cette thèse.

Bien que ces formulaires aient inclus dans la pagination, il n'y aura aucun contenu manquant.

Canada

UNIVERSITÉ DE MONTRÉAL

ÉCOLE POLYTECHNIQUE DE MONTRÉAL

Cette thèse intitulée:

METHANOL-TO-OLEFINS IN A FLUIDIZED BED:

EXPERIMENTAL AND MODELLING STUDY

présentée par: KAARSHOLM Mads

en vue l'obtention du diplôme de: Philosophiae Doctor

a été dûment acceptée par le jury d'examen constitué:

M. LEGROS Robert, Ph.D., président

M. PATIENCE Gregory S., Ph.D., membre et directeur de recherche

M. CHAOUKI Jamal, Ph.D., membre et codirecteur de recherche

M. FRADETTE Louis, Ph.D., membre

M. LATTNER James R., Ph.D., membre

ACKNOWLEDGEMENTS

I would like to express my sincere gratitude to the people that have helped and guided me in this work and without whom it would not have been possible. First of all I would like to thank my supervisors at École Polytechnique de Montréal *Professor Gregory S. Patience* and *Professor Jamal Chaouki* for their guidance, encouragement and fruitful discussion both while I was in Montreal and during my time at Haldor Topsøe in Denmark. I would also like to thank my supervisors at Haldor Topsøe *Roberta Cenni*, *Finn Joensen* and *Jesper Nerlov* for guidance and inspiration.

My thanks go to my friends and family - especially to *Kamilla Hansen* for support and understanding during the last four years. I would also like to thank my fellow Ph.D students at École Polytechnique de Montréal *Ali Shekari* and *Jean-Philippe Laviolette* for their friendship, help and interesting discussion during my time in Montréal. My thanks also go to *Banafsheh Rafii* and *Julia Duchastel-Legare* for their valuable help in the laboratories.

I would also like to thank the technical staff both at École Polytechnique de Montréal and at Haldor Topsøe. A special thank go to *Daniel Dumas*, *Jean Huard* and *Robert Delisle* for support to the experimental setups. I am also thankful to *Kim Ravn* and

Svend-Erik Mikkelsen for their help with the fixed bed experiments at Haldor Topsøe and to *Peter Rahbek* for his help with spray drying of the catalyst

Finally I would like to thank Haldor Topsøe A/S and the Danish Ministry of Science Technology and Innovation for financial support making this work possible.

RÉSUMÉ

Dans cette thèse, la transformation du méthanol en oléfines (MTO) a été étudiée principalement dans un lit fluidisé et aussi dans un lit fixe. Cette réaction peut se diviser en 2 parties : la déshydratation du méthanol en éther diméthylique (DME) et la formation d'hydrocarbures à partir du mélange méthanol/DME. Dans les conditions habituellement utilisées pour le procédé MTO – approximativement entre 450 et 500°C, la première réaction est très rapide et généralement considérée à l'équilibre en tout temps. À des températures plus basses, typiquement inférieures à 300°C, la formation d'hydrocarbures est pratiquement nulle et la réaction de déshydratation du méthanol en DME peut ne plus être à l'équilibre. C'est le cas de plusieurs procédés industriels où la déshydratation du méthanol se fait dans un réacteur conçu à cette fin, pour limiter l'augmentation de la température inhérente au procédé MTO. Le catalyseur utilisé dans cette étude est basé sur de la zéolite ZSM-5 et modifié avec du phosphore pour réduire la formation de méthane. Le travail réalisé a été divisé en trois étapes : d'abord, la déshydratation du méthanol en DME a été étudiée dans un lit fluidisé; ensuite, la réaction MTO a été analysée dans un lit fixe ; enfin, des études cinétiques ont été menées dans un lit fluidisé et un modèle représentant l'ensemble de ces réactions complexes a été proposé.

La transformation du méthanol en DME a été étudiée dans un réacteur à lit fluidisé en quartz, de 46 mm de diamètre, pour examiner la cinétique de la réaction et les effets du transfert de matière sur celle-ci. L'analyse des produits a été effectuée par un

spectromètre de masse (SM) et en partie par chromatographie en phase gazeuse (CG). Le SM fournit des mesures en ligne et en temps réel, ce qui permet de détecter facilement les variations des conditions de réaction et de déterminer les régimes permanents. Les expériences ont été réalisées à partir du méthanol dilué dans de l'argon, à quatre concentrations distinctes : 5, 15, 30 et 33 mol% et à trois températures différentes : 250, 275 et 325°C. À 325°C, - dans certains cas et dépendamment du rapport débit massique et masse de catalyseur (WHSV) - la réaction de déshydratation du méthanol se poursuit au-delà de la formation du DME et produit d'autres hydrocarbures. Ces expériences-là ont été rejetées. Lorences et al., 2006 ont montré que l'hydrodynamique des lits fluidisés peut être assimilée à celle des réacteurs parfaitement mélangés en série (CSTR) quand la vitesse superficielle de gaz est faible et que la dispersion croît avec l'augmentation de la vitesse. Les mesures de Distribution du Temps de Séjour (DTS), réalisées dans le cadre de ce travail, ont permis de caractériser le lit fluidisé comme étant équivalent à 6 réacteurs CSTR, lorsque la vitesse superficielle est égale à 10 fois la vitesse minimale de fluidisation - $u_{mf.}$ Afin d'obtenir des WHSV relativement élevées, même à faibles vitesses superficielles, nous avons varié la masse de catalyseur dans le réacteur de 25 à 200 g. Les conversions expérimentales ont été de l'ordre de 30 à 99+% par rapport à l'équilibre.

Pour l'analyse cinétique, deux réacteurs modèles différents ont été utilisés dans le but de modéliser l'hydrodynamique du lit fluidisé : un modèle à deux phases - phase émulsion et phase bulles - et une série de 6 réacteurs parfaitement mélangés. Un modèle cinétique

de la déshydratation du méthanol en DME a été proposé et comparé à celui de Berĉiĉ et Levec (1992).

Plusieurs séries de paramètres cinétiques ont été trouvées en couplant les deux modèles hydrodynamiques avec les deux modèles cinétiques et par optimisation des données expérimentales aux trois plus faibles concentrations de méthanol.

L'analyse des résultats a montré que le modèle cinétique proposé avec le modèle des n-CSTR en série permet d'obtenir les prédictions les plus proches des données expérimentales et des prédictions excellentes pour les plus grandes concentrations de méthanol. Le modèle hydrodynamique n-réacteurs parfaitement mélangés, couplé au modèle cinétique proposé ou à celui emprunté dans la littérature, donne les meilleurs résultats, quoique le modèle du lit fluidisé n'ait pas été rejeté.

Cette étude a montré qu'une expérience cinétique dans un lit fluidisé à petite échelle a des avantages pour les réactions exothermiques, car elle élimine les incertitudes liées aux points chauds et aux gradients de température.

Pour utiliser les n-CSTR en série comme réacteur modèle, il faut maintenir une vitesse superficielle de gaz relativement faible. Par contre, à cause des contraintes sur les vitesses superficielles et la masse de catalyseur, les conversions à des températures données peuvent être limitées.

Le procédé MTO a été étudié dans plusieurs lits fixes de faible diamètre. Les mécanismes de la réaction principale et de la désactivation ont été analysés pour différentes WHSV, compositions à l'entrée et longueurs de réacteur (3, 6 et 8 mm).

La chromatographie en phase gazeuse a été utilisée pour déterminer la distribution des produits de la réaction. Les composés à faibles nombres de carbone ont été analysés individuellement, alors que les fractions de C_4 aromatiques et de C_{5+} non aromatiques ont été regroupées. Ces expériences suggèrent que les C_{5+} non aromatiques sont des produits intermédiaires de la réaction MTO, conduisant à la formation de propylène et de butylène (et non d'éthylène) par des réactions de craquage supplémentaires. La production d'éthylène se fait, quant à elle, par division des aromatiques (principalement des xylènes et des triméthylbenzènes), ce qui concorde avec les travaux de Svelle et al. (2006). Le méthane, qui est prédominant à de faibles conversions du méthanol/DME et à des taux élevés de WHSV, doit probablement se former directement à partir du méthanol ou du DME et non des hydrocarbures supérieurs.

La désactivation du catalyseur est très sensible à la WHSV et croît avec celle-ci. Par conséquent, la capacité du réacteur à transformer le méthanol dépend du flux à l'entrée. La composition de ce flux a également une influence significative sur la désactivation du catalyseur et la composition des produits. Des pressions partielles basses de méthanol favorisent la production d'oléfines, mais elles réduisent la capacité du réacteur à transformer le méthanol. Ceci contredit les travaux de Chen et al. (2000) montrant que la désactivation du catalyseur est fonction de la quantité de méthanol converti et de la température et non de WHSV.

La troisième partie de la thèse traite de la réaction MTO dans un lit fluidisé. Les effets de la composition de l'alimentation, de la température et de la WHSV ont été analysés dans le même réacteur que celui de la déshydratation du méthanol. En alimentant en 1-

hexène d'une part et en méthanol d'autre part, nous avons proposé un mécanisme probable de réaction. La composition des produits de réaction ne change pas de façon significative avec une alimentation en méthanol. Dans le cas de l'alimentation en hexène, les différences majeures sont une production significativement plus basse de méthane et une plus grande formation d'éthylène. Ces observations confirment les résultats obtenus dans un lit fixe, selon lesquels le méthane se forme directement à partir du méthanol et/ou du DME, et l'éthylène est produit par craquage secondaire.

Un modèle cinétique a été proposé en se basant sur le mécanisme « lot d'hydrocarbures », où les oléfines sont produites par des réactions réversibles à partir d'un lot d'hydrocarbures supérieurs.

Tel qu'observé dans les expériences antérieures réalisées dans des lits fluidisés et fixes, le méthane est supposé se former à partir du méthanol. Les aromatiques sont considérées comme étant C_9H_{12} et les paraffines, tout comme le propane, sont produits directement à partir du propylène.

Pour la réaction MTO en lit fluidisé, le modèle hydrodynamique à deux phases a été choisi. En effet, comme la hauteur du lit était généralement beaucoup plus élevée que dans les expériences de déshydratation du méthanol, la taille des bulles était plus grande. De plus, ce modèle à deux phases n'avait pas été rejeté lors de l'étude de déshydratation du méthanol.

Le modèle prédit bien la production d'oléfines légères, mais moins bien celle des paraffines et des fractions $C_{6.}$, ceci s'expliquant par le fait que les aromatiques, les paraffines et les oléfines sont agglomérés et qu'ils présentent des mécanismes de réaction différents.

ABSTRACT

In this thesis the Methanol To Olefin (MTO) reaction has been studied in fixed bed and fluid bed with emphasis on the fluid bed. The reaction from methanol to olefins can be divided into two parts: dehydration of methanol to dimethyl ether (DME) and reaction of methanol/DME mixture to hydrocarbons, including paraffins, olefins and aromatics. Under reaction conditions for the MTO process app. 450-500°C the methanol to DME reaction is very fast and it is usually considered to be in equilibrium at any time. At lower temperatures, below about 300°C, hydrocarbon formation is essentially absent and the methanol/DME reaction can not be considered in equilibrium. This is the case for Lurgi methanol to propylene (MTP) process where the dehydration of methanol takes place in a separate reactor to limit the temperature increase during the MTO reaction. The MTO reaction is catalysed by an acidic catalyst and in this study the used catalyst is based on a ZSM-5 zeolite and was modified with phosphorous to reduce methane formation. The catalyst used in this study was based on a ZSM-5 zeolite and was modified with phosphorous to reduce methane formation. The work has been divided into three parts: first the methanol to DME reaction is studied in fluidized bed. Second the MTO process is investigated in fixed bed and last kinetic studies of the MTO reaction is conducted in fluidized bed and a model for the complex reaction is proposed.

The methanol to DME reaction has been studied in a 4.6 mm inner diameter quartz fluidized bed reactor to investigate the reaction kinetics and effect of mass transfer on the reaction. Analysis of the products was conducted by mass spectrometer (MS) and in part by gas chromatograph (GC). The MS provides real time measurements and changes in reaction conditions are therefore easy to detect and steady state conditions can be determined. The experiments were performed with methanol diluted in argon at four different concentrations (5, 15, 30 and 33 mol%) and at three temperatures (250, 275 and 325°C). At 325°C the reactions in some cases, depending on the weight hourly space velocity, WHSV, proceeded beyond DME formation, forming hydrocarbons and these results were omitted. Lorences et al., 2006 have shown that the hydrodynamics of the fluid bed can be approximated by CSTR's in series at low gas velocities and with increasing gas velocity the dispersion increases. Residence time distribution (RTD) measurements showed that the fluid bed could be modelled as 6 CSTR's in series at a flow of approximately 10 times $u_{mf.}$ To get at larger WHSV range while still keeping the gas velocity low, the catalyst inventory in the fluid bed was varied in the range 25 – 200g. Conversion to equilibrium in the experiments was in the range 30 – 99+%.

Two different reactor models have been used for the fluid bed during the kinetic analysis. A two phase fluid bed model with interphase mass transfer and a n-CSTR in series model. A kinetic model for the methanol to DME reaction have been proposed and compared to the literature model of Berĉiĉ and Levec, 1992.

The kinetic parameters were found by coupling the two kinetic models with the two reactor models and optimizing them to the experimental data at the three lowest

methanol concentrations. The analysis showed that the proposed kinetics with the n-CSTR's in series model gave the best fit to the experimental data and that the predictions of the data at the highest methanol concentrations was excellent. The n-CSTR reactor model gave the best result for both the proposed model and the literature model although the fluid bed model was not significantly worse.

The study showed that kinetic experiment in a small scale fluid bed has advantages for exothermic reactions since uncertainties regarding hotspots or temperature gradients can be eliminated. To be able to use the n-CSTR's in series reactor model the gas velocities have to be kept relatively low. Given the restraints on gas velocities and catalyst inventory the conversion range at a given temperature can be limited.

The methanol to olefin reaction has been studied in small diameter fixed bed reactors with different diameters. By changing the WHSV, feed composition and reactor size (3, 6 and 8 mm) the reaction pathways and deactivation patterns were studied. GC measurement was used to determine the product distribution. The small components was analysed separately while the C_4, aromatics and C_{5+} (without aromatics) fraction are lumped. These studies suggest that non-aromatic C_{5+} hydrocarbons are intermediates in the MTO reaction, forming propylene and butylene (but not ethylene) by secondary cracking reactions. Ethylene production paralleled the aromatics formation suggesting that ethylene are formed by splitting off from aromatics (mainly xylenes and trimethylbenzenes) which is in accordance with labelling studies of Svelle et al., 2006. Methane predominated the products at low oxygenate conversion and high WHSV

which suggest that methane is formed from methanol and/or DME and not from reactions by higher hydrocarbons.

Deactivation of the catalyst was highly dependent on the space velocity with increasing deactivation as the WHSV was increased. As a result the methanol capacity of the catalyst was dependent on the feed rate. The feed composition also has a high influence on the deactivation and product distribution. Low partial pressure of methanol favours olefin production but at the same time decreases the methanol capacity. This contradicts the findings of Chen et al., 2000 who found that deactivation was based on methanol converted and temperature and not WHSV.

The third part on the thesis treats the MTO reaction in fluidized bed. The effect of feed composition, temperature and WHSV was investigated in the same reactor setup in which the methanol dehydration reaction was studied. Feeding 1-hexene in argon and co-feeding 1-hexene with methanol in argon was used to investigate the reaction mechanism. The product distribution obtained by feeding 1-hexene did not change significantly from a methanol feed. The main difference being the methane production which was considerably lower when feeding 1-hexene confirming the observations in fixed bed, that methane originates directly from methanol and/or DME. Ethylene was also found to be a major part of the product distribution from 1-hexene suggesting that ethylene is a part of the secondary cracking reactions.

A kinetic model has been proposed which is based on the hydrocarbon pool mechanism where the olefins are produced through reversible reactions with a larger hydrocarbon

species. Methane is considered to be formed from DME in accordance to the findings from fixed and fluidized bed. Aromatics are considered as C_9H_{12} and paraffins as propane both are formed directly from propylene.

For the MTO reaction in a fluidized bed, the two phase model was chosen as the hydrodynamic model. This was because the bed height was generally higher than in the experiments with methanol dehydration resulting in larger bubbles and since the gas velocity spanned a larger range. Further, the two phase model did not perform significantly worse than the n-CSTR model for the methanol dehydration. The model predicts the light olefins fractions well but some problems were observed with the paraffin and C_{6+} fractions. The latter because aromatic, paraffins and olefins are lumped together which have different reaction patterns.

CONDENSÉ EN FRANÇAIS

Dans cette thèse, la réaction transformant le méthanol en oléfines (MTO) a été étudiée principalement dans un lit fluidisé et aussi dans un lit fixe. Cette réaction peut être divisée en deux sous-ensembles de réactions : la déshydratation du méthanol en éther diméthylique (DME) et les réactions du mélange de méthanol/DME conduisant à la formation d'hydrocarbures. Dans les conditions habituellement utilisées pour la transformation MTO, approximativement 450 à 500°C, la réaction de déshydratation du méthanol est très rapide et peut être considérée à l'équilibre. À des températures plus faibles, typiquement inférieures à 300°C, la formation d'hydrocarbures est pratiquement nulle et la réaction de déshydratation peut ne plus être à l'équilibre. C'est le cas de plusieurs procédés industriels où cette réaction a lieu dans un réacteur qui lui est spécifique, afin de limiter l'augmentation de température inhérente à la transformation MTO. Le catalyseur utilisé pour ces réactions est un mélange de 10% de ZSM-5, avec un rapport de Si/Al de 140, qui a été fixé dans une matrice de Si/Al, constituée de Catapal B, de Levasil 100s/30% et de kaolin. Ce mélange a été séché par atomisation puis calciné à 550°C pendant 4h. Le diamètre moyen des particules obtenues était de 100 µm. Cette poudre a d'abord été mélangée dans une solution de $(NH_3)_2HPO_4$, ensuite séchée puis calcinée afin d'obtenir un catalyseur contenant 1.5% de phosphore. Ce dernier a été ajouté pour réduire la formation de méthane.

Le travail réalisé se divise en trois étapes : en premier lieu, la réaction de déshydratation du méthanol a été étudiée en utilisant un lit fluidisé. La réaction MTO a été investiguée

dans un lit fixe dans une deuxième étape, et dans un lit fluidisé dans une étape finale. Ainsi, un modèle cinétique représentant l'ensemble de ces réactions complexes a été proposé.

La réaction de déshydratation du méthanol a été étudiée dans un réacteur fluidisé en quartz de 46mm de diamètre. Ce réacteur a permis d'investiguer aussi bien les effets de transfert de matière que la réaction chimique intrinsèque. Les analyses des concentrations des produits de la réaction ont été réalisées par un spectromètre de masse (SM) et en partie par chromatographie en phase gazeuse (GC). Comme le SM permet des mesures en ligne, les changements dans les conditions de réaction sont facilement détectables et les régimes permanents peuvent être déterminés. Les expériences ont été réalisées avec du méthanol dilué dans de l'argon à quatre concentrations distinctes : 5, 15, 30 et 33 mol% et à trois températures différentes : 250, 275 et 325°C. A 325°C, dépendamment du rapport débit massique et de la quantité de catalyseur (WHSV), la réaction de déshydratation du méthanol peut conduire à la formation d'autres hydrocarbures que le DME. Ces cas-là ont été ignorés. Lorences et coll. (2006) ont montré que l'hydrodynamique des lits fluidisés peut être assimilée à celle des réacteurs parfaitement mélangés en série à faibles vitesses superficielles. Les mesures de Distribution du Temps de Séjour (DTS), réalisées dans le cadre de ce travail, ont permis de caractériser le lit fluidisé comme étant équivalent à 6 réacteurs parfaitement mélangés en série, lorsque la vitesse superficielle est égale à 10 fois la vitesse minimale de fluidisation. Afin d'obtenir des WHSV relativement élevées même à faibles vitesses

superficielles, la quantité de catalyseur a été variée de 25 à 200g. Les conversions expérimentales obtenues ont été de l'ordre de 30 à 99+% par rapport à l'équilibre.

Afin d'analyser la cinétique de réaction, deux réacteurs modèles différents ont été utilisés pour modéliser l'hydrodynamique du lit fluidisé. Le premier est un modèle à deux-phases (phase émulsion et phase bulles). La réaction a lieu seulement dans la phase émulsion. Le gaz est considéré en écoulement piston, alors que la phase émulsion est parfaitement mélangée. Le coefficient de transfert de matière entre les deux phases est donné par la corrélation de Sit et Grace (1981). Le coefficient de diffusion moléculaire du méthanol a été assumé égal à 0.4cm^2/s. Le diamètre des bulles a été calculé en fonction de la hauteur du lit, en utilisant la corrélation de Mori et Wen (1975). Le deuxième modèle hydrodynamique considéré est une série de 6 réacteurs parfaitement mélangés, obtenu par DTS. Un modèle cinétique de la réaction de déshydratation du méthanol en DME a été proposé en considérant i) aussi bien la réaction principale que la réaction inverse, ii) l'absorption de l'eau et du méthanol (équation 1).

$$-r_{MeOH} = \frac{kC_M^2\left(1-\dfrac{C_D C_W}{C_M^2 K_{eq}}\right)}{\left(1+K_M C_M + K_W C_W\right)^2} \qquad (1)$$

Ce modèle a été comparé à celui de Berčič et Levec (1992) (Équation 2)

$$-r_{MeOH} = \frac{k\ K_M^2\left(C_M^2 - C_w C_E / K_{eq}\right)}{\left(1+2\left(K_M C_M\right)^{0.5} + K_W C_w\right)^4} \qquad (2)$$

Plusieurs séries de paramètres cinétiques ont été trouvées en couplant les deux modèles hydrodynamiques avec les deux modèles cinétiques et par optimisation des données expérimentales obtenues aux trois plus faibles concentrations de méthanol. L'analyse des résultats a montré que le modèle cinétique proposé (équation 1), obtenu en utilisant n-réacteurs parfaitement mélangés, permet d'obtenir les prédictions les plus proches des données expérimentales. De plus, l'extrapolation de ce modèle aux données obtenues pour les plus grandes concentrations de méthanol était excellente. Le modèle hydrodynamique n-réacteurs parfaitement mélangés, couplé soit au modèle cinétique proposé soit au modèle cinétique de la littérature, donne de meilleurs résultats (valeur de R^2 respectivement égale à 0.934 et 0.910), même si le modèle à deux phases ne peut pas être rejeté (valeur de R^2 respectivement égale à 0.918 et 0.9006).

Cette étude a aussi montré qu'une expérience cinétique dans un lit fluidisé à petite échelle a des avantages pour les réactions exothermiques, car elle élimine les incertitudes liées aux points chauds et aux gradients de température. Pour utiliser les n-réacteurs parfaitement mélangés comme réacteur modèle, il faut maintenir une vitesse superficielle relativement faible. Par contre, avec les contraintes sur les vitesses superficielles et la masse de catalyseur, les conversions à des températures données peuvent être limitées.

La réaction MTO a été étudiée dans plusieurs lits fixes de faible diamètre. Les mécanismes de la réaction principale et de la désactivation ont été analysés pour différentes WHSV, compositions à l'entrée et longueurs de réacteur (3, 6 et 8 mm). La chromatographie en phase gazeuse a été utilisée pour déterminer la composition des

produits de la réaction. Les composés à faibles nombres de carbone ont été analysés individuellement, alors que les fractions de C_4 et de C_{5+} (non aromatiques) ont été mesurées comme un tout. Ces expériences ont suggéré que les hydrocarbures non aromatiques C_{5+} sont des intermédiaires de la réaction MTO conduisant à la formation de propylène et de butylène (mais pas d'éthylène) par un craquage supplémentaire. La production d'éthylène se produit, quant à elle, par divisions des aromatiques (principalement xylènes et triméthylbenzènes), ce qui concorde avec les travaux de Svelle et coll. (2006). Par contre, le méthane qui est prédominant à de faibles conversions du méthanol/DME et à des taux élevés de WHSV doit certainement se former directement à partir du méthanol ou du DME et non à partir des hydrocarbures supérieurs.

La désactivation du catalyseur est très sensible à la WHSV et croît avec celle-ci. Par conséquent, la capacité du catalyseur à transformer le méthanol dépend du flux à l'entrée du réacteur. La composition de ce flux influence beaucoup la désactivation du catalyseur et la composition des produits. De faibles pressions partielles de méthanol favorisent la production d'oléfines, mais elles réduisent la capacité du catalyseur à transformer le méthanol. Ceci est en contradiction avec les travaux de Chen et coll. (2000), qui ont montré que la désactivation du catalyseur est fonction de la quantité de méthanol converti et de la température et non de WHSV.

Par des inspections visuelles, le catalyseur désactivé est constitué essentiellement de 3 zones : une zone à l'entrée, faiblement désactivée, où la réaction de déshydratation du méthanol a lieu; une zone intermédiaire noire (présence de coke), où la production

d'oléfines est prépondérante; et une zone post-réaction, où la présence du coke est plutôt limitée, très probablement à cause des réactions de craquage secondaire d'oxygénés qui consomment du carbone.

La troisième partie de la thèse traite de la réaction MTO dans un lit fluidisé. Les effets de la composition de l'alimentation, de la température et de la WHSV ont été analysés dans le même réacteur que celui de la réaction de déshydratation (voir première partie du travail). En alimentant un mélange 1-hexène/argon d'une part et un mélange 1-hexène/méthanol/argon d'autre part, nous avons proposé un mécanisme probable de réaction. La distribution des produits de réaction n'a pas changé de façon significative avec une alimentation en méthanol. Avec l'hexène, les différences majeures sont la plus faible formation de méthane et la plus grande formation d'éthylène. Ceci confirme l'étude réalisée en lit fixe concluant que i)le méthane est produit principalement à partir du méthanol ou DME, ii)l'éthylène est produit par craquage secondaire.

Plusieurs cinétiques de cette réaction ont été proposées dans la littérature. Cependant, la plupart d'entre elles se basent sur l'utilisation d'un catalyseur de type zéolite SAPO et ne prennent pas en compte la formation d'hydrocarbures supérieurs, car les pores de ce catalyseur ne permettent pas le passage des grosses molécules. Les modèles basés sur des catalyseurs de type ZSM-5 ont été développés principalement pour la réaction méthanol-gazoline, qui combinent les oléfines légères. Quelques rares modèles, tels que celui de Schoenfelder et coll. (1994), traitent les oléfines légères individuellement, mais ne tiennent pas compte du craquage secondaire des hydrocarbures lourds. Un modèle

cinétique a été proposé en se basant sur le mécanisme « lot d'hydrocarbures », où les oléfines sont produites par de réactions réversibles à partir d'un lot d'hydrocarbures supérieurs. La figure 1 montre un schéma du modèle proposé. Comme l'indiquent les conclusions antérieures, le méthane est supposé se former à partir du méthanol/DME. Les aromatiques sont considérés comme étant C_9H_{12} et les paraffines, tout comme le propane, sont produits directement à partir du propylène.

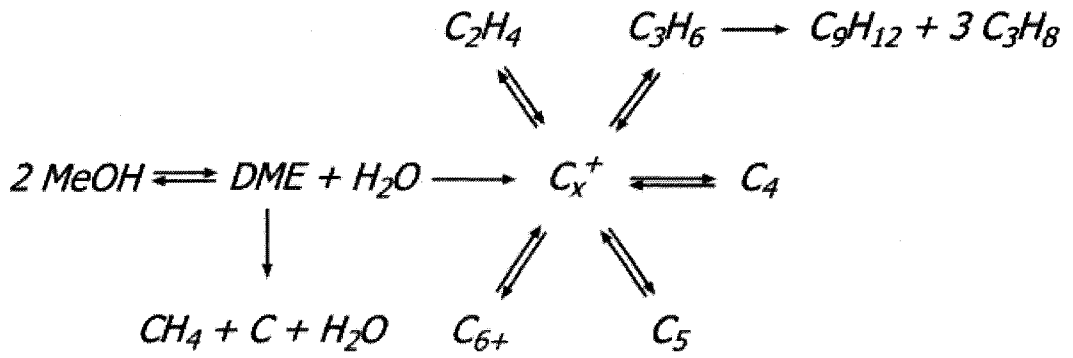

Figure 1: Schéma du modèle cinétique proposé

Pour la réaction MTO en lit fluidisé, le modèle hydrodynamique à deux phases a été choisi. En effet, comme la hauteur du lit était généralement beaucoup plus élevée que dans les expériences réalisées dans la première partie de ce travail, la taille des bulles était donc plus grande. Par ailleurs, ce modèle n'a pas été rejeté lors de l'étude de déshydratation du méthanol. Les valeurs des constantes cinétiques du modèle ont été estimées en ajustant les prédictions du modèle (hydrodynamique + cinétique) proposé avec les données expérimentales. Le modèle prédit bien la formation d'oléfines légères, mais moins bien la production des paraffines et des fractions C_{6+}.

TABLE OF CONTENTS

ACKNOWLEDGEMENTS ..... *iv*
RÉSUMÉ ..... *vi*
ABSTRACT ..... *xii*
CONDENSÉ EN FRANÇAIS ..... *xvii*
TABLE OF CONTENTS ..... *xxiv*
LIST OF TABLES ..... *xxvii*
LIST OF FIGURES ..... *xxix*
LIST OF FIGURES ..... *xxix*
LIST OF SYMBOLS ..... *xxxvi*
Chapter 1 Introduction *1*
Chapter 2 Literature study *8*
2.1 Introduction **8**
2.2 Zeolites **9**
2.2.1 ZSM-5 9
2.2.2 SAPO-34 11
2.3 Mechanisms **12**
2.4 Reaction conditions **17**
2.4.1 Temperature effect 17
2.4.2 Pressure effect 18
2.4.3 Catalyst deactivation 19
2.4.4 Effect of water 20
2.4.5 Gas residence time 21
2.5 Kinetic **22**
2.6 Processes **32**
2.6.1 Industrial Processes 37
2.6.1.1 Lurgi Process 38
2.6.1.2 UOP/Hydro Process 39
2.6.1.3 Mobil Process 40
Chapter 3 Objective and methodology *42*
3.1 Objective **43**
3.2 Methodology **44**
3.2.1 Catalyst 44
3.2.2 Fixed bed experiments 44
3.2.3 Fluid bed experiments 45
3.2.4 Kinetic model 47

Chapter 4 MeOH to DME in Bubbling Fluid Bed: Experimental and Modelling 48*

4.1 Presentation of the article 48

4.2 MeOH to DME in Bubbling Fluidized Bed: Experimental and Modelling 49

4.2.1 Abstract 49
4.2.2 Introduction 50
4.2.3 Experimental 54
4.2.3.1 Equipment 54
4.2.3.2 Catalyst 55
4.2.3.3 Experimental conditions 56
4.2.4 Experimental results 57
4.2.4.1 RTD 57
4.2.4.2 Methanol to DME 60
4.2.5 Modeling 64
4.2.5.1 Kinetics 64
4.2.5.2 Fluid bed model 66
4.2.6 Modelling result and discussion 70
4.2.7 Conclusion 75
4.2.8 Nomenclature 76
4.2.9 Literature Cited 78

Chapter 5 Phosphorous modified ZSM-5: Deactivation and product distribution for MTO 83*

5.1 Presentation of the article 83

5.2 Phosphorous modified ZSM-5: Deactivation and product distribution for MTO 84

5.2.1 Abstract 84
5.2.2 Introduction 84
5.2.3 Experimental 87
5.2.3.1 Catalyst 87
5.2.3.2 Reactor setup 87
5.2.3.3 Procedure 89
5.2.4 Results 89
5.2.5 Conclusions 98
5.2.6 References 99

Chapter 6 Trends in the MTO reaction by MS 103

6.1 Introduction 103

6.2 Experimental 103

6.3 Results and discussion 104

6.4 Conclusion 107

Chapter 7 Kinetic modelling of MTO reaction over ZSM-5 in fluid bed 109*

7.1 Presentation of the article 109

7.2 Kinetic modelling of MTO reaction over ZSM-5 in fluid bed 110

7.2.1 Abstract 110
7.2.2 Introduction 111

7.2.3 Experimental 114
7.2.3.1 Equipment 114
7.2.3.2 Catalyst 115
7.2.3.3 Experimental conditions 116
7.2.4 Experimental data 117
7.2.5 Fluid bed model 125
7.2.6 Kinetic model 128
7.2.7 Modelling results 132
7.2.8 Conclusion 137
7.2.9 Nomenclature 138
7.2.10 References 141

Chapter 8 General discussion 146

8.1 Elevation of the catalyst with glass beads 148

8.2 Kinetic and Modelling of the MTO reaction 150

Chapter 9 Conclusion and recommendations 154

9.1 General conclusions 154

9.2 Recommendation 157
9.2.1 Kinetics in fluidized bed 157
9.2.2 MTO reaction kinetic 157
9.2.3 Equilibrium inside the catalyst? 158

References 159

Appendix A - Catalyst preparation 173

Appendix B - Fluidized bed reactors used 176

LIST OF TABLES

Table 2-1: Product distribution of the MTO reaction in fluid bed at 482°C and 102 kPa methanol partial pressure (Tabak and Yurchak, 1990).....33

Table 2-2: Properties of the H-ZSM-5 and the catalyst used in the.....34

Table 4-1: Particle properties of the catalyst.....56

Table 4-2: n-CSTR model parameters for the RTD experiments done at u_0 0.052m/s 58

Table 4-3: Experimental data obtained – all flows are listed at STP conditions.....61

Table 4-4: Kinetic models including the reverse term. 64

Table 4-5: Hydrodynamic correlations – the correlation for bubble diameter is in cm and not in meters.....69

Table 4-6: Best fit parameters for the kinetic model Equation 4-5 and the level of fit to the experimental data. 70

Table 4-7: Best fit parameters for model of Berĉiĉ and Levec (1992) and the level of fit to the experimental data.....70

Table 4-8: Fixed bed experiments in a 4 mm inner diameter quartz reactor. 74

Table 5-1: Product distribution after 2 hours on stream in the 3 and 6 mm diameter reactors.....91

Table 7-1: Particle properties of the catalyst.....116

Table 7-2: Carbon deposition on the MTO catalyst.....118

Table 7-3: Experimental results from the fluid bed experiments – product distribution is given in carbon % *100ml H_2 was co-feed with methanol and argon 119

Table 7-4: Hydrodynamic correlations 128

Table 7-5: Kinetic model with optimized parameters for k_0 and activation energy k* is calculate with a reference temperature of 500°C 132

Table B-1: Dimensions of the 7.79 cm inner diameter reactor..... 177

LIST OF FIGURES

Figure 1: Schéma du modèle cinétique proposé xxiii

Figure 2-1: Methanol to hydrocarbon reaction path at 371°C (Chang, 1984) 9

Figure 2-2: Structure of the MFI framework (International Zeolite Association, 2006) 10

Figure 2-3: Schematic drawing of an acid site on a ZSM-5 11

Figure 2-4: Structure of the CHA framework (International Zeolite Association, 2006) 12

Figure 2-5: Schematic drawing of the oxonium ylide mechanism (Stöcker, 1999) ... 14

Figure 2-6: Reaction for the free radical mechanism (Chang et al., 1989) 15

Figure 2-7: The hydrocarbon pool mechanism (Dahl and Kolboe, 1994) 16

Figure 2-8: Ethylene formation by reaction of methanol withmethylbenzenes. (Aguayo et al., 2005) 16

Figure 2-9: Product distribution of the MTO reactionat high, low and atmospheric pressure (Chang, 1984) 18

Figure 2-10: Evolution with time on stream of the composition of the lumps of the kinetic scheme, in three successive reaction–regeneration cycles in fixed bed. Reaction conditions: temperature, 773 K, space time, 0.093 (kg of catalyst) h (kg of methanol)$^{-1}$; water content in the feed, 50 wt%. Points: experimental results. Solid lines: calculated (Gayubo et al., 2003) 28

Figure 2-11: Scheme and kinetic model for the MTO-reaction by Schoenfelder et al. (1994) 29

Figure 2-12: Reaction scheme for the MTO reaction by Bos et al. (1995) 30

Figure 2-13: Evolution of the mass fractions of each lump, until steady state is reached at three different temperatures, space time 0.040 $g_{cat}h/g_{MeOH}$ and average solid residence time 0.866h^{-1} (Ortega et al., 1998) 34

Figure 2-14: Contours of the relative production rate of light olefins for different residence times in the reactor and regenerator. Temperature 420°C space time 0.021 $g_{cat}h/g_{MeOH}$ (Gayubo et al. 2000) 35

Figure 2-15: Comparison between measured (symbols) and predicted (lines) product distribution of the CFB reactor at a temperature of 500°C (Schoenfelder et al, 1994) 37

Figure 2-16: Flow diagram of Lurgi MTP® Process (Stöcker 2003) 39

Figure 2-17: Simplified flow diagram of the UOP/Hydro MTO Process (Houdek and Andersen 2005) 40

Figure 4-1: Drawing of the glass fluidized bed with glass beads, catalyst and thermocouple 54

Figure 4-2: Schematic diagram of the experimental setup 55

Figure 4-3: RTD experimental results over the fluid bed with a gas velocity of 5.4 cm/s. A) reactor loaded with 540g glass beads B) Reactor loaded with 540g glass beads and 50g of catalyst C) Reactor loaded with 220g of

catalyst. Experimental data represented by dots and n-CSTR model with a line. 59

Figure 4-4: MS results from experiments done at 275°C with 25 g of catalyst 62

Figure 4-5: Conversion of methanol to DME and water based on equilibrium conversion as function of catalyst amount at five different gas velocities (experiment 20 - 39). Lines are the model predictions using kinetic model equation 4-5 and 6 CSTR's in series. 63

Figure 4-6: Schematic of the two phase fluid bed model 68

Figure 4-7: Model predictions vs. experimental with 6 CSTR's in series. ▪ Model Eq. 4-5; • Model of Berĉiĉ and Levec (1992) 72

Figure 4-8: Effect of the molar diffusion coefficient with the use of the best fit parameters for 6-CSTR's in series with the two phase model and the kinetic model of Equation 4-5. The experimental points are at 275°C and a superficial gas velocity of 7.79 cm/s 73

Figure 5-1: Experimental setup 88

Figure 5-2: MTO product distribution at 500°C in the 6 mm inner diameter reactor with 10% methanol in nitrogen feed: (a) WHSV 0.22 h^{-1} (dashed lines due to missing data) , (b) WHSV 0.43 h^{-1} 90

Figure 5-3: Hydrocarbon distribution as a function of oxygenate conversion. Based on experiments in Table 1 at 500°C 92

Figure 5-4: Hydrocarbon distribution as a function of oxygenate conversion. Based on experiment at 500°C in 8 mm inner diameter reactor with pure methanol feed. WHSV 2.37 h^{-1}. 93

Figure 5-5: Pore size distribution of fresh, coked and regenerated catalyst. 96

Figure 5-6: Catalyst coking at t = 0, 10, 20, 50, 110, 170, 1310 minutes in the 6 mm reactor, 10% MeOH in nitrogen, T=500°C, WHSV 0.43 g(MeOH)/gcat/h (gas flows from the top down through the bed). 97

Figure 6-1: MS traces during the MTO reaction with temperature increments of 50°C from 250°C to 550°C. A) Methanol, B) DME, C) Hydrocarbons and D) Methane. 105

Figure 6-2: Product distribution from the MTO in the temperature interval 450 – 550°C with several different feed compositions 106

Figure 6-3: Comparison between ethene and other hydrocarbon concentration for the MTO reaction 107

Figure 7-1: Drawing of the glass fluid bed reactor – glass beads are used to elevate the catalyst for catalyst amounts below 100g 114

Figure 7-2: Schematic diagram of the experimental setup 115

Figure 7-3: Comparison between experimental data and equilibrium composition of the C2 – C6 olefins in the temperature range 400 – 550°C a) ethylene and propylene b)C_4, C_5,C_6 121

Figure 7-4: Product distribution vs. residence time with methanol/Argon feed (molar ratio 1:1) over ZSM-5 at 550°C. Δ: conversion , ●: ethylene, ■: propylene, ◆: propane, ▲: C_4, □: C_5, ○: C_{6+} 122

Figure 7-5: Product distribution vs. residence time with methanol/Argon feed (molar ratio 1:1) over ZSM-5 at 500°C. Δ: conversion , ●: ethylene, ■: propylene, ◆: propane, ▲: C_4, □: C_5, ○: C_{6+} 123

Figure 7-6: Product distribution vs. residence time with methanol/Argon feed (molar ratio 1:1) over ZSM-5 at 450°C. Δ: conversion , ●: ethylene, ■: propylene, ◆: propane, ▲: C_4, □: C_5, ○: C_{6+} 124

Figure 7-7: Product distribution vs. residence time with pure methanol feed over ZSM-5 at 500°C. Δ: conversion , ●: ethylene,■: propylene, ◆: propane, ▲: C_4, □: C_5, ○: C_{6+} 124

Figure 7-8: Schematic drawing of the fluid bed model. 126

Figure 7-9: Product distribution of reaction over ZSM-5 with three different feed compositions and a total inlet flow rate of 1.57 L/min at 500°C 1) Methanol/Argon molar ratio 1:2 2) Methanol/1-hexene/Argon molar ratio 9:1:20 and 3) 1-hexene/Argon molar ratio 1:2 129

Figure 7-10: Schematic drawing of the kinetic model 131

Figure 7-11: Comparison of the calculated product distribution to the measured data. 134

Figure 7-12: Measured (points) and calculated (lines) data at 550°C with methanol/argon (ratio 1:1) feed as function of residence time in the fluid

bed. Δ(····): conversion: ●(—): ethylene,■(---): propylene, ▲(····): C_4, □(—): C_5, ○(---): C_{6+}. 135

Figure 7-13: Measured (points) and calculated (lines) data at 500°C with methanol/argon feed (ratio 1:1) as function of residence time in the fluid bed. Δ(····): conversion: ●(—): ethylene, ■(---): propylene, ▲(····): C_4, □(—): C_5, ○(---): C_{6+}. 135

Figure 7-14: Measured (points) and calculated (lines) data at 450°C with methanol/argon feed (ratio 1:1) as function of residence time in the fluid bed. Δ(····): conversion: ●(—): ethylene,■(---): propylene, ▲(····): C_4, □(—): C_5, ○(---): C_{6+}. 136

Figure 7-15: Measured (points) and calculated (lines) data at 500°C with methanol feed ratio 1:1 as function of residence time in the fluid bed. Δ(····): conversion: ●(—): ethylene,■(---): propylene, ▲(····): C_4, □(—): C_5, ○(---): C_{6+}. 137

Figure 8-1: Particle size distribution of the MTO catalyst, sand and glass beads used – measured was preformed n a Horiba LA-950 150

Figure 8-2: Calculated values with the use of the model of Schoenfelder et al. (1994) versus the obtained experimental data from fluidized bed..... 151

Figure A-1: Methane formation with time at different phosphor loadings of the fluid bed catalyst. 174

Figure A-2: picture of the spray dried particles 175

Figure B-1: Drawing of the 3" inner diameter fluid bed Legend: 1) feed inlet, 2) windbox, 3) distribution grid 4) solid outlet, 5) fluid bed region, 6) sampling/measuring ports, 7) freeboard, 8) electrical heating, 9) solid inlet, 10) disengagement zone 177

Figure B-2: Schematic diagram of the 3" fluidized bed setup 179

Figure B-3: 4.1cm inner diameter fluidized bed reactor.....181

LIST OF SYMBOLS

Chapter 2

A, B, C, D	lump of oxygenates , :CH_2, light olefins, and the remaining components
a	Remaining catalyst activity due to coke deposition
c	weight percentage of coke on the catalyst, kg/(100kg_{cat})
C_j	Concentration of component j,
d_p	particle diameter, μm
E(t)	Residence-time distribution function
k_i	Kinetic constant for component i, h^{-1}
k_{di}	Kinetic constant for deactivation for component i, h^{-1}
k_i^0	Kinetic constant for component i for zero coke concentration, h^{-1}
N	Number of tanks in CSTR model
P	Pressure, bar
Q	Volumetric flow rate, m^3/s
r_i	Reaction rate for component i,
r_{i0}	Reaction rate of fresh catalyst for component i,
t	Time
t_m	Mean residence time, s
V_j	Volume of tank j, m^3
x_i	Molar fraction of component i, mol/mol
X_i	Weight fraction of component i, kg/kg

Pe	= Peclet number ($Pe = U_gL/D$)
r_i	= Reaction rate of component i (kmol/kg·s)
$t_{½}$	= Halftime (s)
t_m	= Mean residence time (s)
u_{mf}	= Minimum fluidization velocity (m/s)
u_{mb}	= Minimum bubbling velocity (m/s)
u_b	= Bubble velocity (m/s)
u_0	= Superficial gas velocity (m/s)
V_e	= Volume of emulsion (m^3)
W	= Catalyst weight (kg)
Q	= Gas flow (ml/min)
X	= Total conversion
x	= Mole fraction
y	= Mole fraction of gas
z	= Height in bed (m)

Greek symbols

δ	= Bubble phase volumetric fraction
ε_{mf}	= Void fraction at minimum fluidization
μ	= Gas viscosity (kg/m·s)
σ^2	= Variance
ρ_p	= Particle density (kg/m^3)
ρ_{tapped}	= Tapped density (kg/m^3)

α	Remaining catalyst activity due to irreversible deactivation
β	Catalyst activity paramenter

Chapter 4

A_t	= Cross-sectional area of the fluid bed (m^2)
C	= Molar concentration ($kmol/m^3$)
$\mathcal{D}$	= Molar diffusion coefficient (m^2/s)
D_t	= Reactor diameter (m)
d_p	= Mean particle diameter (m)
d_b	= Bubble diameter (m)
d_{b0}	= Initial bubble diameter at the distributor (m)
d_{bm}	= Maximum bubble diameter (m)
E_a	= Activation energy (kJ/mol)
F	= Fine fraction
F_b	= Flow rate in bubble phase (kmol/s)
F_e	= Flow rate in emulsion phase (kmol/s)
g	= gravity (m/s^2)
K_{eq}	= Equilibrium constant
k	= Reaction rate constant ($m^6/kmol \cdot s$)
K_{be}	= Bubble to emulsion mass transfer coefficient (s^{-1})
k_{be}	= Bubble to emulsion mass transfer coefficient (m/s)
N	= Number of CSTR's

ρ_{mf} = Minimum fluidization density (kg/m^3)

ρ_g = Gas density (kg/m^3)

τ = Residence time (s)

Subscripts

exp = Experimental

calc = Calculated

n = CSTR number

i = species

be = Bubble to emulsion

b = Bubble

e =Emulsion

Chapter 7

A_t = Cross-sectional area of the fluid bed (m^2)

C = Molar concentration (kmol/m^3)

C_x^+ = Hydrocarbon pool species (Decene)

D = Molar diffusion coefficient (m^2/s)

D_t = Reactor diameter (m)

dp = Particle diameter (m)

d_b = Bubble diameter (m)

d_{b0} = Initial bubble diameter at the distributor (m)

d_{bm} = Maximum bubble diameter (m)

E_a = Activation energy (kJ/mol)

F = Fine fraction

F = Flow rate (kmol/s)

g = gravity (m/s^2)

h = Height in bed (m)

K_{eq} = Equilibrium constant

k_i = Reaction rate constant (m^6/kmol·s)

K_{be} = Bubble to emulsion mass transfer coefficient (s^{-1})

k_{be} = Bubble to emulsion mass transfer coefficient (m/s)

N = Total number of components in the system

r_i = Reaction rate of component i (kmol/kg·s)

T = Temperature (K)

u_{mf} = Minimum fluidization velocity (m/s)

u_{mb} = Minimum bubbling velocity (m/s)

u_b = Bubble velocity (m/s)

u_0 = Superficial gas velocity (m/s)

V_e = Volume of emulsion (m^3)

W = Catalyst weight (kg)

y = Mole fraction

Greek symbols

Γ = Gas expansion due to reaction

δ = Bubble phase volumetric fraction

ε_{mf} = Void fraction at minimum fluidization

ε_{cat} = Void fraction of the catalyst

μ = Gas viscosity (kg/m·s)

ρ_p = Particle density (kg/m^3)

ρ_b = Bulk density (kg/m^3)

ρ_{tapped} = Tapped density (kg/m^3)

ρ_{mf} = Minimum fluidization density (kg/m^3)

ρ_g = Gas density (kg/m^3)

Subscripts

e = Emulsion Phase

b = Bubble Phase

i = Component index

n = CSTR in series

exp = experimental data

cal = calculated value

Chapter 1
Introduction

In the recent years the demand for the light olefins ethylene and propylene has increased with the largest growth in propylene. Propylene is mainly produced from steam cracking units which produces about twice as much ethylene compared to propylene. With the increases propylene/ethylene ratio in the global demand there is a need to produce propylene from other sources. Fluidized catalytic cracking units are currently filling this gab in production but it is expected that it will not be able to cover the demand and alternative sources are needed (Andersen, 2003; Houdek and Andersen, 2005). A large part of the worlds natural gas resources are located in regions where the need is low or non existent and transport to the gas market is expensive. These remote or stranded natural gas fields therefore offer low cost gas for on-site chemical production. One way to utilize the stranded natural gas is to produce methanol in large scale plants 5,000 – 10,000 MTD. Methanol from these plants offers a cheap feedstock for a Methanol To Olefin (MTO) plant. Olefin production from a MTO facility are comparative with naphtha crackers when the crude oil price is around 16$ per barrel (Houdek and Andersen, 2005). With the recent increase in oil price the MTO process is competitive with standard olefin technology and a good way to use stranded natural gas resources when coupled with a mega-methanol plant.

Several companies already offer MTO technology for large scale olefin production. Lurgi has the Methanol To Propylene (MTP) process which converts methanol to propylene with a selectivity of approximately 70%. The process is based on fixed bed reactors in series with a ZSM-5 zeolite as the active catalyst. Several plants are planned/under construction with the majority located in China (Lurgi, 2008). UOP/Hydro offers a MTO technology based on fluidized bed reactors with a SAPO-34 zoelite as the catalyst, which is continually regenerated to reduce deactivation due to coking. The first commercial plant is scheduled to come online in 2012 and consists of the MTO technology coupled with an olefin cracking unit to increase the light olefin yield (UOP, 2008). Exxonmobil have conducted extensive research in the process and have demonstrated a fluid bed MTO process.

Although research in the methanol to olefin reaction has been ongoing since the late 1970's, there are still several aspects that are poorly understood. The fundamental reaction to form the first C-C bond is still disputed and several different reaction mechanisms have been proposed over the years. The kinetics of the reaction are complicated with a large amount of products including most hydrocarbons from methane to polymethylated-benzenes. Depending on the type of zoelite, the product spectrum can vary between a narrow range of $C_1 - C_5$ for the SAPO zeolite to $C_1 - C_{10}$ for the ZSM-5. The product distribution depends on the pore structure of the zeolites with narrow pores leading to a narrow product spectrum. The formation of the hydrocarbons is taking place inside cages in the zeolite which are able to accommodate molecules larger than what

can be transported out of the zeolite pores. Molecules unable to diffuse out of the pores become trapped and lead to catalyst deactivation. The deactivation rate of the catalyst depends on the pore structure and pore diameter. The SAPO catalysts which have narrow pores deactivate rapidly while the ZSM-5 activity remains for a longer period of time. For all commercial purposes of the MTO reaction both types of catalysts need to be regenerated at regular intervals to maintain the desired activity. In the present study the focus have been on the ZSM-5 zeolite.

Kinetic studies are normally conducted in fixed beds or Berty reactors since the hydrodynamics of the reactor is well understood and decoupling of the reaction kinetics from the reactor hydrodynamic is well established. In this work, a fluidized bed is employed for the kinetic study for the following reasons:

- The MTO reaction is exothermic and heat transfer limitations in a fixed bed can result in hot spots or radial and axial gradients creating uncertainty of the actual reaction temperature. In a fluidized bed solid circulation will ensure a uniform temperature profile in the bed, due to high heat transfer of the solids
- Deactivation of the catalyst in a fluidized bed is homogeneous throughout the bed while in a fixed bed a deactivation front will progress through the bed resulting in different levels of catalyst activity in the reactor
- MTO Fluid bed catalyst with a broad particle distribution and an average particle size around 100μm can be use directly whereas fixed bed experiments will require larger particles to avoid undesired pressure drop over the bed.

Possible effects of altering the particle size to fit fixed bed experiments are also avoided.

Using a fluidized bed to conduct kinetic experiments raises the concern about decoupling the hydrodynamic from the kinetics since gas-phase fluid bed hydrodynamics are more complicated than the fixed bed and not as well established. Lorences et al. 2006 showed that at gas velocities above u_{mf} the fluid bed can be modelled well with both the dispersion model as well as the n-CSTR in series model. At the beginning of the bubbling fluidization regime the bed characteristics deviate more and more from plug flow conditions. Several two and three phase models with varying complexity have been developed over the years to describe the hydrodynamics of the fluidized bed. Due to the complex kinetics of the MTO reaction it is desired to minimize the complexity of the hydrodynamic model while still being able to separate the two. A simple two phase fluidized bed model including an emulsion and a bubble phase is therefore well suited for this purpose. A study of the hydrodynamics in the fluid bed is therefore of importance to be able to validate the model.

The methanol to dimethylether (DME) reaction is used in the study of the hydrodynamics of the fluid bed. In contrast to the MTO reaction, the methanol to DME reaction is equimolar and the reaction is much less complicated and the kinetics are established in the literature (Berĉiĉ and Levec, 1992, Mollavali et al. 2008). The fluid bed model is evaluated through methanol to DME experiments and residence time

distribution measurements (RTD) to characterize the flow. The RTD measurements are preformed by switching between air and argon and monitor the argon response as function of time. The main effect of these experiments is to establish the mass transfer between the bubble and emulsion phase in the hydrodynamic model which is one of the main uncertainties.

Deactivation of the catalyst has a large influence on the MTO process and the catalyst has to be either continuously or periodically regenerated to maintain the activity. The product distribution is dependent on the deactivation of the catalyst and the continuous regeneration in a circulation fluidized bed reactor is therefore beneficial for steady-state operation. The deactivation rate of the catalyst is critical; several parameters affect the rate and include: temperature, methanol and water partial pressure. Fixed bed experiments are excellent to study these effects on deactivation. As the catalyst deactivates the number of active sites decreases. By gradually reducing the number of active sites on the catalyst some insight into the reaction mechanism can be obtained as more intermediate species are present in the product distribution.

The general mechanism of the MTO reaction has been disputed for several years but in the recent years the hydrocarbon pool mechanism proposed by Dahl and Kolboe (1993) has gained widespread acceptance. The hydrocarbon pool consists of $(CH_2)_n$ located inside the cage of the zeolite which reacts to the lower olefins. The light olefins are formed by reaction of methanol with polymethylated benzenes which then splits off

olefins after rearrangement under formation to a lower order polymethylated benzene. From carbon isotopic labeling experiments Bjørgen et al (2007) found that the mechanism between SAPO and ZSM-5 differ regarding the polymethylated benzenes that are active in the formation of the light olefins. They also proposed that the reaction consists of two parallel mechanisms one consisting of a modified hydrocarbon mechanism for benzene and ethylene the other with alkene methylations and interconversion of propene and higher alkenes.

As mentioned above the mechanism is highly complicated but the majority of the kinetic reaction schemes proposed over the years have consisted of a few lumped species which capture main trends in the reaction. Only a few kinetic models include the light olefin species as individual components and these kinetics are for the SAPO type catalysts and neglect the higher hydrocarbon species. It is well known that cracking of higher olefins over ZSM-5 is an important reaction mechanism and including it in the kinetic reactions can prove to be important. In this work a kinetic model based on the hydrocarbon pool mechanism is developed for the MTO reaction over ZSM-5 which includes the light hydrocarbons as separate components while also including the cracking and oligomerization reactions for the higher olefins.

Gas chromatograph (GC) and mass spectrometer (MS) are used to analyse the fluid bed MTO experiment. The former gives the product distribution of the hydrocarbons with separate quantification of the light species and lumps based on carbon number for the

C_{4+} hydrocarbons. The MS is able to show trends in the reaction but due to a large overlap between the hydrocarbons precise quantification is difficult. For the methanol to DME reaction, however, the MS is well suited to determine the product distribution.

Chapter 2
Literature study

2.1 Introduction

The Methanol-to-Olefin (MTO) process over a zeolite catalyst has been of great interest since the late 1970's when Chang and Silvestri (1977) first proposed a mechanism for the reaction. It was discovered by accident by two different groups at Mobil. One of the groups was trying to form other oxygen compounds from methanol over a ZSM-5 catalyst while the other was reacting methanol with iso-butane. Both groups produced unwanted hydrocarbons in the gasoline boiling range. Since then, a lot of research has been conducted centred on the methanol to gasoline (MTG) and later the methanol to olefin reaction. Figure 2-1 presents the product distribution of methanol conversion over a ZSM-5 catalyst at 371°C. It shows that the olefin concentration is highly dependent on the space time. Other factors, such as temperature, pressure, Si/Al ratio and deactivation also influence the reaction and will be discussed in the following section.

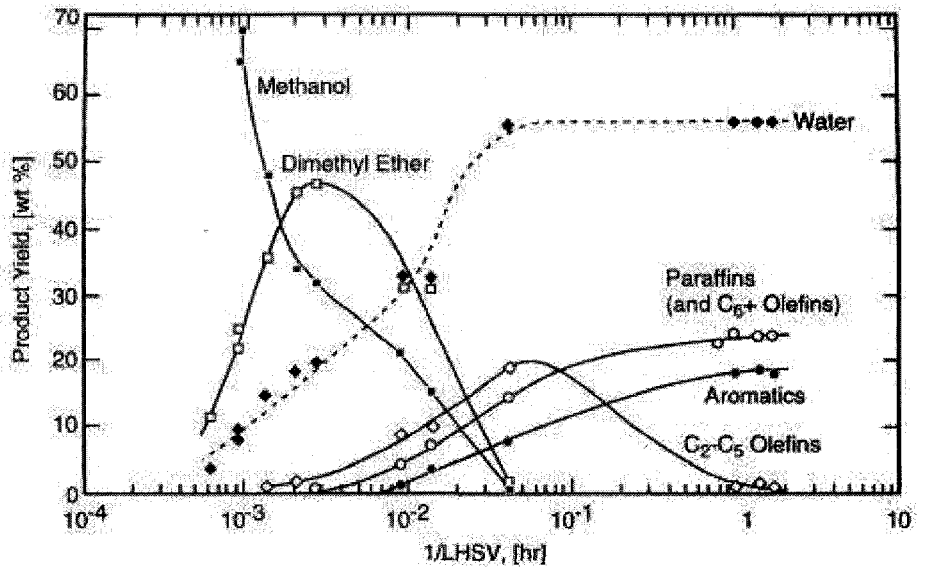

Figure 2-1: Methanol to hydrocarbon reaction path at 371°C (Chang, 1984)

2.2 Zeolites

The MTO reaction is an acid catalyzed reaction and several zeolites are therefore of interest. The two most used zeolites for the MTO reaction are ZSM-5 and SAPO-34 but several others have also been studied, including: MeAPSO-44, SAPO-18, SAPO-44, $ALPO_4$-5, $ALPO_4$-14, and ZKU-4 (Stöcker, 1999). To be able to categorize zeolites, the International Zeolite Association (IZA) has sorted zeolites with framework type codes. The framework type code of ZSM-5 and SAPO-34 is MFI and CHA (International Zeolite Association, 2006). The zeolite used in this project is a ZSM-5 with a Si/Al ratio of 140. The focus will therefore be on this specific zeolite but a brief description of the SAPO-34 zeolite will also be given.

2.2.1 ZSM-5

ZSM-5 has a 3-dimensional channel system with pore sizes of 5.1x5.5 and 5.3x5.6Å in two directions. The channels consist of 10-membered rings with one channel going

straight and parallel to [010] and the other having a sinusoidal structure and running parallel to [001] (Kokotailo, 1978). Cages with larger cross section than the channels are formed where channels meet in both directions. In these cages, larger molecules can form but are not able to pass through the channels and are trapped inside the zeolite, leading to blockage of the pore system. A drawing of the MFI structure is shown in Figure 2-2.

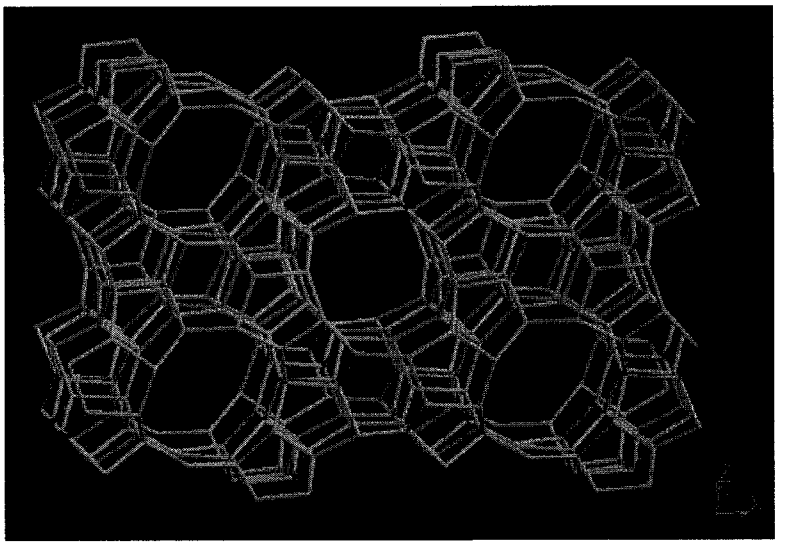

Figure 2-2: Structure of the MFI framework (International Zeolite Association, 2006)

ZSM-5 consists of Silica and Alumina in tetrahedral coordination with oxygen. The introduction of alumina into a tetrahedral framework results in Brøndsted acid sites where a proton is loosely bound to the framework as shown in Figure 2-3. This form of ZSM-5 is also called H-ZSM-5 (Chang, 1983). In the MTO reaction, the product distribution over a ZSM-5 is wide, giving products in the range of C_1 to polymethylatated benzenes with the main products being propylene and butylenes. It is

catalyzed by the acid sites. The reaction rate and product distribution are influenced by the numbers of acid sites in the zeolite. Since it is the amount of alumina that governs the acidity of the ZSM-5 zeolite, the acid strength can be represented by the Si/Al ratio. Chang et al. (1984) investigated the effect of different Si/Al ratios between 17 and 835 at 500°C. For every ratio, it was found that all the catalysts had a maximum olefin production at a space time where the conversion of oxygenates was complete. As the Si/Al ratio is increased, the contact time for complete conversion of oxygenates increases. The maximum production of olefins was found to be dependent on the Si/Al ratio with an optimum around 250.

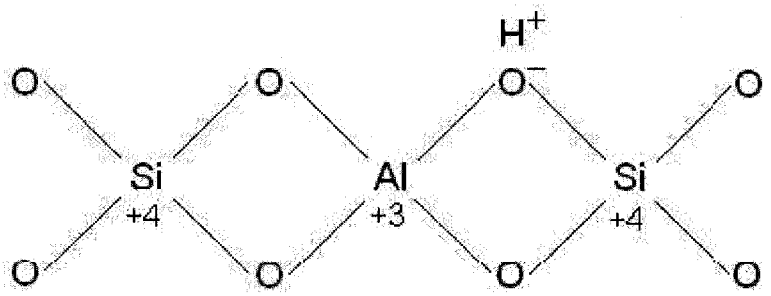

Figure 2-3: Schematic drawing of an acid site on a ZSM-5

2.2.2 SAPO-34

SAPO-34 is a silica-aluminophosphate zeolite with a CHA framework structure. It has a 3-dimensional pore structure with 3.8Å diameter channels (International Zeolite Association, 2006). A schematic drawing of the CHA framework is given in Figure 2-4. As in the case of the MFI structure, the CHA structure also has internal cages that allow formation of larger molecules but since the channels are narrower than in the case of the

MFI, only smaller molecules are able to pass through the channels. The SAPO-34 gives a narrower product spectrum then the ZSM-5 but the coking rate is higher due to entrapment of larger molecules (Stöcker, 1999).

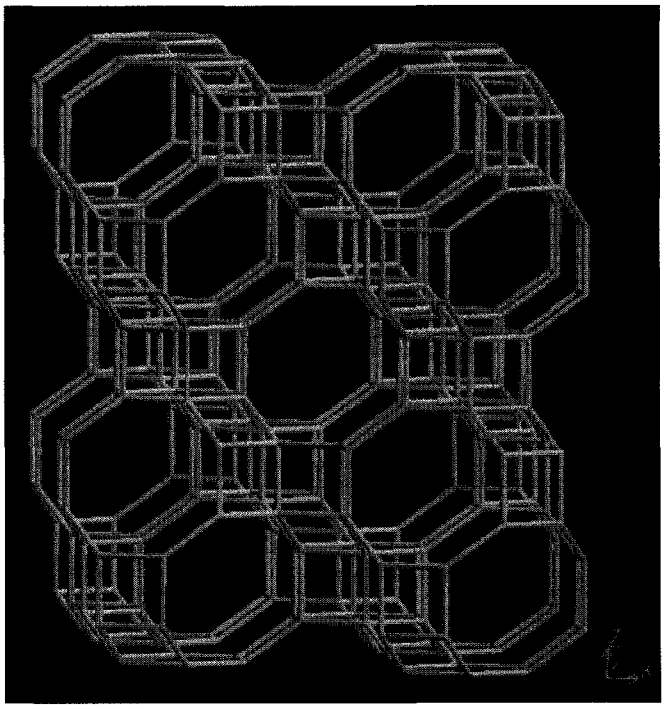

Figure 2-4: Structure of the CHA framework (International Zeolite Association, 2006)

2.3 Mechanisms

Many mechanisms have been proposed, mainly concerning the formation of the first C-C bond. There is a general consensus of the dehydration of methanol to DME and the reaction of light olefins to paraffins, higher olefins and aromatics are known to be formed from hydrocarbon chemistry in acidic media, where the reaction proceeds via a classical carbenium mechanism with hydrocarbon transfer. A short description of the different mechanisms from the first C-C bond are given below.

In the **oxonium ylide mechanism,** dimethyl ether interacts with a Brønsted acid site on the catalyst to form a dimethyl oxonium ion. The oxonium ion then reacts with DME to form a trimethyl oxonium ion that is then deprotonated by an acid site to form a dimethyl oxonium methyl ylide on the surface. Next the dimethyl oxonium ion either undergoes a Stevens rearrangement or an intermolecular methylation leading to a methylethyl ether and ethyldimethyl oxonium ion, respectively. Ethylene is then formed by β-elimination of either of the two components. A schematic drawing is shown in Figure 2-5. Many studies have been preformed to verify the existence of the oxonium ions and the zeolites ability to abstract a proton from the oxonium ions to form the ylides but no definitive answers have been found (Stöcker, 1999).

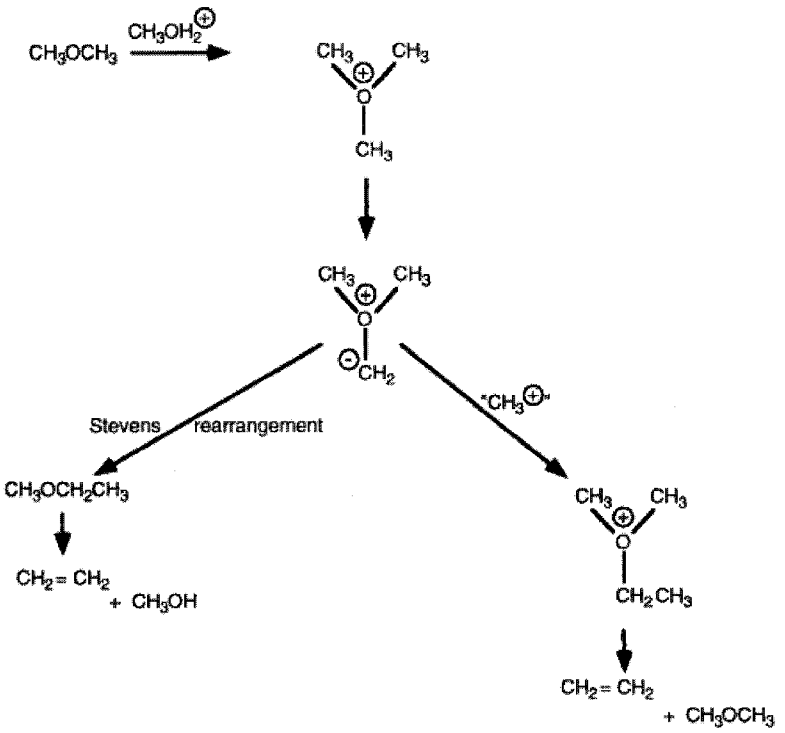

Figure 2-5: Schematic drawing of the oxonium ylide mechanism (Stöcker, 1999)

The carbene mechanism involves a surface associated carbene and is based on α-elimination of water from methanol. The resulting carbene then either reacts with another carbene to olefins or reacts with methanol or DME by concurrent sp^3 insertion. It is not yet clear if the carbene is formed by cooperative action of acid and basic sties on the catalyst or by decomposition on the surface (Stöcker, 1999).

The free radical mechanism involves the participation of free radicals in the conversion of methanol to hydrocarbons. Clarke et al. (1986) found that DME could be a source of methyl radicals as they identified free radicals in the reaction of DME over

ZSM-5. Chang et al. (1989) suggested a reaction path for the free radical mechanism which is shown in Figure 2-6.

$$
\begin{array}{rcl}
CH_3OH + ZOH & \longrightarrow & CH_3O - Z + H_2O \\
CH_3O - Z + R\bullet & \longrightarrow & \bullet CH_2O - Z + RH \\
\bullet CH_2O - Z + ZO & \longrightarrow & ZO : \ : CH_2 \\
 & & \updownarrow \qquad\qquad +ZO\bullet \\
 & & Z - O - CH_2^- \\
HR + ZO\bullet & \longrightarrow & R\bullet + ZOH
\end{array}
$$

Figure 2-6: Reaction for the free radical mechanism (Chang et al., 1989)

The mechanisms proposed for the methanol to hydrocarbon reaction may be classified in two groups (Dahl and Kolboe, 1994).

Consecutive type mechanisms:

$$
\begin{aligned}
&2C_1 \longrightarrow C_2H_4 + H_2O \\
&C_2H_4 + C_1 \longrightarrow C_3H_6 \\
&C_3H_6 + C_1 \longrightarrow C_4H_8 \ldots.
\end{aligned}
$$

Parallel-type mechanisms:

$$
C_1 \left\{ \begin{array}{l} \rightarrow C_2H_4 \\ \rightarrow C_3H_6 \\ \rightarrow C_4H_8 \end{array} \right.
$$

Based on experiments with co-feeding ^{13}C-methanol, ethanol and water over a SAPO-34 catalyst, Dahl and Kolboe (1993) found that only a small part of the propylene formed was made from addition of methanol to ethanol. This favours the parallel-type mechanism and on this basis they proposed a modified parallel mechanism based on $(CH_2)_n$ known as the "Hydrocarbon pool mechanism" depicted in Figure 2-7.

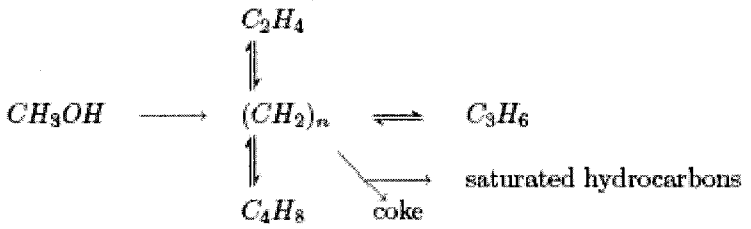

Figure 2-7: The hydrocarbon pool mechanism (Dahl and Kolboe, 1994)

Recent studies by Svelle et al. (2006) Bjørgen et al. (2004) and Haw et al. (2003) have suggested polymethylated benzenes play an important role in the in the formation of the light olefins. The polymethylated benzenes are formed in the cages of the catalyst and act as the reaction sites for the MTO process. It is believed that methanol reacts with polymethylated benzenes which then splits off olefins after rearrangements under formation of a lower order polymethylated benzene which then again can be methylated by methanol. A schematic drawing is given in Figure 2-8

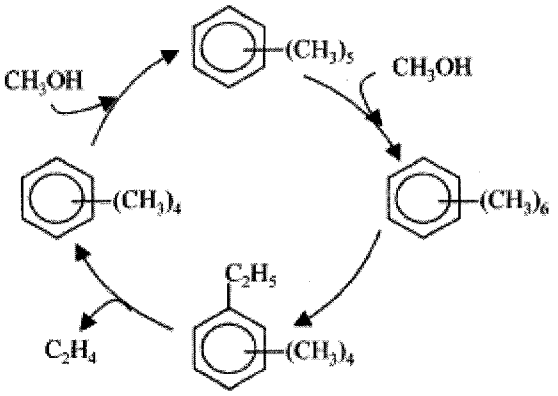

Figure 2-8: Ethylene formation by reaction of methanol withmethylbenzenes. (Aguayo et al., 2005)

2.4 Reaction conditions

The MTO reaction is highly dependent on the operation conditions and acidity of the zeolite. Several investigations of the MTO and the related MTG reactions have been done over the last thirty years in connection to the reaction conditions. The following section describes the effect of the main variables that influence the reaction and include: temperature, pressure, water co-feed, residence time and catalyst coking.

2.4.1 Temperature effect

The MTO reaction is very temperature dependent with respect to the product distribution. At low temperatures of about 300 – 400°C, a high level of aromatic and heavy hydrocarbons are formed that lie in the gasoline boiling range. This is the typical temperature range for the MTG reaction. For the MTO reaction, the typical operation temperature is 400 – 500°C. The selectivity of the olefins generally increases with temperature. Above 500°C, the formation of methane, CO and H_2 begins to increase significantly (Keil, 1999; Chang, 1984). Dewaele et al. (1999) studied the temperature effect on the product distribution of olefins over an H-ZSM-5 catalyst. They found that the ethylene to propylene ratio increases with temperature (from 0.05 at 375°C and up to 0.35 at 475 °C) while the ratio between the higher olefins (C_3-C_5) remains unchanged. Shoenfelder et al. (1994) conducted experiments in a riser reactor at 400, 450 and 500°C with a catalyst containing 25% H-ZSM-5. They found that ethylene production decreased with increasing temperature while propylene increased slightly. Further, the overall selectivity towards olefins was increased with temperature.

2.4.2 Pressure effect

Several authors have investigated the effect of pressure on the MTO reaction (Chang, 1984, Dewaele et al, 1999). By reducing the partial pressure of methanol, the reaction of olefins to higher hydrocarbons is slowed considerably. Figure 2-9 illustrates the effect of pressure observed during the studies in the late 70'ties at 370°C. The effect of pressure is significant and it is desirable to run the reaction at a low pressure to optimize the olefin production.

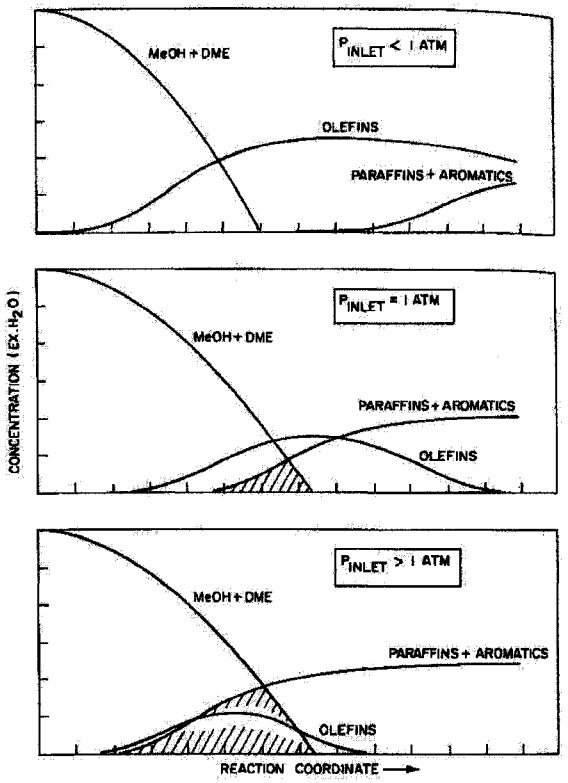

Figure 2-9: Product distribution of the MTO reactionat high, low and atmospheric pressure (Chang, 1984)

2.4.3 Catalyst deactivation

Deactivation of the ZSM-5 based catalyst is relatively slow compared to other catalysts like the SAPO-34, which is due to the ZSM-5 larger pore sizes. The deactivation of the catalyst can happen by three different mechanisms (Stöcker, 1999):

- Deposition of carbon residue both on the outer surface and inside the catalyst pores,
- Irreversible activity loss due to the effect of steam on the zeolite structure, and
- Structural changes due to high temperature during the regeneration of the catalyst.

The rate of carbon deposition on the catalyst depends on the acidity of the catalyst and the operating conditions (temperature, space velocity, feed composition).
A large part of the catalyst coking is due to the formation of higher hydrocarbons that are unable to escape the catalyst since they are larger than the catalyst pores. It was found that the acidity (Si/Al ratio) of the catalyst has a significant influence on the coking rate. By decreasing the Si/Al ratio, the production of higher hydrocarbons increases and thus increases the coking rate.

Irreversible activity loss occurs because of the dealumination of the catalyst caused by steam. The level of dealumination is affected by the water content during the reaction

together with the reaction temperature. As the water content and/or temperature increase, the dealumination becomes increasingly important (Gayubo et al., 2003).

The dealumination caused by the high temperature during regeneration can be avoided by regeneration of the catalyst below the calcination temperature (Gayubo et al., 2004a).

2.4.4 Effect of water

Water plays an important role in the MTO process: it reduces the deactivation rate due to coke deposition; it changes the product distribution, increasing the selectivity to light olefins; and, it increases the dealumination rate, which leads to irreversible deactivation of the catalyst. The importance of water has been investigated by several authors (Gayubo et al., 2004a; Aguayo et al., 2005; Wu and Anthony, 2001; Möller at al. 1999; Campbell et al., 1996).

Campbell et al. (1996) showed that dealumination of the ZSM-5 catalyst during the MTG reaction is caused by the high water vapour pressure. Möller at al. (1999) investigated the effect of co-feeding water in a jet loop reactor and found that water reduced the conversion of methanol probably because it reduces the number of active sites in the catalyst.

Wu and Anthony (2001) investigated the effect of co-feeding water with methanol at different water/methanol ratios at 400°C in a fixed bed reactor on SAPO-34. They found that increasing the mole fraction of water in the feed to 0.74-0.8 increased by eight times

the amount of methanol that the catalyst could process before methanol breakthrough was observed. Further, the selectivity to olefins was increased. The reason for the increased lifetime and higher olefin production is attributed to water occupying the strong acid sites in the catalyst thus preventing olefin oligomerization and coking on the sites.

The effect of water in the temperature interval 400-500°C on the deactivation was studied by Gayubo et al. (2004a). Pure methanol and methanol/water with a 1:1 mass ratio was fed to a fixed bed reactor and after 2h on stream, the catalyst was regenerated. After two reaction/ regeneration cycles, the acidity of the catalyst was measured by NH_3 TPD. They found that irreversible deactivation becomes important above 450°C when water is co-fed at a mass ratio of 1:1. Irreversible deactivation became evident with pure methanol feed above 500°C.

2.4.5 Gas residence time

Residence time influences the product distribution of the MTO process. At high gas residence time, the main products are higher hydrocarbons in the gasoline boiling range. As the residence time decreases, the product distribution changes favouring the production of light olefins (see Figure 2-1) (Chang, 1984). At very low residence time the main product is ethylene or propylene. Dessau (1986) conducted experiments on ZSM-5 with a very low aluminium content (Si/Al=1670). The experiments were done at reduced partial pressure of methanol with nitrogen as the diluent. Results showed that propylene was the main product and that ethylene was formed by secondary reactions.

Chu and Chang (1984) conducted experiments with a ZSM-5 catalyst with higher aluminium content. At 500°C and low methanol partial pressure, they found that the main product was ethylene. The residence time during these experiments were, however, higher than the ones used by Dessau (1986).

2.5 Kinetic

Kinetic models are important in the design of chemical reactors and thus a lot of work has been devoted to develop suitable models for the MTO/MTG reaction. The models can be divided into two categories:

- Lumped models that group similar components into one including oxygenates, olefins, heavy hydrocarbons and light gases.
- Detailed models that are based on elemental reactions where all species are accounted for.

The lumped model is more common since they are easier to use than the detailed models and are often accurate enough for most purposes. In the MTO/MTG process where the mechanisms for methanol conversion to hydrocarbons are not fully understood, a detailed model may be equally inaccurate as lumped models.

Several kinetics/reaction paths have been proposed for the MTO and MTG process since the late seventies when Chang and Silvestri (1977) proposed the first model (Equation 2-1). The methanol/DME equilibrium is reached very fast and, in the initial studies, the

two oxygenates are treated as a single kinetic species. Methanol and DME are then converted to light olefins and finally the olefins react to paraffins, higher olefins and aromatics.

$$2CH_3OH \underset{+H_2O}{\overset{-H_2O}{\rightleftharpoons}} CH_3OCH_3 \xrightarrow{-H_2O} C_2^{=} - C_5^{=} \longrightarrow \begin{array}{c} paraffins \\ aromatics \\ cycloparaffins \\ C_{6+}\ olefins \end{array} \tag{2-1}$$

Many models have been developed since Chang and Silvestri (1977) proposed their model. Keil (1999) gives a summary of the model development of both lumped and detailed models. Chen and Reagan (1979) found that oxygenates disappearance was autocatalytic over ZSM-5 and proposed the following reactions:

$$\begin{aligned} &A \xrightarrow{k_1} B \\ &A + B \xrightarrow{k_2} B \\ &B \xrightarrow{k_3} C \end{aligned} \tag{2-2}$$

Where A are oxygenates, B olefins and C aromatics and paraffins. Chang (1980) expanded the model to include $^{\cdot}CH_2$. It was based on the following conditions and constraints:

- Methanol and DME are always at equilibrium and can be treated as a single kinetic species.
- Generation of the reactive intermediate is first order in oxygenates.
- Consumption of the reactive intermediate is first order in oxygenates.
- Olefins can be treated as a single kinetic species.

- Disappearance of olefins is first order in olefins.

The conditions led to the following set of reactions:

$$\begin{aligned} &A \xrightarrow{k_1} B \\ &A + B \xrightarrow{k_2} C \\ &B + C \xrightarrow{k_3} C \\ &C \xrightarrow{k_4} D \end{aligned} \tag{2-3}$$

Where A is oxygenates, B ($^{\cdot}CH_2$) and C olefins and D aromatics and paraffins.

The kinetics first given by Chang (1980) has been modified by Anthony (1981) and is given in Equation 2-4 below.

$$\begin{aligned} \frac{-dA}{dt} &= k_1 A + k_2 AB \\ \frac{-dB}{dt} &= k_1 A - k_2 AB - k_3 C \\ \frac{-dC}{dt} &= k_2 AB - k_4 C \end{aligned} \tag{2-4}$$

Similar models have been proposed by Sedran et al. (1990), Schipper and Krambeck (1986) and Gayubo et al. (1996). Sedran et al. (1990) proposed three different models that take the light olefins into account as separate species. In one case the formation of the olefins is divided into three reactions in a consecutive type mechanism. Oxygenates react to ethylene and the higher olefins are formed by reaction between lighter olefins and oxygenates. The model of Schipper and Krambeck (1986) was used in the MTG process of Mobil. Here, methanol and DME are considered to be in equilibrium and react to form light olefins. The light olefins can polymerize to form heavy hydrocarbons and the heavy hydrocarbons can react with oxygenates and light olefins to produce additional heavy hydrocarbons. Gayubo et al. (1996) proposed two alternative models.

One is a modification of Chen's (1980) model (Equation 3) where the third step is substituted by $B+C_1$ (C_1= ethylene + propylene) $\rightarrow$ C_2 (higher olefins). In the second model, oxygenates are absorbed on the acid sites and an absorbed oxygenate reacts with a non-absorbed oxygenate to form the light olefin. Based on experiments in a fixed bed reactor at 300-375°C for different contact times, Gayubo et al. (1996) found that the fitting of the models of Chen and Reagan (1979) and Schipper and Krambeck (1986) was superior to the others.

Novella et al. (1988) modelled the process with methanol, DME and three lumps: gaseous olefins, liquid hydrocarbons and gaseous paraffins. DME reacts to olefins and olefins react to both liquid hydrocarbons and paraffins (two reactions). They considered the reaction to heavy hydrocarbons and paraffins to be both second order in olefins. They introduced a temperature dependent induction time on the reaction from olefins to heavy hydrocarbons and paraffins that represent the necessary space time for the formation of olefins from the dehydration of methanol and DME. The model shows good agreement to the experimental results in the 320-420°C temperature interval.

Schipper and Krambeck (1986) introduced a catalyst activity parameter β which accounted for both activity loss due to coking (a) and permanent deactivation (α).

$$\beta = \alpha \cdot a \tag{2-5}$$

The reaction rate, r_i, of the different lumps/components are then calculated as the product of the reaction rate with a fresh catalyst, r_{i0}, and the catalyst activity parameter given by Equation 2-5.

$$r_i = \beta \cdot r_{i0} \tag{2-6}$$

The permanent deactivation kinetic is:

$$\frac{d\alpha}{dt} = -K_\alpha \cdot \alpha^h \tag{2-7}$$

The activity loss due to coking of the catalyst is:

$$\frac{da}{dt} = -k_d (\alpha \cdot a)^d \tag{2-8}$$

The total deactivation, β, can then be found to be:

$$\frac{d\beta}{dt} = \alpha\left[-k_d(\alpha \cdot a)^d - K_\alpha \alpha^{h-2}(\alpha \cdot a)\right] \tag{2-9}$$

Benito et al. (1996) studied catalytic deactivation and found that a composition dependent deactivation kinetic expression was necessary to characterize of the MTG process. In their work, activity loss due to coking was calculated by:

$$\frac{-da}{dt} = \left[\sum (k_{di} X_i)\right] a^d \tag{2-10}$$

Where k_{di} is the kinetic constant for deactivation by coke deposition for lump i and a is defined as $a = \frac{r_i}{r_{i0}}$

Gayubo and co-workers presented a kinetic model for the MTG process with eight reactions involving six components/lumps including coke and water (Gayubo et al., 2001; Gayubo et al., 2004b). The effect of water was included in the reaction kinetic as a

term in the denominator in the kinetic equations of the form ($1+k_W X_W$). By including this term, agreement between the model prediction and experiments was improved with pure methanol feed as well as with feed consisting of methanol/water mixtures.

The recovered activity in the regeneration of the catalyst was also investigated and the following empirical equation was proposed:

$$a_0 = 1 - (1-a)\exp\left[-\left(b_1 t_c + b_2 t_c^2\right)\right] \tag{2-11}$$

Where a_0 is the initial activity after the regeneration, t_c is the combustion time during regeneration. The parameters a, b_1 and b_2 were found to be:

$$a - 5.00(\pm 1.43)\cdot 10^{-3}$$
$$b_1 = 1.38(\pm 0.11)\cdot 10^{-1}$$
$$b_2 = 6.13(\pm 0.50)\cdot 10^{-4}$$

Gayubo et al. (2003) included the activity loss by coke deposition and irreversible deactivation for the MTO process, the reaction kinetics were based on their previous work mentioned above. The activity was defined similar to Equation 2-5. Several models for the irreversible deactivation were studied. The most suitable model was given by:

$$-\frac{d\alpha}{dt} = k_{dir} X_W^2 \alpha \tag{2-12}$$

The model was experimentally verified in three successive reaction-regeneration cycles with feed consisting of 50% MeOH and 50% water. Results form the simulation is shown in Figure 2-10.

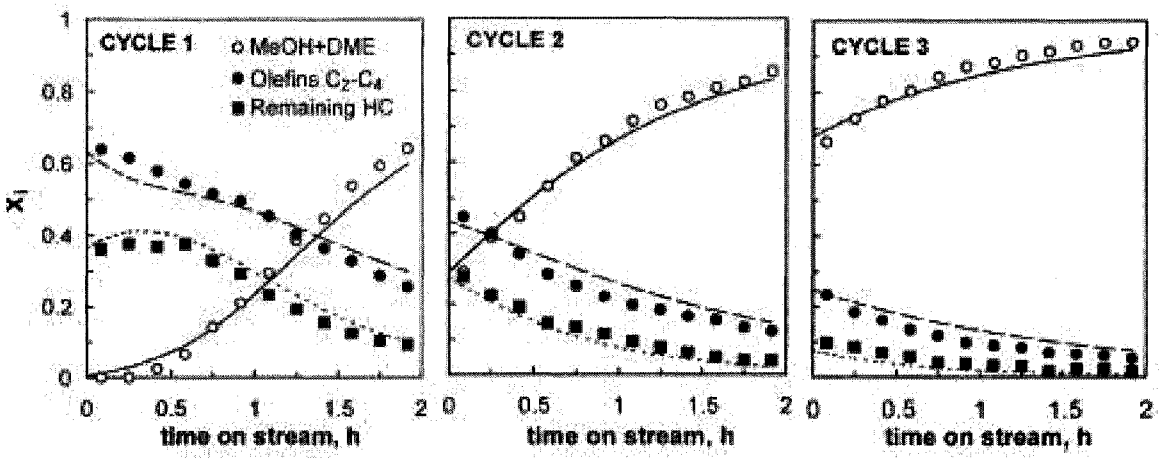

Figure 2-10: Evolution with time on stream of the composition of the lumps of the kinetic scheme, in three successive reaction–regeneration cycles in fixed bed. Reaction conditions: temperature, 773 K, space time, 0.093 (kg of catalyst) h (kg of methanol)$^{-1}$; water content in the feed, 50 wt%. Points: experimental results. Solid lines: calculated (Gayubo et al., 2003)

Most models describe the trends in the MTG/MTO process but fail to characterize the individual olefin components, which are important in the MTO process. Schoenfelder et al. (1994) developed a lump model given in Figure 2-11 for the MTO process. The catalyst used was based on a ZSM-5 zeolite. Based on experiments run in a Berty reactor at temperatures between 400 - 500°C, the kinetic constants were found at 5 different temperatures. The parameters found were in agreement with the Arrhenius law. The model was used in conjunction with a one-dimensional circulating fluidized bed model in the calculations of the MTO process in. The model was able to predict the product distribution fairly well on fresh catalyst but is unable to characterize the effect of time on stream since coke deposition on the catalyst was not included.

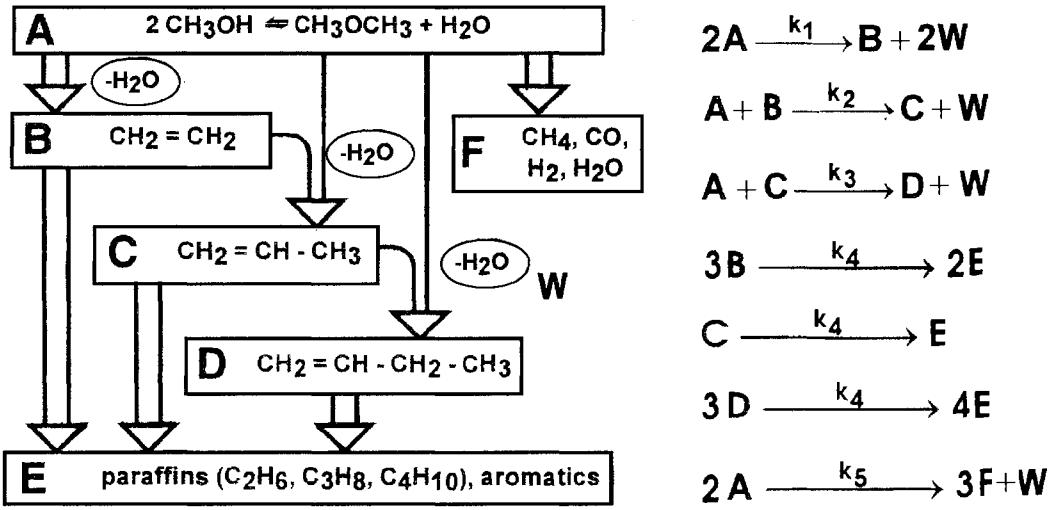

Figure 2-11: Scheme and kinetic model for the MTO-reaction by Schoenfelder et al. (1994)

Bos et al. (1995) proposed a kinetic model for a SAPO-34 based catalyst. The model was developed on fixed bed experiments conducted over a very short time span to avoid coking. To include the coking effect the experiments were done on samples containing 3.7, 8.9 and 12.3 wt % coke. The reaction scheme developed is given in Figure 2-12. From experimental data with butylenes as feed gas and model predictions, it was concluded that the reaction from ethane to coke should be excluded form the reaction scheme (k_{13}=0). The final model consisted of 6 components lumps plus coke described by 12 reactions. The final model is given in equations 2-13 – 2-16.

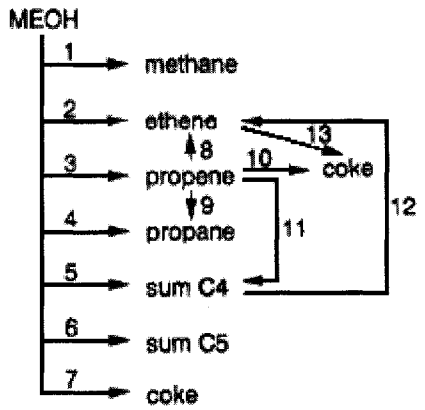

Figure 2-12: Reaction scheme for the MTO reaction by Bos et al. (1995)

$$r_i = k_i x_{MeOH} P \quad i = 1-7 \tag{2-13}$$

$$r_8 = k_8 x_{C3=} P x_{MeOH} P \tag{2-14}$$

$$r_i = k_i x_{C3=} P \quad i = 9-11 \tag{2-15}$$

Four different correlations were investigated for the coke dependency of the reaction. They found that an exponential dependency (Eq. 2-16) best represented the coking effect.

$$k_i(c) = k_i^0 e^{-a_i c} \tag{2-16}$$

where a_i is an empirical deactivation constant and c is weight percentage of coke.

Detailed kinetic models have been proposed that describe the production of each component in the process (Park and Froment, 2001a; Park and Froment, 2001b; Mihail et al., 1983a; Michail et al., 1983b). Mihail et al. (1983a) developed their model using the following approach:

- Stoichiometric matrix of all the components found in the experimental results
- Choice of a set of linear independent reactions
- Reactions are deleted or supplemented in accordance to data in the literature
- Kinetic parameters are fitted to experimental data

In the stoichiometric matrix, they included 16 components (up to C_5) with the rank of 3 (C, H, O), from that 13 independent reactions were chosen. By deleting and supplemented these reactions, the final model comprised of 27 reactions. Mihail et al. (1983b) expanded the model to higher hydrocarbons (olefins and paraffins up to C_7 and methylated benzene up to C_{12}) which resulted in a reaction network with 53 reactions.

Maria and Muntean (1987) simplified the olefin model of Mihail et al. (1983a). With the use of numerical methods and experimental data, the reaction model was reduced by eliminating reactions with limited impact on the final result. This reduced of the kinetic model to only include 14 reactions.

Park and Froment (2001a) developed a detailed kinetic model based on elementary steps for the MTO process over an H-ZSM-5 catalyst. The elementary steps to describe the formation of the primary olefins production included 8 different mechanisms due to the large number of possible reactions for the formation of the first C-C bond. The total number of parameters in the reaction network amounted to 500. The number of parameters was reduced with the use of the single-event concept and the Evans-Polanyi

relation and thermodynamic constraints. This reduced the number of parameters to 33. The parameters were obtained by optimizing the model to experimental data with the use of sequential quadratic programming and the Levenberg-Marquardt routine. Through this, the best mechanism for the primary product formation was found to be between oxonium methyl ylide and dimethyloxonium ion (Park and Froment, 2001b).

2.6 Processes

The MTO reaction has mainly been investigated in fixed beds (Chu and Chang, 1984; Park and Froment; 2001b; Gayubo et al., 2003; Stöcker, 1999) but due to the high exothermicity of the reaction and coking rate of the ZSM-5 and SAPO catalysts, a fixed bed may be less suited compared to a fluid bed. In the case of fast deactivation for an industrial process, the regeneration should take place in the same reactor with successive reaction-regeneration cycles or circulation of the catalyst between a reaction and a regeneration reactor (Gayubo et al, 2000). The exothermic reaction can be a problem in a fixed bed which will operate under non isothermal conditions resulting in hot spots. Several researchers have reduced this problem in fixed bed by using a dehydration reactor before the MTO reactor hence reducing both the energy production and coking in the MTO reactor (Sapre, 1997; Tabak and Yurchak, 1990).

A fluidized bed or circulating fluid bed (CFB) will be a more obvious choice due to the advantages it offers with respect to high heat transfer between gas and solid combined with rapid solid mixing, insuring isothermal conditions. Furthermore, a CFB offers

continually regeneration of the catalyst while avoiding the need for several reactors in series.

Tabak and Yurchak, (1990) give the product distribution of fluid bed experiments performed by Exxon-Mobil in their pilot plant. The operation conditions were 482°C with partial pressure of methanol of 100 kPa in the feed and the reaction was run to almost complete methanol conversion. A breakdown of the product distribution in their experiments is shown in Table 2-1. They consider the fluid bed reactor to be the best suited for the MTO reaction since it allows for steady-state operation at maximum olefin production at complete methanol conversion and makes it easy to remove the reaction heat with the use of heating coils in the bed.

Table 2-1: Product distribution of the MTO reaction in fluid bed at 482°C and 102 kPa methanol partial pressure (Tabak and Yurchak, 1990)

Product	C_1	C_2	C_3	C_4	$C_{2=}$	$C_{3=}$	$C_{4=}$	C_5-C_{11}	oxygenates
Wt % hydrocarbons	1.4	0.3	2.3	3.9	5.0	31.8	19.6	35.7	0.3

Ortega et al. (1998) have studied the lumped product distribution (oxygenates, light olefins and other hydrocarbons) over a HZSM-5 containing catalyst. The properties of the catalyst are given in Table 2-2. The experiments were performed in a 30 mm internal diameter fluid bed with solid circulation.

Table 2-2: Properties of the H-ZSM-5 and the catalyst used in the experiments of Ortega et al. (1998)

	HZSM-5 zeolite	catalyst[a]
Si/Al ratio	24	
Bronsted/Lewis ratio	2.9	
crystallinity	97%	
crystal size, μm	6.3	
particle size, mm		0.3–0.5
apparent density, $g \cdot cm^{-3}$	0.94	1.21
BET surface area, $m^2 \cdot g^{-1}$	420	124
pore volume, $cm^3 \cdot g^{-1}$	0.65	0.43
micropore volume, $cm^3 \cdot g^{-1}$ (99% of diameter < 0.7 nm)	0.17	
pore volume distribution of the catalyst, vol %		
$d_p < 10^{-3}\ \mu m$	8.1	
10^{-3} to $10^{-2}\ \mu m$	14.7	
10^{-2} to 2 μm	77.2	
zeolite acidity measurements	**NH_3**	***tert*-butylamine**
total acidity, (mmol of base)$\cdot g^{-1}$	0.51	0.46
temperature peaks in the TPD	422 °C	304 °C

[a] Composition: zeolite, 25 wt %; bentonite, 30 wt %; alumina, 45 wt %.

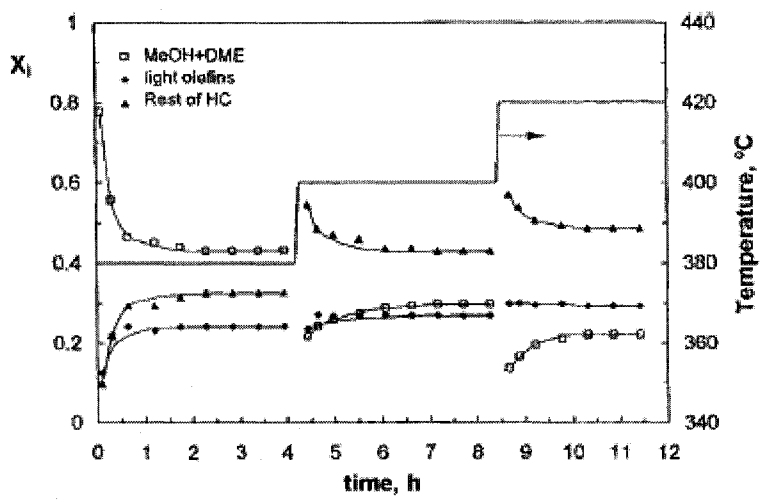

Figure 2-13: Evolution of the mass fractions of each lump, until steady state is reached at three different temperatures, space time 0.040 $g_{cat}h/g_{MeOH}$ and average solid residence time $0.866h^{-1}$ (Ortega et al., 1998)

The reaction was carried out between 380 and 420°C at space times between 0.022 to 0.0040 $g_{cat}h/g_{MeOH}$. The product distribution as a function of time is shown in Figure

2-13. The authors attribute the initial approach to steady state to increasing catalyst mass in the fluid bed while the approach to equilibrium when the temperature is increased is due to increased catalyst deactivation.

Gayubo et al. (2000) continued the investigation of the effect of residence time on reaction and regeneration operations on the process together with the space time and temperature. The regeneration was conducted at 550°C. By optimizing the light olefin production based on catalyst residence time, it was found that the time on stream during the reaction and regeneration is dependent on each other. Figure 2-14 shows a contour plot of the results. The production rate is highest when the residence time in the reactor is about 3 times longer than in the regenerator. Experiments conducted with increasing methanol flow rate at temperatures between 380 and 420°C showed that the light olefin production was substantially increased with decreased residence time and that the effect of temperature was highest at low residence times.

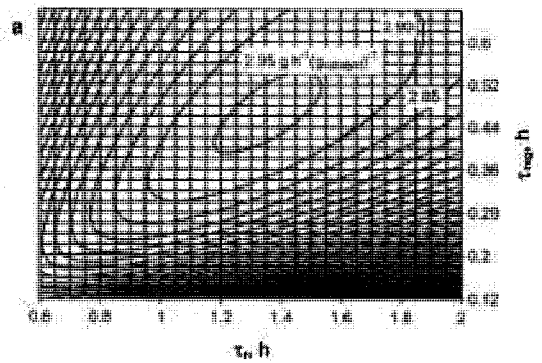

Figure 2-14: Contours of the relative production rate of light olefins for different residence times in the reactor and regenerator. Temperature 420°C space time 0.021 $g_{cat}h/g_{MeOH}$ (Gayubo et al. 2000)

Schoenfelder et al. (1994) investigated the MTO reaction in a CFB consisting of a riser made of six tube sections with an inner diameter of 30 mm and a height of 11m, a

stripper and a regenerator. They used catalyst consisting of 25% H-ZSM-5 with a Si/Al ratio of 400 the mean Sauter diameter of the fluid bed catalyst was 100μm. To derive the kinetics, experiments were conducted in a Berty reactor system. The riser was modelled using four zones; bottom zone described by a bubble phase and a suspension phase, a splash zone modelled as a CSTR, a recirculation zone described by a lean phase and a dense phase and an exit zone modelled as a CSTR. Experiments in the CFB were conducted at 400, 450 and 500°C and at different space velocities. The product distribution obtained consisted mainly of olefins and at 500°C the olefin yield reached 97% and went through a maximum propylene production. Figure 2-15 compares the product distribution of the experiments at 500°C against the predicted yield from their model. The model predicts the overall behaviour of the system but some deviations are evident especially at low $WHSV^{-1}$ and it does not catch the maximum in propylene yield seen from the experimental results.

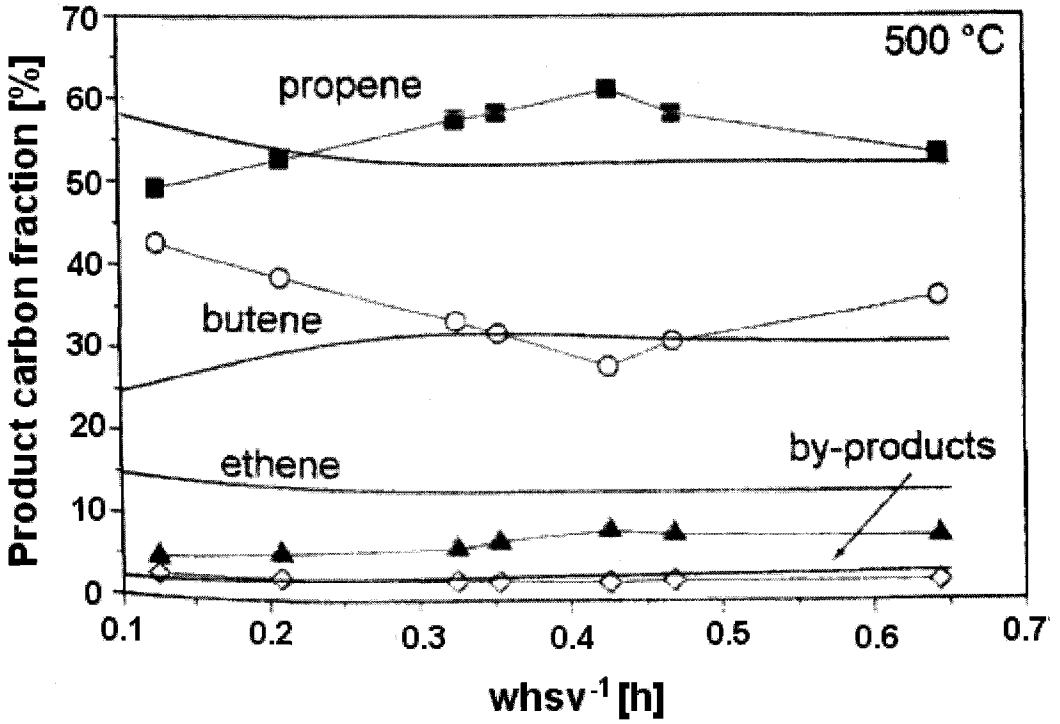

Figure 2-15: Comparison between measured (symbols) and predicted (lines) product distribution of the CFB reactor at a temperature of 500°C (Schoenfelder et al, 1994)

2.6.1 Industrial Processes

There are currently three companies that offer/have the technology for large scale production of methanol to olefin (MTO). They include UOP/Hydro, Lurgi and Exxon-Mobil. The strategy of the three companies are quite different: Lurgi offers fixed bed technology using a ZSM-5 zeolite in there catalyst; UOP/Hydro offers a fluid bed/riser process where the catalyst is continuously regenerated, the zeolite used is SAPO-34; and, Exxon-Mobil has many patents on MTO processes, they are concentrated around high velocity riser reactors with catalyst regeneration in a fluid bed, like UOP/Hydro, they also use the SAPO-34 zeolite catalyst. Further description of the processes is given below.

2.6.1.1 Lurgi Process

For several years Lurgi and Statoil have run a demonstration unit in Norway. This has led to the first contract on an industrial scale MTP unit that is to be built in Iran for the Fanavaran Petrochemical Company. The plant will have an annual capacity of 100,000 MT of propylene (Lurgi, 2005).

The Lurgi MTP process relies on fixed beds where methanol is first partially converted to DME. From the pre-converter a split stream is sent to the first fixed bed reactor of three which is run in series. The remaining feed from the pre-converter is sent to the second and third reactor. After purification and separation, the unwanted olefins are re-circulated to the first reactor together with some water. A schematic diagram of the process is given in Figure 2-16. The final product consists of approximately 70% propylene, 20% gasoline and some LPG and fuel gas. The process is based on a ZSM-5 zeolite from Süd-chemie and the process is operated at slightly elevated pressure (about 0.3 - 0.6 barg) and in a temperature range of 420 - 490°C (Ondrey, 2005). Due to coking, the fixed bed reactors have to be regenerated and one extra reactor is needed for continuous production.

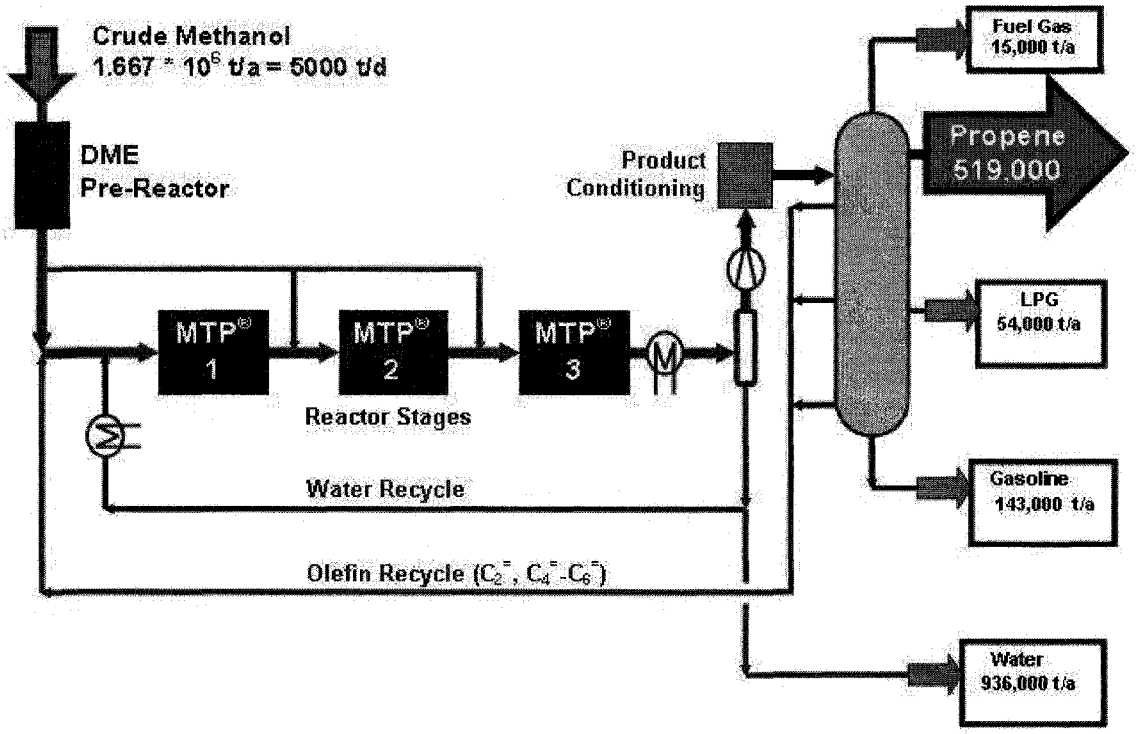

Figure 2-16: Flow diagram of Lurgi MTP® Process (Stöcker 2003)

2.6.1.2 UOP/Hydro Process

UOP and Norsk Hydro have put over 10 years of development into the MTO process and have been operating a 1 ton methanol a day demo unit in Norway since 1995. The technology is based on fluid bed technology with continuous catalyst regeneration in a separate fluid bed. A schematic drawing of the process is given in Figure 2-17. The catalyst is based on a SAPO-34 catalyst designated MTO-100, with a pore size of 3.8Å. The operating temperature is 350-550°C and the operating pressure is 1-3 barg. The olefin yield is around 80% where about 10% is butylenes. The ethylene to propylene ratio can be varied from 0.75 to 1.5 depending on process conditions, with the highest total olefin yield at a ratio of 1. Based on the demonstration unit, catalyst tests and

process calculations, the process can be scaled up to 1000 kt olefin a year (Houdek and Andersen 2005;Andersen, 2003).

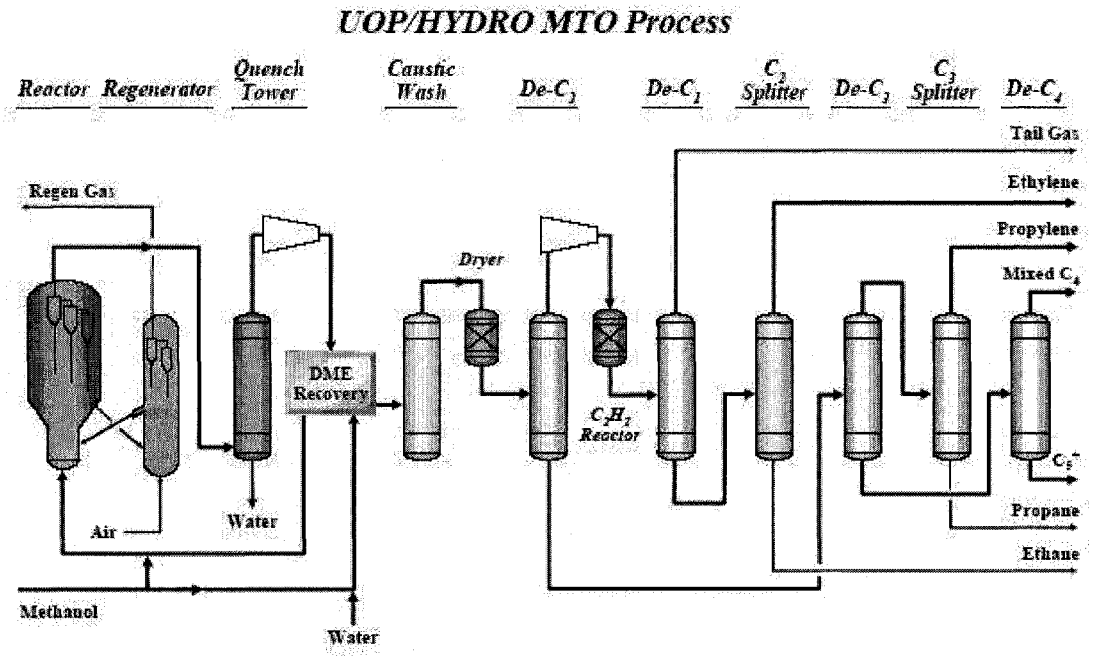

Figure 2-17: Simplified flow diagram of the UOP/Hydro MTO Process (Houdek and Andersen 2005)

2.6.1.3 Mobil Process

Exxon-Mobil has a long history in MTO and has completed a lot of research in the field over the last three decades. They have run a 4000 t/year fluid-bed demonstration plant at Wesseling (Germany), which had previously been used to demonstrate their methanol to gasoline (MTG) process (Stöcker, 1999).

In recent years, Exxon-Mobil has concentrated on process design and optimization, which is reflected in the patent literature where several different processes for the MTO reaction have been patented with the use of both ZSM-5 and SAPO based catalysts (Chisholm et al. 2003, Beech et al. 2004, Coute et al. 2004, Lattner et al. 2005).

Chisholm et al. (2003) patented a process where the MTO reaction is carried out in a riser reactor; the gas/solid mixture from the riser is then separated in a fluid bed with internal cyclones by means of gravity and the cyclones. Part of the catalyst is re-circulated to the riser while another part is sent to a stripping zone where the absorbed hydrocarbons are stripped with an inert gas. The stripped catalyst is then sent to a fluid bed where it is regenerated and then re-circulated to the riser. The space velocity in the riser is preferably above 4 m/s and the WHSV in the range of 20 h^{-1} to 500 h^{-1}. The partial pressure of the feed is preferably between 0.2 to 5 bars and the temperature between 350°C and 550°C and a feed stock conversion of 75-95%.

The reason to recycle some of the catalyst without regenerating it is because the coke loading should be 1-2 carbon atoms pr. acid site for optimal operation. The catalyst should be regenerated at 550 - 700°C and at a pressure between 2.07 and 4.14 bars. The oxygen containing stream consists of 0.01 to 5% of oxygen and the residence time is most preferably between one and 100 minutes.

Beech et al. (2004) have patented four different riser reactor configurations with external regeneration. They all include a feed inlet at the bottom of the riser and exit through the top which is inside a vessel. The separation of the gas and solids are done by both gravity and cyclones. In one case the riser reactors are located near the side of the separation vessel while in the other cases the riser reactors are centred in the vessel. A part of the catalyst is sent to regeneration in a fluid bed and then reintroduced into the vessel. The remaining catalyst is led to the bottom of the riser reactors. To control the catalyst flow, solid flow regulators are used.

Chapter 3
Objective and methodology

As described in the literature study, a significant amount of research has been conducted on the MTO process. In general, the light hydrocarbons have been lumped together both experimentally and in the kinetic analyses, which limit the utility of this research with respect to optimizing the olefin product mix (that is, ethylene versus propylene or butylene). A model capable of predicting the light olefin yield is crucial for both the design of down-stream product separation but also for the product value. Some models include the light olefins as separate species, like the model of Schoenfelder et al. (1994), but don't take the higher olefins produced in the ZMS-5 zeolite into account. The model proposed by Bos et al. (1995) includes deactivation from coking but it only considers ethylene and propylene as the light olefins since it is based on the SAPO-34 zeolite. For the ZSM-5 zeolite, the catalyst system used in this study, propylene and butylenes are the main products.

Kinetic studies in fluidized bed systems represent significant experimental and modelling challenges. Although the bed temperature is uniform and the solids are completely backmixed, the gas phase hydrodynamics are complex: bubbles form at the grid and rise through a gas-solid emulsion at elevated velocities. The challenge will be to establish experimental conditions that minimize these phenomena.

3.1 Objective

The objectives of this thesis can be formulated as:

- Investigate the mechanism of the MTO process in order to,

- Develop a kinetic model for the methanol to propylene process in a fluid bed with respect to conditions such as temperature, space velocity and feed composition. The model must include the main olefins: ethylene, propylene and C_4 as separate components.

- Determine the kinetic parameters of the proposed reaction kinetic for the MTO reaction

To reach the objectives the following tasks have been preformed

Kinetic study of the methanol to DME reaction in fluid bed

The kinetic of the methanol to DME reaction was studied in the fluid bed. The reaction kinetics over a ZSM-5 based catalyst were studied in the temperature range of 250 – 325°C where and at a wide range of WHSV and feed compositions. A kinetic model was derived and this model was coupled together with hydrodynamic models to characterize the fluidized bed.

Catalyst investigation in fixed bed
The catalyst will be studied in fixed bed to evaluate the effect of residence time, temperature and feed composition on the product distribution and deactivation. Special focus was put on the effect of space velocity on the deactivation rate of the catalyst.

Kinetic study of the MTO reaction in fluidized beds
Kinetic experiments were conducted in a fluidized bed to investigate the effect on temperature, WHSV and feed composition. 1-hexene was feed to the reactor to examine the reaction network. The goal was to gain a better understanding of the reaction pathways and with this understanding develop a kinetic model for the MTO reaction which takes into account the main olefins, ethylene, propylene and C_4 as separate components.

3.2 Methodology

3.2.1 Catalyst

The catalytic system used in this work was based on a ZSM-5 from Zeolyst designated CBV 28014 with a Si/Al ratio of 140. The ZSM-5 zeolite was imbedded in a silica/alumina matrix during spray drying and impregnated with 1.5 wt % phosphorous to reduce methane formation. A description of the catalyst is given in Appendix A.

3.2.2 Fixed bed experiments

The experiments were conducted in a 9 mm inner diameter quartz reactor into which a 3 or 6 mm inner diameter quartz reactor could be inserted. The vessel was heated electrically and the temperature was regulated with a PID controller. The reference

temperature was measured at the wall and a second thermocouple monitored the temperature just below the catalyst bed. The feed stream was prepared by passing nitrogen through two bubble flasks containing MeOH: the first was at room temperature (approx. 22°C) and the second at 16°C to ensure that nitrogen was saturated by methanol yielding 10% methanol in the feed. The product stream was analyzed by FID on a Hewlett Packard 5890 series-II GC. Equipped with a pre-column (Porapak Q 80/100 mesh size – 0.5 m x 2.16 mm ID x 1/8" OD packed column in stainless steel) followed by a capillary column: CP-PoraPLOT Al2O3, KCl – 10 m x 530 μm x 5 μm. For some of the experiments a GC with a TCD measured the CO/CO_2 and other light gases.

3.2.3 Fluid bed experiments

Methanol to DME

Methanol to DME experiments were preformed in a 4.6 cm inner diameter glass fluidized bed a description of the system is given in Chapter 4.2.3. Other fluidized bed reactors have also been used, mainly for the MTO reaction, but methanol decomposition in the distributor was found to be significant. Further description of the other fluidized bed reactors are given in Appendix B. The feed stream consists of 5, 15, 30 and 33 mol% methanol and in argon which was preheated before it enter the fluid bed. The superficial gas velocity in the fluid bed was between 0.5 and 8.0 cm/s. The velocity was kept low to ensure that catalyst stays in the fluid bed and to avoid changing the hydrodynamic significantly. To have a higher span of WHSV's the catalyst inventory was varied between 25 and 200g. Due to poor heating just above the distributor plate in the fluid bed the catalyst was elevated into the heating zone. Glass beads with a

minimum fluidisation velocity above the maximum gas velocity were used to elevate the catalyst into the heating zone.

Product distribution was monitored online on a MS with reference measurements by GC to help calibrate and determine uncertainties on the MS measurements. Using a MS has several advantages including fast response to changes in product distribution and determination of by products.

MTO experiments

To establish when deactivation begins to influence the product distribution during operation long term experiments (one day) have been conducted in order to be able to design experiments where deactivation do not influence the results. The effect of regeneration was investigated and the coke content of the catalyst was measured in a thermal gravimetric analyser (TGA)

To gain insight into the kinetics of the MTO reaction, experiments at different flow rates (1.3 – 10 cm/s) and temperatures (400 – 550°C) were conducted and the catalyst bed height was varied to obtain a larger range of residence times. The effect of water and dilution with argon were investigated by using different feed compositions: pure methanol, methanol/water and methanol/argon mixtures. 1-Hexene was also used both as feed and co-feed with methanol to gain insight into the reaction mechanism. By only feeding 1-hexene the reaction pattern of the larger olefin can be investigated which will be important in the development of a kinetic for the MTO reaction.

The product distribution was analysed by GC and trends in the reaction monitored on MS.

3.2.4 Kinetic model

Based on the fluid bed experiments and literature knowledge a kinetic model for the reaction is proposed. The model is based on the hydrocarbon pool mechanism with a high molecular weight molecule, C_x^+ as the hydrocarbon pool species. The model is implemented together with a fluid bed model with a bubble and emulsion phase where all catalyst is considered to be in the emulsion phase.

Chapter 4
MeOH to DME in Bubbling Fluid Bed: Experimental and Modelling*

4.1 Presentation of the article

The article looks at the modelling of a bubbling fluidized bed with a relatively well known reaction methanol to DME over a ZSM-5 containing catalyst. Experimental data for the methanol to DME reaction is obtained in a small fluid bed reactor (4.6 cm ID) at 250°C - 325°C with different feed mixtures of methanol and argon. The data is analysed with the use of MS and GC. A reaction kinetic model is proposed for the methanol dehydration reaction and its performance is compared to the literature model of Berĉiĉ and Levec (1992). The fluidized bed is modelled with both a detailed fluid bed model and a CSTR in series model. Coupling the proposed reaction kinetic with the CSTR in series model gives a superior performance in the prediction the conversion in the fluidized bed.

The fluid bed is shown to be a viable reactor type for kinetic measurements of the exothermic dehydration reaction.

*This article was submitted to Canadian Journal of Chemical Engineering

4.2 MeOH to DME in Bubbling Fluidized Bed: Experimental and Modelling

Mads Kaarsholm*, Finn Joensen†, Roberta Cenni†, Jamal Chaouki, Gregory S. Patience

Department of chemical engineering, École Polytechnique de Montréal, Canada

†Haldor Topsøe A/S, Denmark

4.2.1 Abstract

Methanol dehydration over a ZSM-5 containing catalyst in a fluidized bed reactor at 250 – 325°C gave conversion of 30 – 100% to the equilibrium. Side reactions were negligible at low temperatures while hydrocarbon formation was more significant at 325°C. Online gas analysis by MS provided real time measurements that allowed for fast determination of steady state conditions.

Residence time distribution (RTD) measurements of the flow pattern are performed and are shown to mimic plug flow at low catalyst amount with increases dispersion as catalyst is added. At the highest catalyst loading the RTD measurements can be modelled by a n-CSTR in series model with 6 CSTR's. Both a detailed fluid bed model and the CSTR in series model have been used to characterise the hydrodynamics. Dehydration reaction kinetics are proposed that include the reverse reaction and is compared to a literature model. Coupling n-CSTR model with the proposed kinetics

* Corresponding auther. Tel: + 45 45 27 22 55
E-mail address: mkaa@topsoe.dk

gives a superior fit and good predictions at other reaction conditions. The fluid bed is shown to be a viable reactor type for kinetic measurements of the exothermic reaction and other exothermic reactions where hotspots or temperature gradients are a concern in fixed bed could benefit from fluid bed kinetic measurements.

Keywords: Methanol dehydration, DME, Fluidized bed, n-CSTR in series, Reaction kinetics

4.2.2 Introduction

The dehydration of methanol over an acidic catalyst is an important reaction for the production of dimethyl ether (DME). DME is considered as one of the best alternatives to diesel fuel with decreased NO_x, CO and hydrocarbon emissions with both lower particle emissions and global warming potential than conventional fuels (Semelsberger et al., 2006; Gray and Webster, 2001). The reaction is also important as the first step to produce olefins (MTO) or gasoline (MTG) (Keil, 1999).

Several authors have investigated the dehydration reaction over different catalysts e.g. alumina, silica-alumina or acidic iron exchange resins. Most kinetic expressions are based on either the Langmuir-Hinshelwood or the Eley-Rideal mechanisms and takes the adsorption of water and methanol into account but leaves out the contribution of DME since the absorption constant is insignificant compared to the others. A summary of models can be found in Berĉiĉ and Levec, 1992 and Mollavali et al., 2008 who both studied the intrinsic reaction kinetics. Almost all of the kinetic expressions assume irreversible reaction and only a few incorporate the reversible reaction to account for the

decrease in reaction rate close to equilibrium which is critical for most industrial applications.

Often reaction rate kinetics is measured in reactors under differential conditions. The main advantage of the fixed bed is that the flow pattern can be assumed to be ideal-plug flow and a simple well described reactor model can therefore be used to model the reaction together with the reaction kinetics. Fixed beds do have some limitations that must be considered. In reactions where deactivation is important the catalyst deactivation is likely to progress down the bed resulting in a non uniform activity down the bed (Kaarsholm et al., 2007). For highly exothermal reactions temperature gradients and/or hot spots are problematic and the exact reaction temperature can be difficult to measure precisely. For intrinsic measurements the catalyst particles have to be small to avoid transport gradients but this leads to higher pressure drop over the bed. Fluidized bed reactors have the advantage of isothermal operation due to rapid heat transfer by solid circulations, limiting temperature uncertainties considerable compared to fixed bed. Due to the solids back-mixing the catalyst have a uniform state e.g. the deactivation of the catalyst is uniform as is the temperature. The greatest drawback of the fluidized bed is the gas flow which is less than ideal due to the presence of bubbles. The effect of bubbles has been investigated for several decades and a large number of mathematical models have been proposed to model the hydrodynamic of the fluidized bed (Kunii and Levenspiel, 1991).

Over the years many models for the bubbling fluidized bed have been proposed including single phase models with axial dispersion which have been shown to work

well at low gas velocities (Lorences et al. 2006) and multiphase models. Horio and Wen (1977) divides multiphase models into three groups: level 1 is described as two phase models with several adjustable parameters that are not directly related to the bubble side this include the Van Deemter model (Van Deemter, 1961) and the model of May (1959). Level 2 models relate the bed parameters to the bubble size that is treated as a constant or a fitted parameter. A model that is included in this group is the model of Kunii and Levenspiel (1968) where the bubble diameter is measured by frequency probes. The third level of the bubbling models include the bubble diameter as a function of height and may also include grid region and freeboard effects. Many of the models proposed in the recent years are included in this level and include the models of Werther and Hartge, (2004), Christensen et al. (2008) and Radmanesh et al (2006). Hetsroni (1982) shows that two phase systems with plug flow in the bubble phase and either plug flow or a well mixed reactor model for the emulsion with mass transfer between the phases can give reasonable predictions of fluidized bed reactor performance.

The mass transfer between the bubble and emulsion phases is a key parameter for the fluid bed reactor models with regard to both overall reactor effectiveness and in reactor scale-up. Two different models for the interphase mass transfer coefficient between the bubble and emulsion phase are usually used either it is calculated by a correlation of Sit and Grace (1981) or the interphase mass transfer between the bubble and wake and between wake and bubble is calculated separately to get the overall interphase mass transfer (Kunii and Levenspiel, 1991). Sit and Grace (1981) developed a correlation for the interphase mass transfer coefficient between the bubble and emulsion phase based on

studies of bubble interaction and coalescing in a 2D experimental setup which was then extended to three dimensions.

Shaikh and Batran (2007) have further expanded the mass transfer term by including film resistance on the bubble side alongside the mass transfer coefficient between the emulsion and bubble phase. They conclude that this term is important when the reactant is in a mixture or for fast reactions.

In this article, the methanol to DME reaction in a gas-solid bubbling bed will be investigated at a range of gas velocities and bed heights. The reaction was studied in a fluid bed reactor for several reasons. The catalyst used is a fluid bed catalyst and to avoid a high pressure drop over a fixed bed the catalyst have to be pelletized and crushed to increase the particle size which could change the surface properties of the catalyst. Hot spots or a reaction front with a resulting temperature gradient down the fixed bed is also a concern due to the exothermic reaction. These problems are avoided in a fluid bed and thus better controls of the experiments are possible. Low gas flows are used in the fluidized bed to operate as close to ideal gas flow as possible and RTD measurements are conducted to characterise the flow. The kinetics of the reaction are investigated and both a two phase fluid bed model and an n-CSTR's in series model is used. The goal is to look at the feasibility of doing the kinetic study in a fluid bed.

4.2.3 Experimental

4.2.3.1 Equipment

The experiments were carried out in a 46 mm inner diameter quartz fluid bed (Figure 4-1) with a 66 mm inner diameter disengagement zone.

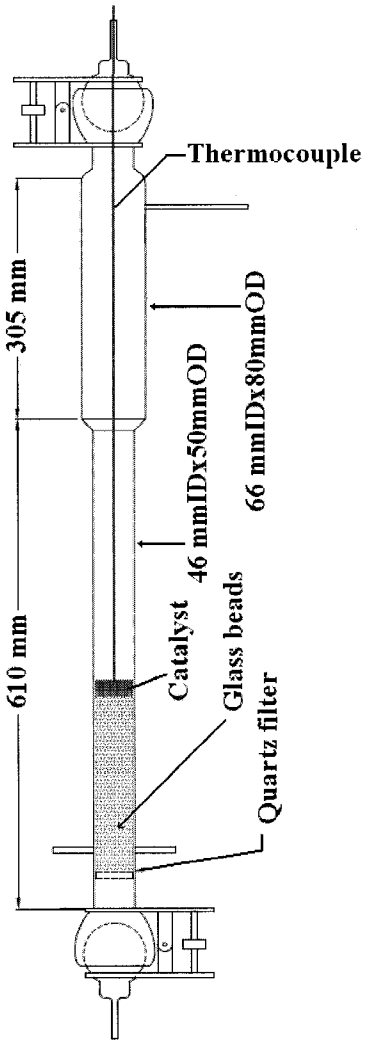

Figure 4-1: Drawing of the glass fluidized bed with glass beads, catalyst and thermocouple

The gas is distributed through a quartz frit. The reactor temperature is maintained by two electrical band heaters, one located in the fluidized bed zone and one in the disengagement zone. A thermocouple is inserted in the middle of the reaction zone and

the band heaters are controlled by temperature measurements on the outside wall of the reactor. Liquid methanol is fed from a dual piston pump and the gas is metered by one of two gas inlet lines both controlled by a Brooks mass flow controller (MFC). The inlet stream is preheated to 150°C to ensure liquid feed is entirely vaporized. The effluent gas was analysed by a Hiden mass spectrometer QIC-20 (MS) and a Varian CP3800 GC. A diagram of the system is shown in Figure 4-2

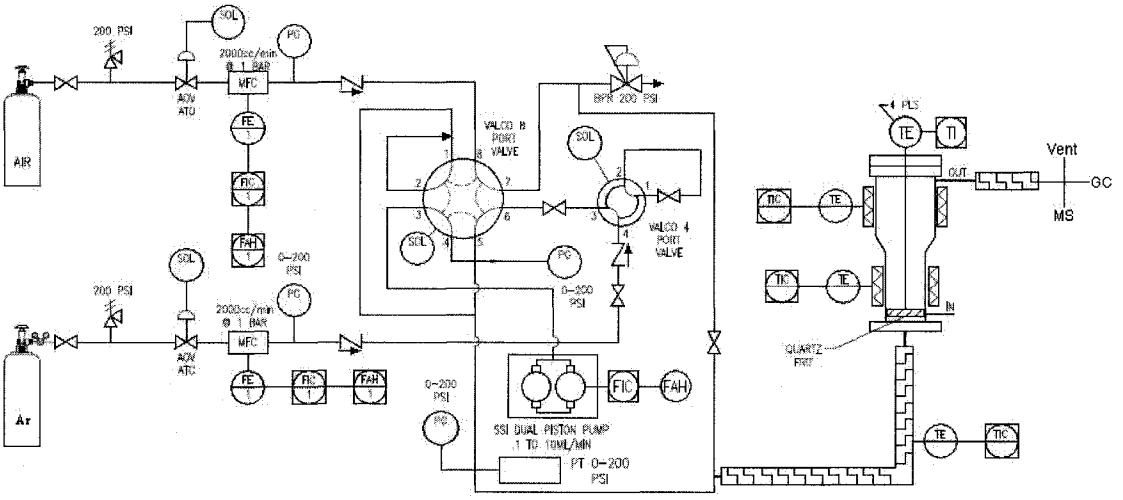

Figure 4-2: Schematic diagram of the experimental setup

4.2.3.2 Catalyst

The catalyst is composed of 10% CBV28014 (Zeolyst) imbedded in a Si/Al matrix consisting of Catapal B, Levasil 100s/30% and kaolin which was spray dried then calcined in air at 550°C for 4 h. The powder was contacted with a $(NH_4)_2HPO_4$ solution and then dried and calcined so that the resulting catalyst contained 1.5% phosphorous. The particle size distribution was measured on a Horiba LA-950 and the mean particle diameter was measured to 108 μm. The minimum fluidization velocity at ambient

temperature and pressure was measured to 0.005 m/s in a 76 mm perspex column in which the tapped particle density and density at minimum fluidization were also measured. The catalyst properties are listed in Table 4-1.

Table 4-1: Particle properties of the catalyst

d_p < 45	0.4	200 < d_p > 229	2.9
45 < d_p < 68	4.7	229 < d_p < 262	1.6
68 < d_p < 89	16.6	262 < d_p < 350	1.3
89 < d_p < 102	15.5	d_p	108 μm
102 < d_p < 117	16.7	u_{mf}	0.0051 m/s
117 < d_p < 133	15.3	ρ_p	1270 kg/m^3
133 < d_p < 153	11.9	ρ_{tapped}	855 kg/m^3
153 < d_p < 175	8.1	ρ_{mf}	744 kg/m^3
175 < d_p < 200	5.0	ε_{mf}	0.405

4.2.3.3 Experimental conditions

Glass beads with a particle diameter of 500 μm were placed at the bottom of the reactor and the catalyst was loaded on top to ensure that the catalyst was adjacent to the band heaters. No mixing of the two solids occurred since the maximum gas velocity used was insufficient fluidize the glass beads. The feed gas consisted of 5, 15, 30, 33 mol% methanol in argon. The superficial gas velocity ranged from 0.45 – 8.4 cm/s and the experiments were conducted with 4 different catalyst loadings 25, 50, 100 and 200g. Experiments ended when the product distribution was stable over a period of a few minutes on the MS.

The MS was calibrated with different known mixtures of water, DME, methanol and argon in the same range as the expected product distribution and the exit composition was also measured on a GC to verify the MS. The retention times of the components

have been validated from binary gas mixtures of argon and the gas of interest except in the case of methanol which was done from a methanol air mixture

RTD measurements were performed on the reactor loaded with 540g of glass beads, 50g of catalyst on top of the glass beads and a third experiment without glass beads and with 220g of catalyst. The experiments were carried out with argon as the tracer gas by switching between air and argon which were controlled by two MFC's. To minimize perturbations the change in gas flow is done by a multiport valve and the gas that is not sent to the reactor is purged. Pressure differences between the two inlet lines are hereby kept at a minimum and MFC delay is avoided. Switching the multiport valve gives a heavyside unit step function which first derivative is the Dirac delta pulse. The change in exit gas compositions was recorded at the exit of the reactor by MS at a frequency of 4.4 Hz

4.2.4 Experimental results

4.2.4.1 RTD

The E-curve from the RTD measurements is shown in Figure 4-3. There is almost no difference in the results form RTD measurements A and B in Figure 4-3 and the effect of adding 50g of catalyst to the 540g of glass beads already in the reactor does not change the flow significantly. Using 220g of catalyst gives a noticeable change in the flow compared to the using only the glass beads (Figure 4-3 C). An increase in the mean residence time is observed which is due to a lower volume of catalyst compared to glass beads. The broadening of the peak shape when 220g of catalyst is used is due to more dispersion and less plug flow behaviour as the amount of catalyst is increased.

A n-CSTR model is used to describe the system showing a similar result for the experiments with glass beads and glass beads plus catalyst. With 220g of catalyst in the bed only half the number of CSTR's is needed to describe the system. The result of the n-CSTR model is given in Table 4-2. By subtracting the result from reactor with glass beads from the data with 220g of catalyst and accounting for the volume of glass beads the *Pe* number for the bed can be found to 10 which give 6 n-CSTR in series (*Pe*=2(n-1)). The axial dispersion can be obtained from the *Pe* number and gives a value of 0.0008 m^2/s which correspond to the values found by Lorences et al. 2006. The RTD experiments done at ten times the minimum fluidization velocity shows that the reactor can be approximated by a plug flow with increased dispersion at increased catalyst amount.

Table 4-2: n-CSTR model parameters for the RTD experiments done at u_0 0.052m/s

Catalyst amount	σ^2 (s)	t_m (s)	N	Pe
540g glass beads	573	26.8	28	54
540g glass beads + 50g catalyst	428	26.7	27	52
220g catalyst	618	28.0	15	28

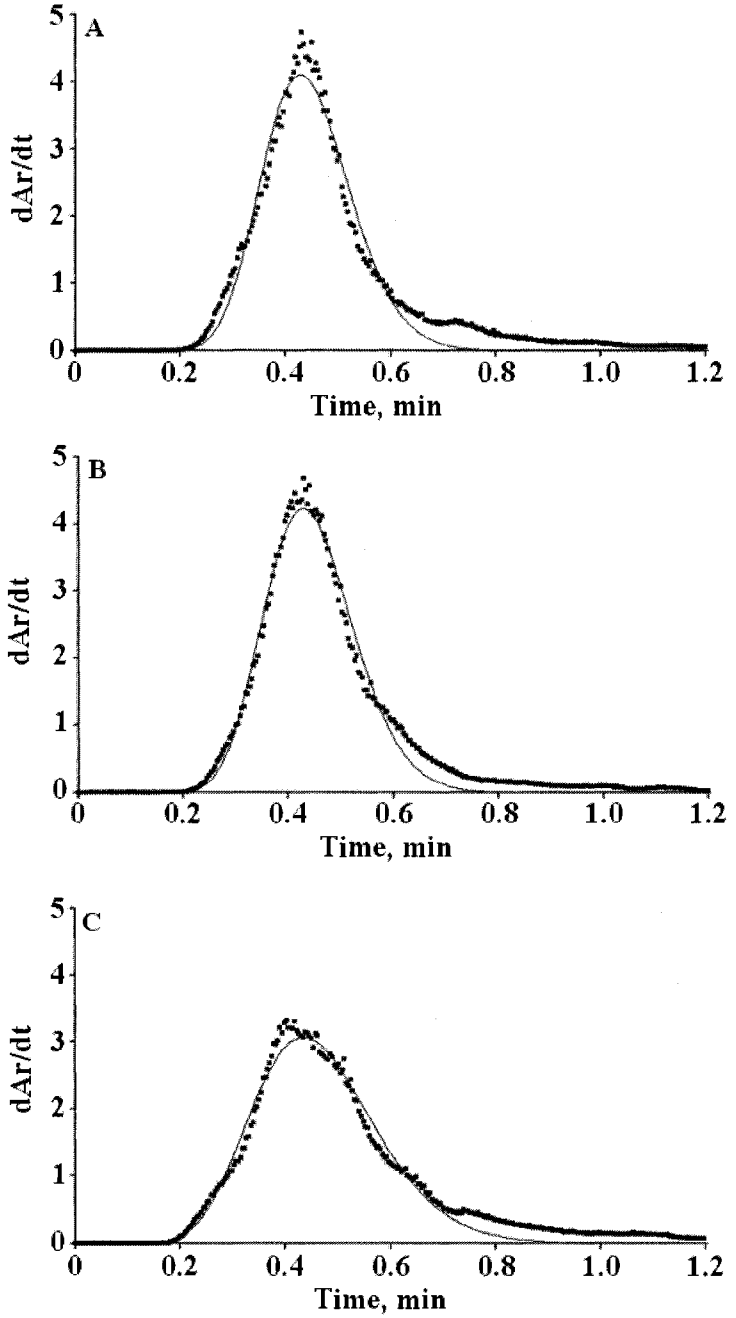

Figure 4-3: RTD experimental results over the fluid bed with a gas velocity of 5.4 cm/s. A) reactor loaded with 540g glass beads B) Reactor loaded with 540g glass beads and 50g of catalyst C) Reactor loaded with 220g of catalyst. Experimental data represented by dots and n-CSTR model with a line.

4.2.4.2 Methanol to DME

The experimental results from the MeOH/DME reaction are given in Table 4-3. The table lists the experimental data with the actual temperature, equilibrium constant, flows, catalyst amount and exit concentrations. A problem with a temperature probe has resulted in a temperature offset in the temperature of experiment 20-46. Based on the uncertainties in the experiments the maximum uncertainty is estimated to be ±2% on the methanol conversion. Methanol conversion is defined as the conversion to equilibrium while the total conversion is the actual conversion of methanol.

MS measurements was set up to measure not only Ar, MeOH, DME and H_2O fractions but also other hydrocarbon fraction to make sure possible side reactions were recorded. Only a few experiments at 325°C are included in the table as MS traces revealed hydrocarbon production in a majority of the data and they have therefore been omitted for analysis. MS results of the experiments 20 - 24 are shown in Figure 4-4. At 30 minutes the gas velocity was close to u_{mf} and the DME and H_2O concentrations were high while methanol concentration was close to equilibrium. After 35 min the gas velocity was increased to 0.89 cm/s and the DME and water concentrations dropped while methanol increased. The same trend is observed for the subsequent feed rate increases. The new product distribution was established within 2-5 minutes depending on flow rate and the change is clearly defined. No propene formation was detected but a low level of methane is present in all the experiments.

Table 4-3: Experimental data obtained – all flows are listed at STP conditions.

Exp. no.	Temp. °C	Cat. g	Q_{MeOH} ml/min	Q_{Ar} ml/min	u_0 cm/s	K_{eq}	y_{MeOH}	y_{DME}	MeOH Conv % ± 2%	Total conv. %
1	250	50	16.8	334	0.67	16.0	0.007	0.020	95.8	85.2
2	250	50	50.5	947	1.92	16.0	0.010	0.021	91.2	81.1
3	250	50	124	2340	4.73	16.0	0.012	0.019	86.3	76.7
4	250	200	50.5	947	1.92	16.0	0.007	0.022	96.1	85.5
5	250	200	124	2334	4.73	16.0	0.008	0.021	93.9	83.5
6	275	50	50.5	947	2.01	12.8	0.009	0.021	94.1	82.6
7	275	50	124	2340	4.95	12.8	0.010	0.020	90.4	79.3
8	250	50	39.3	214	0.49	16.0	0.026	0.064	93.4	83.0
9	250	50	152	858	1.94	16.0	0.050	0.050	74.6	66.4
10	250	50	382	2160	4.88	16.0	0.075	0.038	56.2	50.0
11	275	50	39.3	214	0.51	12.8	0.026	0.065	94.9	83.3
12	275	50	152	858	2.03	12.8	0.034	0.058	87.8	77.1
13	275	50	382	2160	5.12	12.8	0.044	0.053	80.4	70.5
14	250	50	157	355	0.98	16.0	0.089	0.109	79.8	70.9
15	250	50	309	710	1.96	16.0	0.150	0.076	56.6	50.4
16	250	50	792	1840	5.05	16.0	0.209	0.046	34.3	30.5
17	275	50	157	355	1.03	12.8	0.066	0.120	89.4	78.4
18	275	50	309	710	2.05	12.8	0.081	0.111	83.5	73.2
19	275	50	792	1840	5.29	12.8	0.121	0.090	68.2	59.8
20	278	25	78.5	154	0.47	12.5	0.060	0.139	93.9	82.3
21	277	25	157	307	0.94	12.6	0.090	0.125	83.9	73.5
22	278	25	309	613	1.86	12.5	0.122	0.107	72.7	63.7
23	279	25	791	1580	4.82	12.4	0.183	0.075	51.5	45.2
24	277	25	1250	2560	7.79	12.6	0.224	0.053	36.6	31.9
25	280	50	78.5	154	0.47	12.3	0.059	0.140	94.2	82.6
26	277	50	157	307	0.94	12.6	0.075	0.132	88.9	78.0
27	278	50	309	613	1.86	12.5	0.088	0.123	84.1	73.6
28	279	50	791	1580	4.82	12.4	0.138	0.098	67.	58.7
29	278	50	1250	2560	7.71	12.5	0.174	0.077	53.6	47.0
30	278	100	78.5	154	0.47	12.5	0.046	0.146	98.7	86.3
31	279	100	157	307	0.94	12.4	0.053	0.143	96.4	84.3
32	279	100	309	613	1.87	12.4	0.064	0.135	92.3	80.8
33	282	100	791	1580	4.84	12.1	0.093	0.120	82.5	72.2
34	284	100	1250	2560	7.79	11.9	0.115	0.107	74.5	65.0
35	287	200	78.5	154	0.48	11.6	0.044	0.147	99.8	87.0
36	288	200	157	307	0.96	11.5	0.046	0.146	99.1	86.4
37	288	200	309	613	1.90	11.5	0.049	0.143	98.0	85.3
38	289	200	791	1580	4.90	11.4	0.062	0.136	93.5	81.5
39	290	200	1250	2560	7.88	11.3	0.073	0.128	88.9	77.7
40	325	25	78.5	154	0.51	8.66	0.044	0.147	101.8	87.0
41	325	25	157	307	1.01	8.66	0.044	0.148	101.8	87.1
42	325	25	309	613	2.02	8.66	0.054	0.140	98.1	83.8
43	325	25	791	1580	5.22	8.66	0.073	0.130	91.3	78.0
44	325	25	1250	2560	8.37	8.66	0.087	0.121	86.0	73.6
45	325	50	791	1580	5.22	8.66	0.061	0.136	95.6	81.8
46	325	50	1250	2560	8.37	8.66	0.069	0.130	92.5	79.1

The conversion of methanol from the GC – relative to the MeOH/DME equilibrium – was 96.4% in experiment 31 and 88.9% in experiment 39 which was in agreement with the MS. From the GC data the level of methane was found to be 0.25% on carbon basis which is considered to be negligible.

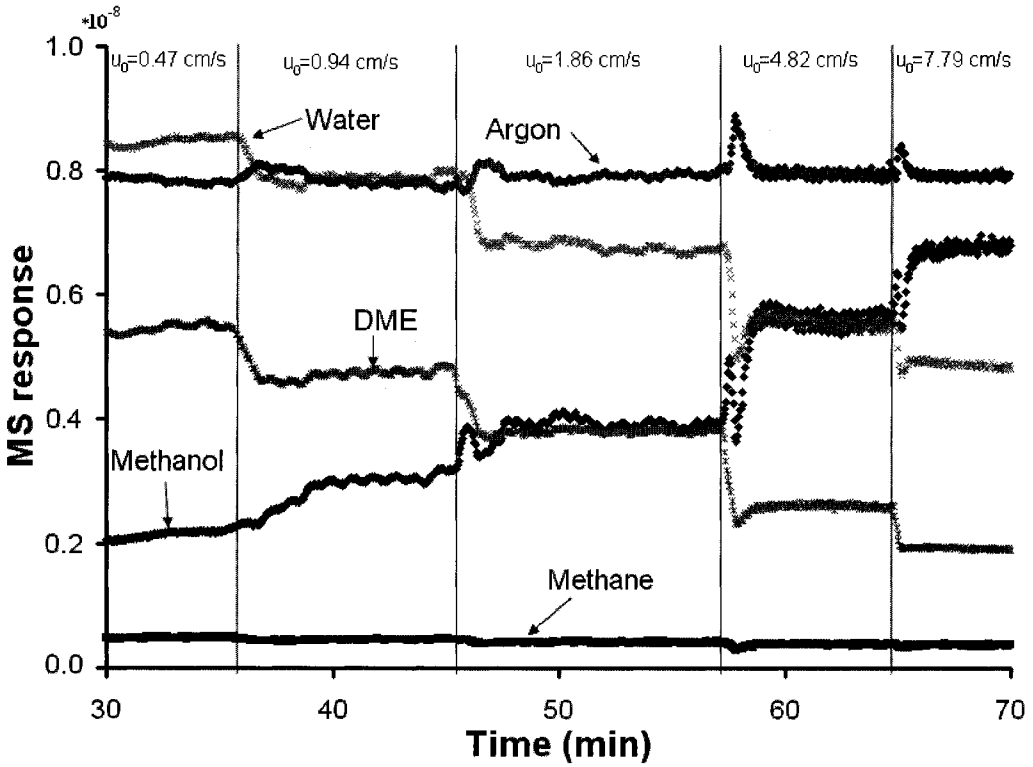

Figure 4-4: MS results from experiments done at 275°C with 25 g of catalyst

Due to a slightly declining background level of water in the MS trace, the water fraction was based on the DME which is valid due to the reaction stoichiometry. A graphical representation of the methanol conversion of experiment 20-39 is shown in

Figure 4-5. The data all follows the same trend with higher conversion as the catalyst amount increases and decreased conversion when the gas velocity is increased. With 200g of catalyst the conversion at the three lowest gas velocities are almost the same and

within full conversion when the uncertainty is taken into account. The increase in velocity compared to catalyst amount also correspond to each other e.g. going from at gas velocity of 0.94g and 50g of catalyst to 1.86cm/s and 100g of catalyst result in approximately the same conversion. At higher gas velocities the same trend is seen with slightly higher conversions by doubling the catalyst amount while increasing the velocity by 60%. At low gas velocity close to u_{mf} conversions are high with only a slight rise in conversion as the catalyst amount is increased. The difference between the data points at 25g and 50g at this velocity is smaller that what would be expected from the other gas velocities. The used experimental parameters are also shown to give a wide conversion range from 30 to almost 100% conversion.

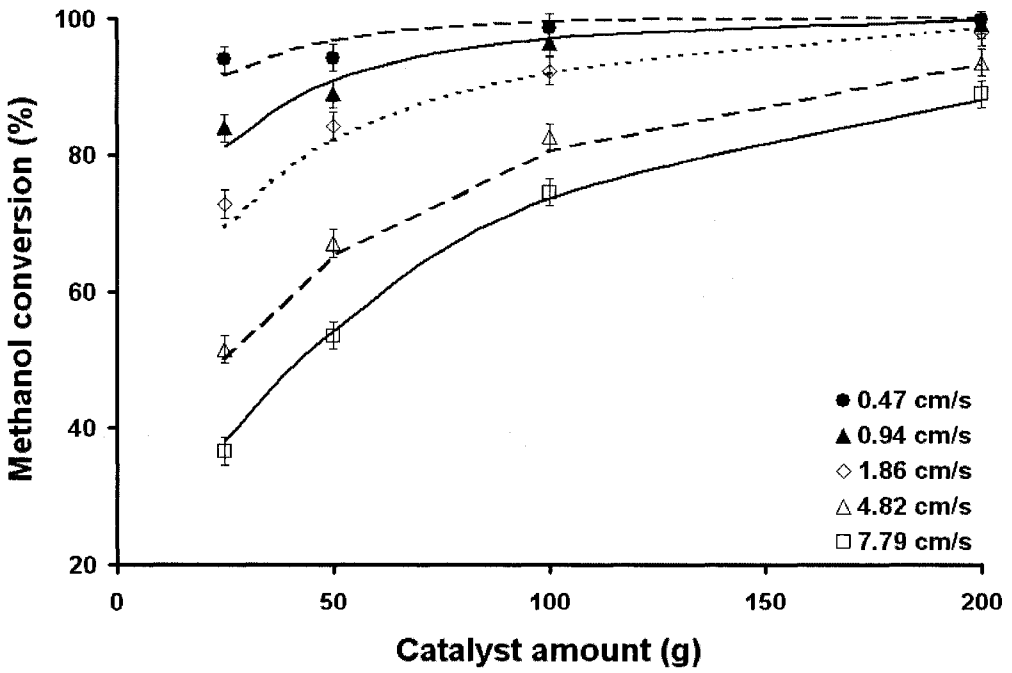

Figure 4-5: Conversion of methanol to DME and water based on equilibrium conversion as function of catalyst amount at five different gas velocities (experiment 20 - 39). Lines are the model predictions using kinetic model equation 4-5 and 6 CSTR's in series.

4.2.5 Modeling

4.2.5.1 Kinetics

Mollavali et al. (2008) recently studied the methanol to DME reaction (Equation 4-1) and summarized the published kinetic models with reaction orders of ½, 1 and 2.

$$2CH_3OH \Leftrightarrow CH_3OCH_3 + H_2O \tag{4-1}$$

Calculations of the reaction order by the half-lives method from the fluid bed data gives a reaction order in the range 1.75 – 2 and therefore a second order reaction has been assumed in this work.

Due to the high conversion levels the reverse reaction also has to be included in the kinetic expression. Literature models that include the equilibrium term are given in Table 4-4. The absorption term of DME is neglected in all of the models because it is much smaller than the absorption of methanol and water (Berĉiĉ and Levec, 1992).

Table 4-4: Kinetic models including the reverse term.

Model	Equation	Ref.
1	$-r_{MeOH} = \dfrac{k\left(C_M - C_w C_D / \left(K_{eq} C_M\right)\right)}{\left(1 + K_M C_M + C_w / K_W\right)}$	Mollavali et al. (2008)
2	$-r_{MeOH} = \dfrac{k\ \left(C_M^2 / C_W - C_D / K_{eq}\right)}{\left(1 + K_M C_M + K_W C_W\right)^2}$	Lu et al. (2004)
3	$-r_{MeOH} = \dfrac{k\ K_M^2 \left(C_M^2 - C_w C_E / K_{eq}\right)}{\left(1 + 2\left(K_M C_M\right)^{0.5} + K_W C_w\right)^4}$	Berĉiĉ and Levec (1992)

A simple model for the for the methanol to DME reaction is proposed where methanol is absorbed on a active site on the catalyst (Equation 4-2), two absorbed methanol species

then react to DME and an absorbed water molecule (Equation 4-3) this reaction is considered to be in the rate determined. Finally the water is desorbed (Equation 4-4).

$$CH_3OH + S \leftrightarrow CH_3OHS \tag{4-2}$$

$$CH_3OHS + CH_3OHS \leftrightarrow CH_3OCH_3 + H_2OS + S \tag{4-3}$$

$$H_2OS \leftrightarrow H_2O + S \tag{4-4}$$

The reaction rate of methanol from Equation 4-2 to 4-4 is given in Equation 4-5 where k follows an Arrhenius relationship. This kinetic expression will be compared to the model of Berĉiĉ and Levec (1992) where the model parameters have been re-estimated to account for the different temperature interval and catalyst composition.

$$-r_{MeOH} = \frac{kC_M^2\left(1-\frac{C_D C_W}{C_M^2 K_{eq}}\right)}{\left(1+K_M C_M + K_W C_W\right)^2} \tag{4-5}$$

Hetsroni (1983) divides first order kinetics into three categories slow, intermediate and fast reactions in fluidized beds based on their reaction rate constant. Slow reactions are controlled by reaction kinetics while intermediate reactions can be controlled by both reaction rate or mass transfer between bubble and emulsion. Fast reactions are characterized by k values above 5 s^{-1} and slow reactions have k values below 0.5 s^{-1}. For a first order reaction $t_{½}$= ln(2)/k and a fast reaction in this view is a reaction with a half-life below 0.14 s and a slow reaction with a half-life above 1.4 s. Using the same criteria for second order reactions, we categorise the methanol dehydration reaction as either

fast, intermediate or slow. The average half-life from the experiments can be calculated by Equation 4-6 ignoring the reverse reaction,

$$t_{½} = \frac{\tau}{\frac{1}{1-X} - 1} \tag{4-6}$$

Where X is the total conversion of methanol and t is the residence time in the bed. For experiment 43, the average half-life is 0.11 s which is below the criteria for a fast reaction and it would be assumed that the mass transport between the emulsion and bubble will play a role in the modelling of this data. For all the experiments below 300°C the half-life is above 0.5 s and the reactions rates are considered to be in the intermediate region. The experimental data with conversion to equilibrium above 95% all have an average half-life above 1.4 s and slow reaction rates which would also be expected for second order reactions close to equilibrium where the reaction rate is reduced.

4.2.5.2 Fluid bed model

The fluid bed has been modelled with a two region model with a bubble phase and an emulsion phase as well as an n-CSTR's in series model with 6 CSTR-s in series. The number of CSTR's in series has been considered to be constant over the range of gas velocities and catalyst inventory. Improving the n-CSTR's in series model with the amount of CSTR's as function of gas velocity and catalyst amount is possible but have not been included in this study. The two phase model is well described in the literature and has recently been used by Werther and Hartge (2004) to model industrial fluidized bed reactors and by Abba et al. (2003) where it was used as part of a comprehensive

model to characterise fluidization from bubbling conditions to fast fluidization. Although the general model is of the same form, different assumptions are made to the hydrodynamic. In this work where the following assumptions are made.

- Gas flow only in the axial direction - dispersion in the radial direction is not considered (with the exception of interphase mass transfer)
- Interphase mass transfer between bubble and emulsion phase
- No catalyst in the bubble phase
- The activity of the catalyst is considered constant e.g. no deactivation due to short reaction time compared to the deactivation time of the catalyst

The mass balance of the bubble and emulsion phases of the model can be written as

Bubble phase:

$$-u_b \frac{\partial C_{i,b}}{\partial z} = K_{be}\left(C_{i,b} - C_{i,e}\right) \tag{4-7}$$

Emulsion phase:

$$u_{mf} \frac{\partial C_{i,e}}{\partial z} = \frac{\delta}{(1-\delta)} K_{be}\left(C_{i,b} - C_{i,e}\right) + (1-\varepsilon_{mf})\rho_p(-r_i) \tag{4-8}$$

The model has been implemented in Fortran as two parallel CSTR in series with mass transfer between the two. The implemented equations are given below and a schematic drawing is shown in Figure 4-6.

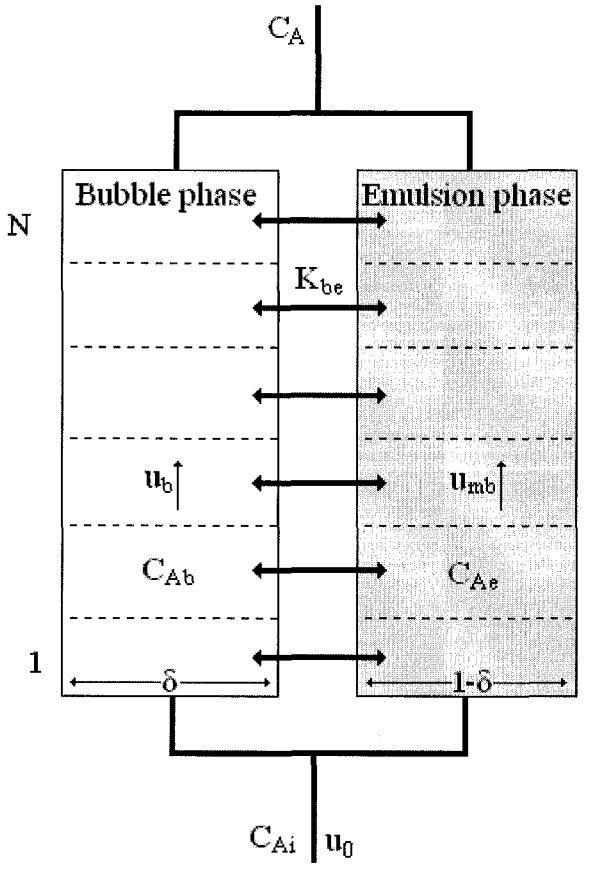

Figure 4-6: Schematic of the two phase fluid bed model

The CSTR volume is based on equal catalyst amount e.g. constant emulsion volume, which makes the CSTR's volume in the bubble phase dependent on the bubble velocity

$$F_b x_{b,i,n} = F_b x_{b,i,n-1} - \frac{\delta}{1-\delta} V_e K_{be} \left(\rho_g x_{b,i,n} - \rho_g x_{e,i,n} \right) \tag{4-9}$$

$$F_e x_{e,i,n} = F_e x_{e,i,n-1} + \frac{\delta}{1-\delta} V_e K_{be} \left(\rho_g x_{b,i,n} - \rho_g x_{e,i,n} \right) + W(-r_i) \tag{4-10}$$

Optimization of parameters have been done with the use of the Simplex method and the error calculations have been evaluated from Equation 4-11

$$R_i^2 = 1 - \frac{\sum_n \left(x_{i,n,cal} - x_{i,n,\exp}\right)^2}{\sum_n \left(x_{i,n,\exp} - \bar{x}_{i,\exp}\right)^2} \tag{4-11}$$

The hydrodynamic correlations used in this work are given in Table 4-5. The mass transfer coefficient correlations used in this work is the one from Sit and Grace (1981). The bubble diameter has been calculated form the correlation of Mori and Wen (1975). Since the used particles are Geldart A particles the minimum bubbling velocity is used in the correlations for the gas in the emulsion phase.

Table 4-5: Hydrodynamic correlations – the correlation for bubble diameter is in cm and not in meters

Variable	Correlation	Ref.
Mass transfer coefficient	$k_{be} = \frac{u_{mb}}{3} + \left(\frac{4D\varepsilon_{mf}\bar{u}_b}{\pi \bar{d}_b}\right)^{1/2}$ $\quad K_{be} = \frac{6k_{be}}{d_b}$	Sit and Grace (1981)
Bubble diameter	$d_b = d_{bm} - (d_{bm} - d_{b0})\exp\left(\frac{-0.3z}{D_t}\right)$ $d_{b0} = 0.00376(u_0 - u_{mb})^2, \quad d_{bm} = 0.652(A_t(u_0 - u_{mb}))^{0.4}$	Mori and Wen (1975)
Bubble velocity	$u_b = u_0 - u_{mb} + 0.711(gd_b)^{1/2}$	
Minimum fluidization velocity	$u_{mf} = \frac{\mu}{d_p \rho_g}\left[\left[(33.7)^2 + 0.0408\left(\frac{d_p^3 \rho_g (\rho_p - \rho_g) g}{\mu^2}\right)\right]^{1/2} - 33.7\right]$	Wen and Yu (1966)
Minimum bubbling	$\frac{u_{mb}}{u_{mf}} = \frac{2300\rho_g^{0.126}\mu^{0.523}\exp(0.716F)}{d_p g^{0.934}(\rho_p - \rho_g)^{0.934}}$	Abrahamsen and Geldart (1980)
Bubble fraction	$\delta = \frac{u_0 - u_{mb}}{u_b - u_{mb}}$	

4.2.6 Modelling result and discussion

All parameters in the fluid bed model besides the molecular diffusion coefficient are given by the experimental conditions or the hydrodynamic correlations. The molecular diffusion coefficient varies between 0.2-0.6 cm^2/s for the binary mixtures and for the modelling of the fluid bed an average value of 0.4 cm^2/s has been used. It has further been found that slight changes in the molecular diffusion coefficient – within the range of the binary mixtures - do not changes the modelling results significantly. The models parameters were fit to the data in experiments 1 to 19. The parameters and level of fit to the experimental data for the fluid bed model and 6 CSTR's in series are given in Table 4-6 and Table 4-7.

Table 4-6: Best fit parameters for the kinetic model Equation 4-5 and the level of fit to the experimental data.

Reactor model	k $m^6/(kg \cdot s \cdot kmol)$	Ea kcal/mol	K_W $m^3/kmol$	K_m $m^3/kmol$	R^2 Exp 1-19	R^2 all exp
Fluid bed	21900	24.5	47000	14000	0.918	0.901
6 CSTR's	21400	22.1	47000	15000	0.934	0.940

Table 4-7: Best fit parameters for model of Berĉiĉ and Levec (1992) and the level of fit to the experimental data.

Reactor model	k kmol/(kg·s)	Ea kcal/mol	K_W $m^3/kmol$	K_m $m^3/kmol$	R^2 Exp 1-19	R^2 all exp
Fliud bed	0.619	33.0	590	48	0.906	0.884
6 CSTR's	0.677	32.2	480	30	0.910	0.925

The heat of adsorption has not been included into the kinetics of the model from Equation 4-5 since the data was not sufficient to obtain reliable results and they have therefore been considered as temperature-independent. For the model of Barĉiĉ and Levec (1992) their values for the heat of adsorption for methanol and water was used. The lack of temperature dependency in the absorption term for the proposed model

might explain some of the difference in the activation energy seen between the two models since the absorption has a significant influence on the reaction. The kinetic model of Equation 4-5 shows the best result when coupled with 6 CSTR's in series compared to the other kinetic and reactor model. Modelling the rest of the data set (experiment 20-46) shows a very good fit to the data derived from the first 19 experiments. In Figure 4-5 the data from experiment 20-39 is plotted together with the model prediction. The overall agreement is very good and only at high conversion does the model over predict the actual conversion. The ability for the CSTR's in series model to predict the reaction with different catalyst inventories even better than the fluid bed model indicates that the mass transfer between the bubble and emulsion phase in the fluid bed is not predominant under the given experimental conditions, which is also indicated by the high conversions levels which would not be expected if mass transfer between the emulsion and bubble was limiting the reaction.

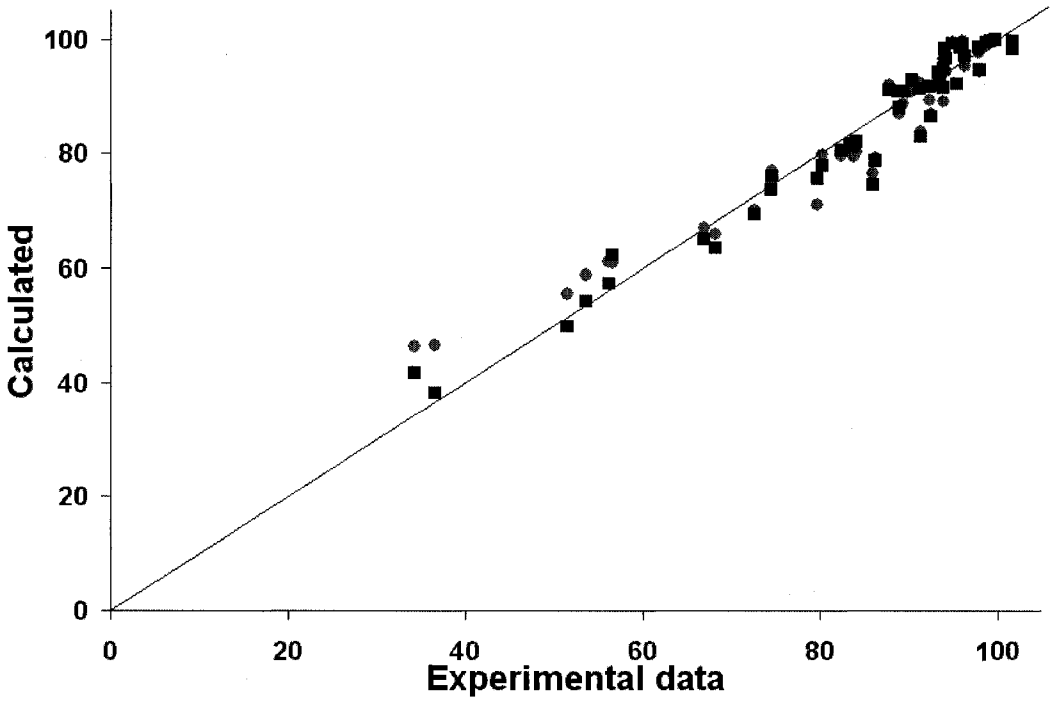

Figure 4-7: Model predictions vs. experimental with 6 CSTR's in series. ▪ Model Eq. 4-5; • Model of Berĉiĉ and Levec (1992)

A parity plot of all the data compared to the model estimations with the use of the kinetic model Equation 4-5 and the model of Barĉiĉ and Levec (1992) are given in Figure 4-7. The model predictions are not that different at high conversions but at low the model given by Equation 4-5 are slightly better. The model shows that the absorption term – which is the different between the two models – have a large influence on the reaction. Overall the predicted conversions are within 5% of the measured values.

The influence of the mass transfer coefficient in the two phase model have been investigated by using the best fit parameters from the CSTR's in series model. In Figure 4-8 the effect of changing the mass transfer coefficient is depicted. The effect at low catalyst inventory is limited and increases as the catalyst amount is increased, which is a

result of the increasing bubble size along the bed. The deviation when 200g of catalyst is used is significant and even with a molar diffusion coefficient ten times the estimated the prediction is off by 5%. Some deviation is expected since the best fit parameters from the CSTR's in series model is used the best fit parameters is however similar and does not change the trends in the figure significantly.

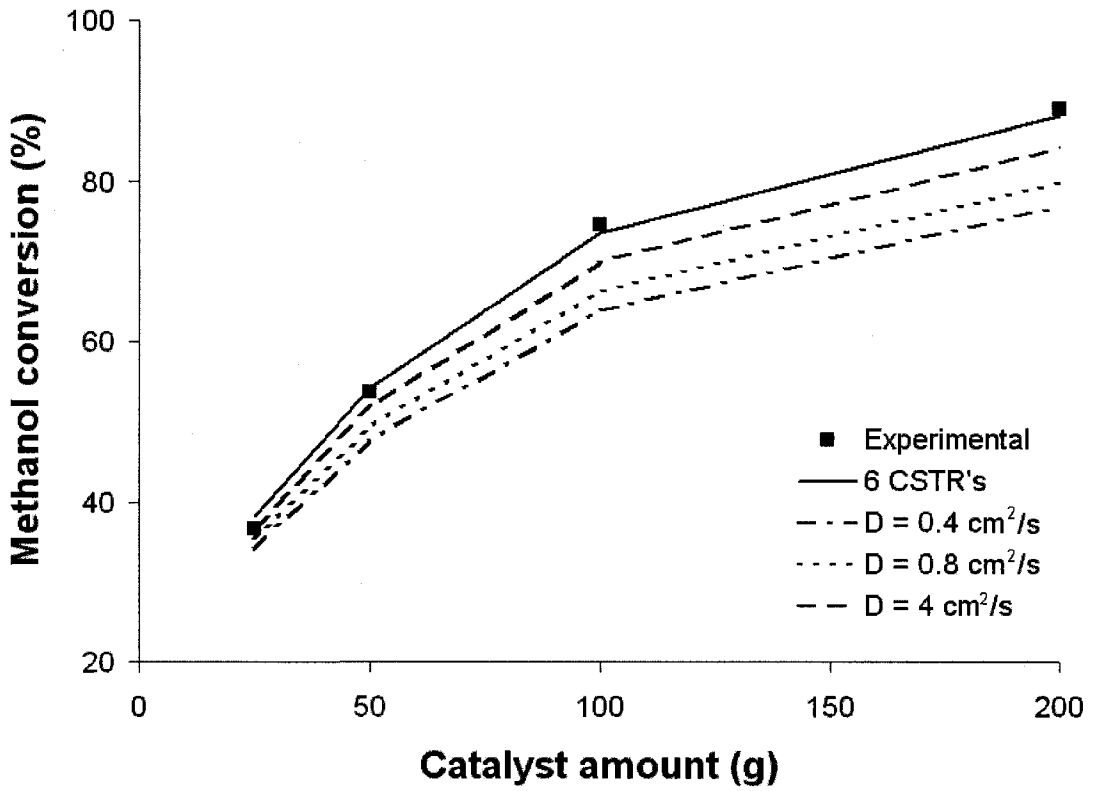

Figure 4-8: Effect of the molar diffusion coefficient with the use of the best fit parameters for 6-CSTR's in series with the two phase model and the kinetic model of Equation 4-5. The experimental points are at 275°C and a superficial gas velocity of 7.79 cm/s

The conversions measured in the present work are relatively high for a standard kinetic study but due to the nature of the fluid bed the operational range is limited. If the gas velocity is increased further the hydrodynamic of the bed could change leading to different hydrodynamics in the kinetic dataset which will have to be accounted for.

Investigations of the limitations in the superficial gas velocity in which the n-CSTR's in series model can be use will therefore be useful but have not been pursued in this work. Decreasing the catalyst inventory further will lead to a very shallow bed and possibility of by-pass has to be considered. Changing the temperature is the best option to investigate a large range of conversions, and lowering the temperature further than the 250°C done in this work would help explore the kinetic at low conversions.

Data from fixed bed experiments in a 4 mm inner diameter quartz reactor together with predictions of the conversion using Equation 4-5 is given in Table 4-8. The predicted conversions is lower then the measured with increasing difference as the reactions temperature is increased. The higher difference between model prediction and experimental data is most likely due to temperature gradients in the bed, caused by the exothermic reaction, which increases with increased reaction temperature and thus higher reaction rate.

Table 4-8: Fixed bed experiments in a 4 mm inner diameter quartz reactor.

Temp. °C	Cat. g	Q_{MeOH} ml/min	Q_{Ar} ml/min	u_0 cm/s	K_{eq}	y_{MeOH}	y_{DME}	MeOH Conv. % ± 2%	Model prediction
250	0.1	1.3	12	3.39	16.0	0.066	0.017	39	50.2
250	0.1	2.8	25	7.05	16.0	0.070	0.015	34	34.1
275	0.1	1.3	12	3.55	12.8	0.027	0.036	83	74.6
275	0.1	2.8	25	7.39	12.8	0.034	0.033	75	58.7
275	0.1	5.6	50	14.8	12.8	0.057	0.022	50	42.8
300	0.1	1.3	12	3.71	10.4	0.016	0.042	97	91.5
300	0.1	2.8	25	7.73	10.4	0.019	0.040	93	80.2
300	0.1	5.6	50	15.5	10.4	0.026	0.037	85	66.0
300	0.1	1.3	12	3.71	10.4	0.014	0.043	99.4	91.5

Using the fluid bed for kinetic measurements of the methanol to DME reactions have in this work been shown to give good results. The isothermal temperature profile of the

fluid bed ensures that the temperature is easily controlled and well known. Since a small temperature uncertainty can easily result in poor estimation of the reaction rate or activation energy it is essential that the temperature is known and hot spots and gradients are avoided. This is difficult in fixed bed when investigating exothermic reactions since hot spots and temperature gradients will affect the result (Fogler, 2005) and one is forced to dilute the catalyst with inert and run experiments at very low conversions to reduce the effect. Diluting the catalyst introduces the possibility of bypassing and it has been shown to influence the observed conversion especially at conversions above 0.4 (Berger et al. 2002).

4.2.7 Conclusion

The reaction kinetics of the exothermic dehydration of methanol to DME have been investigated in a fluidized bed at low gas velocities. A kinetic expression for the methanol to DME reaction has been proposed and the kinetic parameter has been estimated with both a two phase fluid bed model and an n-CSTR's in series as the reactor model. The kinetic model coupled with the n-CSTR model was shown to give superior result compared to the two phase fluid bed model. This was observed with both the proposed model and the literature model of Barĉiĉ and Levec (1992). The fluid bed was shown to be a good reactor type for the kinetic modelling of the methanol to DME reaction due to the isothermal conditions and the conversions that could be obtained at relatively low gas velocities. Other exothermic reactions where hotspots or temperature gradients are of concern during kinetic measurements could benefit from the fluid bed

technology. Due to restraints on the catalyst inventory and gas velocities the conversion range at a given temperature is can be limited.

.

4.2.8 Nomenclature

A_t = Cross-sectional area of the fluid bed (m^2)

C = Molar concentration ($kmol/m^3$)

$\mathcal{D}$ = Molar diffusion coefficient (m^2/s)

D_t = Reactor diameter (m)

d_p = Mean particle diameter (m)

d_b = Bubble diameter (m)

d_{b0} = Initial bubble diameter at the distributor (m)

d_{bm} = Maximum bubble diameter (m)

E_a = Activation energy (kJ/mol)

F = Fine fraction

F_b = Flow rate in bubble phase (kmol/s)

F_e = Flow rate in emulsion phase (kmol/s)

g = gravity (m/s^2)

K_{eq} = Equilibrium constant

k = Reaction rate constant ($m^6/kmol \cdot s$)

K_{be} = Bubble to emulsion mass transfer coefficient (s^{-1})

k_{be} = Bubble to emulsion mass transfer coefficient (m/s)

N = Number of CSTR's

Pe	= Peclet number ($Pe = U_gL/D$)
r_i	= Reaction rate of component i (kmol/kg·s)
$t_{½}$	= Halftime (s)
t_m	= Mean residence time (s)
u_{mf}	= Minimum fluidization velocity (m/s)
u_{mb}	= Minimum bubbling velocity (m/s)
u_b	= Bubble velocity (m/s)
u_0	= Superficial gas velocity (m/s)
V_e	= Volume of emulsion (m^3)
W	= Catalyst weight (kg)
Q	= Gas flow (ml/min)
X	= Total conversion
x	= Mole fraction
y	= Mole fraction of gas
z	= Height in bed (m)

Greek symbols

δ	= Bubble phase volumetric fraction
ε_{mf}	= Void fraction at minimum fluidization
μ	= Gas viscosity (kg/m·s)
σ^2	= Variance
ρ_p	= Particle density (kg/m^3)
ρ_{tapped}	= Tapped density (kg/m^3)

ρ_{mf} = Minimum fluidization density (kg/m^3)

ρ_g = Gas density (kg/m^3)

τ = Residence time (s)

Subscripts

exp = Experimental

calc = Calculated

n = CSTR number

i = species

be = Bubble to emulsion

b = Bubble

e =Emulsion

4.2.9 Literature Cited

Abba, I. A., J. R. Grace, H. T. Bi and M. L. Thompson, "Spanning the flow regimes: Generic Fluidized-bed reactor model," AIChE Journal. **49**, 1838 – 1848 (2003).

Abrahamsen, A. R., and D. Geldart, "Behaviour of gas-fluidized beds of fine powders Part 1. Homogeneous expansion," Powder Technology. **26**, 35 – 46 (1980).

Berĉiĉ, G. and J. Levec, "Intrinsic and Global Reaction Rate of Methanol Dehydration over γ-Al_2O_3 Pellets," Ind. Eng. Chem. Res. **31**, 1035-1040 (1992).

Berger, R. J, J. P. Ramírez, F. Kapteijn and J. A. Moulijn, "Catalyst performance testing: bed dilution revisited" Chem. Eng. Sci. **57**, 4912 – 4932 (2002)

Christensen, D., D. Vervloet, J. Nijenhuis, B.G.M. van Wachem, J.R. van Ommen and M.-O. Coppens, "Insights in distributed secondary gas injection in a bubbling fluidized bed via discrete particle simulations" Powder Technology. **183**, 454 – 466 (2008)

Fogler, H. S. "Elements of chemical reaction engineering" Prentice Hall, 4th edition, 2005

Gray, C. and G. Webster, "A Study of Dimethyl Ether (DME) as an Alternative Fuel for Diesel Engine Applications" Transport Canada Publication No.: TP 13788E, May 2001

Hetsroni, G., "Handbook of Multiphase Systems" Hemisphere-McGraw Hill, 1982

Horio, M. and Wen, C. Y. "An assessment of fluidized-bed modelling" AIChE symposium series, **73**, 9 – 21 (1977)

Kaarsholm, M., F. Joensen, J. Nerlov, R. Cenni, J. Chaouki and G. S. Patience, "Phosphorous modified ZSM-5: Deactivation and product distribution for MTO" Chem. Eng. Sci., **62**, 5527 – 5532 (2007)

Keil, F. J. "Methanol-to-hydrocarbons: process technology" Microporous and Mesoporous Materials, **29**, 49–66 (1999)

Kunii, D. and O. Levenspiel, "Fluidization Engineering," Butterworth-Heinemann series in chemical engineering, Newton, MA (1991).

Kunii, D. and O. Levenspiel, "Bubbling bed model. Model for the flow of gas through a fluidized bed" I&EC Fundamentals. **7(3)**, 446 – 452 (1968)

Lorences, M. J., J.-P. Laviolette, G. S. Patience, M. Alonso and F. V. Díez, "Fluid bed gas RTD : Effect of fines and internals," Power Technology. **168**, 1 – 9 (2006).

Lu, W.-Z., L.-H. Teng and W.D. Xiao, "Simulation and experiment study of dimethyl ether synthesis from syngas in a fluidized-bed reactor" Chem. Eng. Sci. **59**, 5455 – 5464 (2004)

May, W. G., "Fluidized-bed reactor studies" Chemical Engineering Progress, **55(12)**, 49 – 56 (1959)

Mollavali, M., F. Yaripour, H. Atashi, and S. Sahebdelfar, "Intrinsic Kinetic Study of Dimethyl Ether Synthesis from Methanol on γ-Al_2O_3 Catalysts," Ind. Eng. Chem. Res. **47**, 2365-3273 (2008).

Mori, S. and Y. Wen, "Estimation of bubble diameter in gaseous fluidized beds," AIChE Journal. **21(1)**, 109 – 115 (1975).

Radmanesh, R., J. Chaouki, and C. Guy, "Biomass Gasification in a Bubbling Fluidized Bed Reactor: Experiments and Modeling" AIChE Journal. **52(12)**, 4258 – 4272 (2006)

Semelsberger, T. A., R. L. Borup, and H. L. Greene, "Dimethyl ether (DME) as an alternative fuel" Journal of Power Sources. **156,** 497-511 (2006)

Shaikh, A. A. and H. Batran, "On bubble-side transport limitations in catalytic fluid-bed reactors" Chem. Eng. Res. Des. **85**, 1215 – 1218 (2007).

Sit, S. P., and J. R. Grace, "Effect of bubble interaction on interphase mass transfer in gas fluidized beds," Chem. Eng. Sci. **36**, 327 – 335 (1981).

Van Deemter, J. J., "Mixinf and contacting in gas-fluidized beds" Chem. Eng. Sci. **13(3)**, 143 – 154 (1961)

Wen, C.Y., and Y. H. Yu, "Mechanics of fluidization," Chemical Engineering Progress Symposium Series. **62**, 100 – 111 (1966).

Werther, J., and E.-U. Hartge, "Modeling of industrial fluidized-bed reactors," Ind. Eng. Chem. Res. **43,** 5593 – 5604 (2004).

Chapter 5
Phosphorous modified ZSM-5: Deactivation and product distribution for MTO*

5.1 Presentation of the article

The objective of the second article is to investigate the deactivation and product distribution of the phosphorous modified ZMS-5 catalyst in small diameter fixed bed reactors. Both pure methanol and 10% methanol in nitrogen at different feed rates is feed to the reactor showing a substantial change in the amount of methanol converted per catalyst volume before deactivation dependent of feed rate and composition. Secondary cracking reactions of higher olefins are found to be and important route to the lower olefins. For better understanding of the deactivation and change in product distribution the deactivation of the catalyst have been followed during the reaction. Due to the colour change of the catalyst during reaction the coke front down the bed could be followed and three zones identified.

* *Chemical Engineering Science Volume 62, Issues 18-20, September-October 2007, Pages 5527-5532*

5.2 Phosphorous modified ZSM-5: Deactivation and product distribution for MTO

Mads Kaarsholm, Finn Joensen[†], Jesper Nerlov[†], Roberta Cenni[†], Jamal Chaouki, Gregory S. Patience
Department of Chemical Engineering, École Polytechnique de Montréal, Canada
[†]Haldor Topsøe A/S, Denmark

5.2.1 Abstract

The product distribution and deactivation in the MTO process over a phosphorous modified catalyst containing 10% H-ZSM-5 was studied in small diameter fixed bed reactors. These studies suggest that methane is formed directly from methanol and/or dimethyl ether and that non-aromatic C_{5+} hydrocarbons are intermediates in the MTO reaction, forming light olefins ($C_{3=}$ and $C_{4=}$, but *not* ethylene) by secondary cracking reactions. Based on photographs of the catalyst taken during the course of the reaction, three distinct coking patterns were observed that might be attributable to the different reactions. Deactivation time of the catalyst is highly dependent on the contact time, doubling the feed rate decreased the deactivation time by a factor of ten and lowered the olefin production. Changing the feed form pure methanol to 10% methanol in nitrogen reduced methanol capacity of the catalyst considerably, but a slight increase in propylene selectivity was also observed.

Keywords; Zeolites; Catalyst selectivity; ZSM-5; Methanol-to-olefins

5.2.2 Introduction

The methanol to hydrocarbon process over acid zeolites has received significant academic and industrial attention since its discovery in the late 1970's (Chang, 1984). In the last two decades the main focus of this research has been on the methanol-to-olefin

(MTO) part of the reaction due to the increasing demand for light olefins (Chen et al., 2005). This has become even more pronounced with the high price of crude oil. The MTO process is an acid catalyzed reaction of which SAPO-34 and ZSM-5 are the most common catalysts (Stöcker, 1999).

Several kinetics/reaction paths have been proposed for the MTO and MTG process. Chang & Silvestri (1977) proposed the first model.

$$2CH_3OH \underset{+H_2O}{\overset{-H_2O}{\rightleftharpoons}} CH_3OCH_3 \xrightarrow{-H_2O}$$

$$C_2^= - C_5^= \longrightarrow \begin{array}{c} paraffins \\ aromatics \\ cycloparaffins \\ C_{6+}\ olefins \end{array}$$

Equilibrium between MeOH and DME is reached very rapidly. This mixture then reacts to form light olefins followed by paraffins and aromatics. In early kinetic studies, the two oxygenates were treated as a single species (Chang, 1983; Keil, 1999). In addition, the kinetic rates were derived for fresh catalyst and deactivation was ignored. Aguayo et al. (2005) modelled the reaction kinetics and deactivation for both ZSM-5 and SAPO-18 catalysts and accounted for both the deactivation due to coking and irreversible activity loss that occurs with each regeneration cycle. However, their model lumped the light olefins into one component and is therefore unsuitable for differentiating between ethylene and propylene yield.

Detailed models have been proposed by Mihail et al. (1983) and Park and Froment (2001a,b) who characterized the process based on elementary reactions. Mihail et al.

(1983) considered 27 reactions for the C1-C5 fractions and an additional 26 for higher hydrocarbons. Dehertog and Froment (1991) examined the effect of phosphorus on H-ZSM-5 catalysts. They showed that the space velocity had to be reduced by 75% in order to achieve the same conversion compared to the non-modified zeolite. The phosphorus modification was shown to increase the lower olefin yield at low temperatures; at high temperature (480°C), the effect of phosphorus was not as pronounced. Other investigations of P-modified ZSM-5 showed a similar decrease in conversion and increase in selectivity of up to 70 % at complete methanol conversion (Froment et al., 1992).

Chen et al. (2000) investigated the effect of space velocity over a SAPO-34 catalyst. They found that the coking rate was lower with high methanol feed rates under partial methanol conversion conditions. This was also observed for ZSM-5 by Benito et al. (1996). The increased coking rate was largely attributed to the increased conversion of oxygenates and, to a small extent, to the space velocity. Chen et al. (2000) found that the coke content was proportional to the amount of hydrocarbon formed (per mass of catalyst) and independent of space velocity.

In the present study, the effect of space velocity, temperature and reactor diameter on the activity profile of the catalyst is reported. These parameters are important in the design of MTO reactors for both fixed and fluid bed processes.

5.2.3 Experimental

5.2.3.1 Catalyst

The catalyst was made of 10% CBV28014 (from Zeolyst) imbedded in a Si/Al matrix consisting of Catapal B, Levasil 100s/30% and kaoline which was spray dried and calcined in air at 550°C for 4 h. The average particle size of the resulting catalyst was 100 μm. The powder was contacted with a $(NH_3)_2HPO_4$ solution and then dried and calcined so that the resulting catalyst contained 1.5% phosphorous. It was made into tablets, crushed and sieved into a fraction of 400 – 600 μm.

5.2.3.2 Reactor setup

The experimental setup is shown in Figure 5-1. The experiments were conducted in an 8 mm stainless steal reactor and a 9 mm inner diameter quartz reactor into which a 3 or 6 mm inner diameter quartz reactor could be inserted. The outer diameters of the two insertion tubes were 5.0 and 8.0 mm resulting in an annulus between the inner and outer tubes of 2 and 0.5 mm, respectively. The small insertion tube expanded to an outer diameter of 8.2 mm approximately 3 cm above the catalytic bed reducing the length of the larger annulus to a minimum. The vessel was heated electrically and the temperature was regulated with a PID controller. The distance between the 9 mm quartz tube and the heater was 1.75 mm. The reference temperature for control was measured at the wall of the heater. The temperature at the reactor exit was monitored by a thermocouple placed in a thermowell 10 mm below the bed. Additional thermocouples were inserted in the catalyst bed. When the feed gas was switched from nitrogen to a 10% methanol in

nitrogen mixture, the bed temperature rose 3°C. The pressure in the reactor was maintained between 0 - 0.1 barg for all experiments.

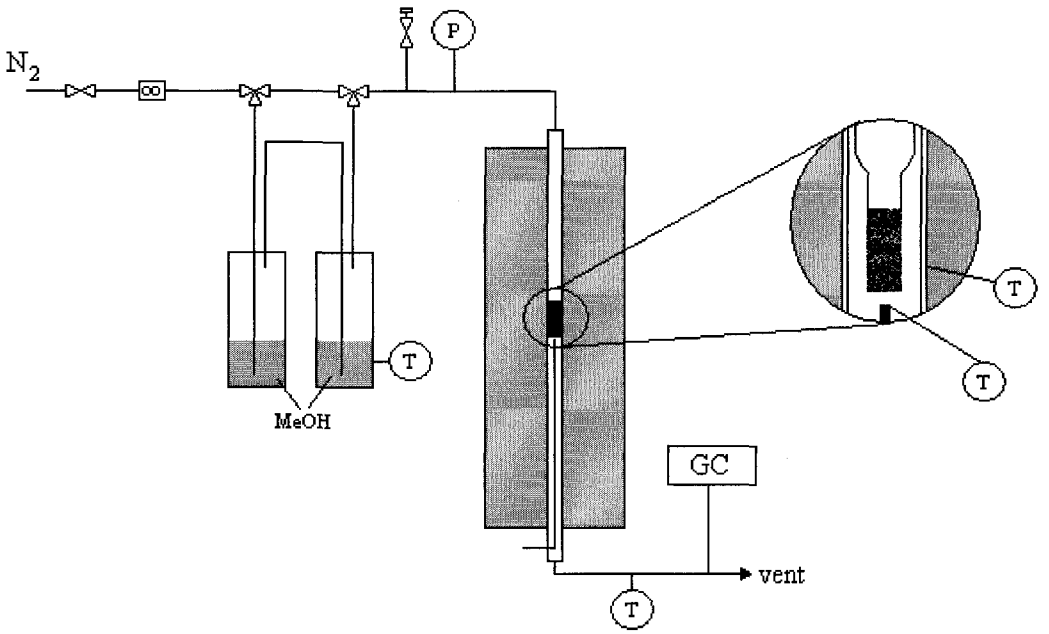

Figure 5-1: Experimental setup

The feed stream was prepared by passing nitrogen through two saturation evaporators containing MeOH: the first was kept at room temperature and the second at 16°C to maintain a 9:1 nitrogen to methanol ratio. A Brooks 5850TR flow controller was used for the nitrogen feed gas. The product stream was analyzed by FID on a Hewlett Packard 5890 series-II GC equipped with a pre-column (Porapak Q 80/100 mesh size – 0.5 mx2.16 mm IDx1/8" OD packed column in stainless steel) followed by a capillary column: CP-PoraPLOT Al2O3, KCl - 10 m x 530 μm x 5 μm. A GC with a TCD measured the CO/CO_2 and other light gases for some experiments.

5.2.3.3 Procedure

The 3 and 6 mm ID reactors were loaded with 0.185 g and 0.53g, respectively, to obtain equal bed lengths. Experiments with 100% MeOH were conducted in the 8 mm reactor with 1 g of catalyst. The reactor was heated to a given set-point in nitrogen before feeding reaction gases. The flow rate was varied between WHSV 0.22 – 2.4 h-1 (based on total catalyst mass). Product gases were analyzed on-line and the experiments were terminated when only equilibrium mixtures of MeOH and DME were detected.

5.2.4 Results

The experiments showed that the space velocity had a significant influence on the deactivation rate and product distribution. Figure 5-2 shows the product distribution at two space velocities and 500°C in the 6 mm reactor. The carbon mass balance was based on C_1-C_9 hydrocarbons only. Production of higher hydrocarbons, CO and CO_2 in the product gas and carbon deposition on the catalyst were neglected. The figure shows that the deactivation rate depends on the methanol feed rate: Methanol breakthrough occurred after 40 h at a WHSV of 0.22 h^{-1} (Figure 5-2a) compared to less than 5 h at a WHSV of 0.43 h^{-1} (Figure 5-2b). By increasing the WHSV to 0.86 h^{-1}, the C_{5+} fraction increased and methanol breakthrough was observed after only a few minutes. The experiments show that the olefin yield decreases with increasing flow rate, which is contrary to some experiments reported in the literature over pure zeolite (Park and Froment, 2001b; Dessau,1986).

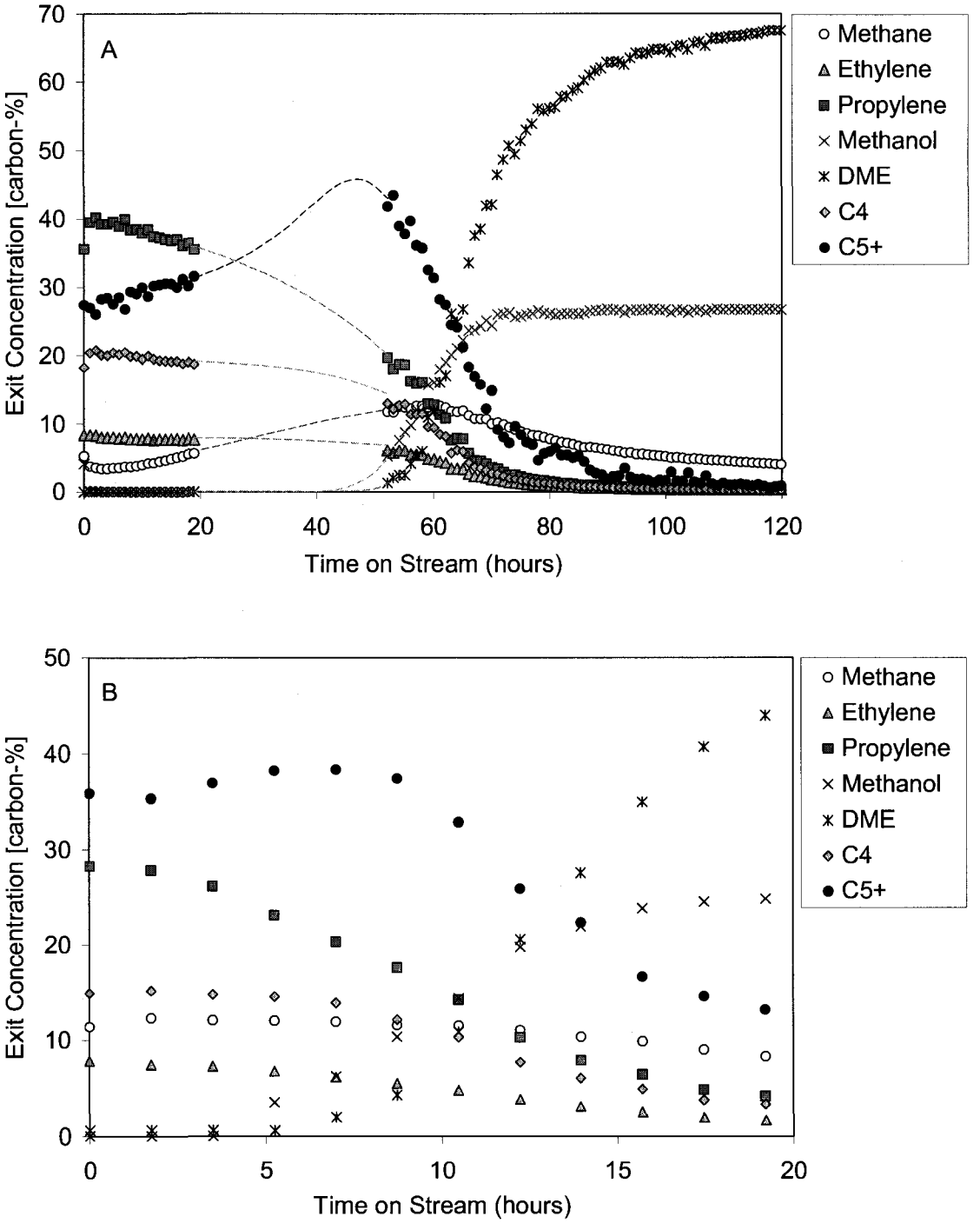

Figure 5-2: MTO product distribution at 500°C in the 6 mm inner diameter reactor with 10% methanol in nitrogen feed: (a) WHSV 0.22 h^{-1} (dashed lines due to missing data) , (b) WHSV 0.43 h^{-1}

The product distribution of the experiments conducted in the 3 and 6 mm reactor after 2 hours on stream is given in Table 5-1Table 5-1. As expected both the yield of light olefins and methane increase with temperatures. However, at 500°C and partial methanol conversion, increased space velocities resulted in a decrease in olefin selectivity. At the highest space velocity (WHSV of 1.43 h^{-1}) in the 3 mm reactor, methane became the dominant hydrocarbon product, accounting for almost half of the total.

Table 5-1: Product distribution after 2 hours on stream in the 3 and 6 mm diameter reactors.

Reactor diameter, mm	3	3	3	6	6	6	6	6
Temperature	500	500	500	500	500	500	450	400
WHSV, h^{-1}	1.47	0.87	0.43	0.86	0.43	0.22	0.23	0.25
Contact time, s	0.18	0.31	0.63	0.32	0.63	1.25	1.24	1.24
Product distribution, %								
Methane	7.2	7.8	7.6	5.3	12	3.6	2	1.2
Ethane	0.3	0.3	0.4	0.2	0.8	0.2	0.1	0.1
Ethylene	0.9	3.1	7.3	2	7.5	8.3	5.4	2.7
Propane	0.1	0.1	0.6	0.1	0.4	0.9	0.6	0.1
Propylene	2	11	32	8.1	28	40	39	16
Methanol	16	22	1	14	0.6	0.1	0	17
DME	69	27	0.1	16	0	0	0.3	28
C_4	1.5	7.8	17	6	15	21	24	11
C_5^+	2.9	21	33	48	35	26	29	24
Sum	99.9	100.1	99	99.7	99.3	100.1	100.4	100.1
Aromatics	0.5	4.6	11.9	7.6	17	13.1	5.8	1.5
Aromatics (in C5+ fraction %)	18.7	21.7	35.4	16	48.1	50.5	19.8	6.3
% MeOH/DME conversion	15	51	98.9	70	99.4	99.9	99.7	55

The first six experiments reported span the regime of partial to essentially full MeOH/DME conversion. The fact that methane predominated at the highest space velocity, where only 15 % of MeOH/DME was converted into hydrocarbons, leads us to

propose that methane forms parallel to the equilibrium reaction from either MeOH or DME, or from both.

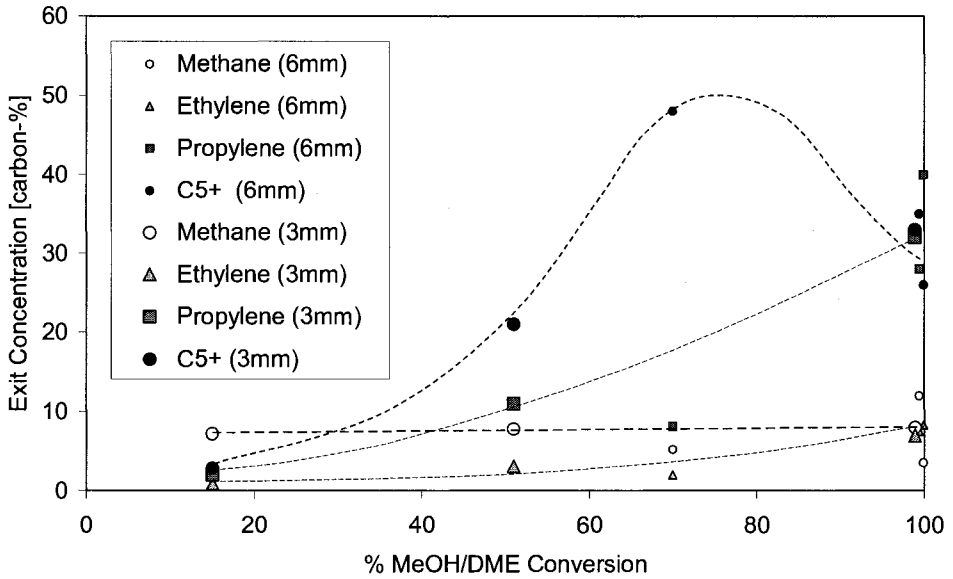

Figure 5-3: Hydrocarbon distribution as a function of oxygenate conversion. Based on experiments in Table 1 at 500°C

At 50-70% MeOH/DME conversion, the C_{5+} fraction predominated, whereas at close to full conversion propylene was the most abundant hydrocarbon. In Figure 5-3, the product distributions shown in Table 5-1 (500°C data) are plotted against the MeOH/DME conversion. The plot demonstrates that: (1) Methane is formed very early in the reaction, before the higher hydrocarbons; (2) At higher conversion, methane levels are largely constant; (3) As reaction progresses, the C_{5+} yield reaches a maximum and subsequently declines while the formation of light olefins accelerates. The latter observation may be rationalized in terms of higher aliphatic (and possibly naphthenic) hydrocarbons undergoing secondary cracking reactions, thus increasing the amount of light products. The data in Table 5-1 show that the C_{5+} fraction at low conversion is low

in aromatics and, therefore, relatively labile with respect to secondary cleavage reactions. The sequence of reactions described above may also explain both the coking pattern (*vide infra*) and the fact that, in experiments conducted at low space velocity with complete MeOH/DME conversion, C_{5+} yields tend to increase as breakthrough approaches. This peak in C_{5+} yields at close to full conversion is apparent from Figure 5-2a and b. It is also evident from Figure 5-4, showing the product distribution as a function of MeOH/DME conversion in an integral experiment conducted with a feed of 100% methanol.

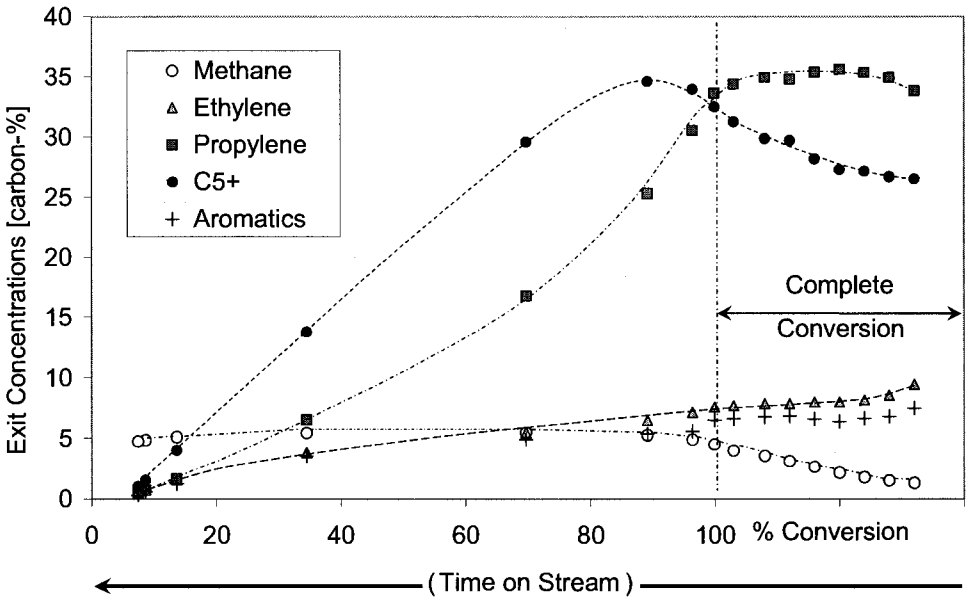

Figure 5-4: Hydrocarbon distribution as a function of oxygenate conversion. Based on experiment at 500°C in 8 mm inner diameter reactor with pure methanol feed. WHSV 2.37 h^{-1}.

Figure 5-4 also shows that the ethylene yield closely parallels that of the aromatics (predominantly xylenes and trimethylbenzenes). This trend agrees with recent data published by Svelle et al. (2006) who concluded that ethylene is formed from xylene and trimethylbenzene intermediates rather than by secondary alkene cracking reactions. Also

apparent from Figure 5-4 is that methane formation gradually increases as breakthrough is approached and subsequently remains virtually constant. This is in full accordance with the suggestions presented above, namely that methane is formed directly from MeOH and DME: In the early stages of the MTO reaction MeOH and DME are completely converted in a narrow zone close to the reactor entrance. As coking progresses the zone where MeOH and DME are present gradually expands through the catalyst bed and the methane formation increases. After breakthrough, i.e., when MeOH and DME extends the full catalyst bed, methane formation reaches a maximum and stays constant thereafter.

We considered channeling as a possible mechanism to account for the lower olefin production at higher flow rates. The average particle diameter to tube ratio in the 8, 6 and 3 mm inner diameter reactors was 16, 12 and 6, respectively, and these values are greater than the standard rule of thumb of 10 for the two larger reactors. In the case of the 3 mm reactor, some channeling might occur over a limited length of the bed. However, channeling is considered to be negligible when the bed length to tube diameter is greater than 10, which is the case of the 3 mm reactor. After unloading the catalyst from the reactor, radial gradients of colour at various distances from the bed entrance were not seen. Finally, all recorded data of the exit composition showed that the MeOH/DME equilibrium was established. Thus, we conclude that channeling effects were insignificant.

In Figure 5-2a breakthrough occurred after less than 50 hours. In a comparative experiment using 100% MeOH as a feed and maintaining almost the same contact time (1.13 sec) the time until breakthrough was 10 hours. Taking into account the total methanol (100% vs 10%) feed and reaction time (10 h vs. < 50 h), the capacity of the catalyst to react is at least twice as high when the feed is 100% MeOH. The increased methanol capacity with pure methanol may be attributable to the higher water vapour pressure that reduces the coking rate (Gayubo et al., 2004). The product distribution was slightly different: with diluted methanol; notably propylene yields were higher whereas the C_4 fraction was lower at the low methanol concentration. Whereas there is virtually no difference in ethylene yields supporting the two different reaction pathways for ethylene and propylene. With pure MeOH feed methane formation was significantly reduced, probably due to the higher water partial pressure

With respect to coking, nitrogen QBET measurements clearly demonstrate a reduction in pore volume of the deactivated catalyst over the entire range, as shown in Figure 5-5. The total pore volume of the fresh, coked and regenerated samples were 0.207, 0.0973 and 0.202 cm^3/g. The lower volume maybe attributable to two mechanisms: accumulated surface carbon deposition and blocking of the pore entrances to the pores. The regenerated catalyst was treated with air at 500°C and, in the region of 20 to 1000 Å, its pore volume distribution is identical to that of the fresh catalyst. However, in the rage of 13-20 Å there appears to be a minor difference between the two. The pore volume of the coked catalyst was unexpectedly higher in this region.

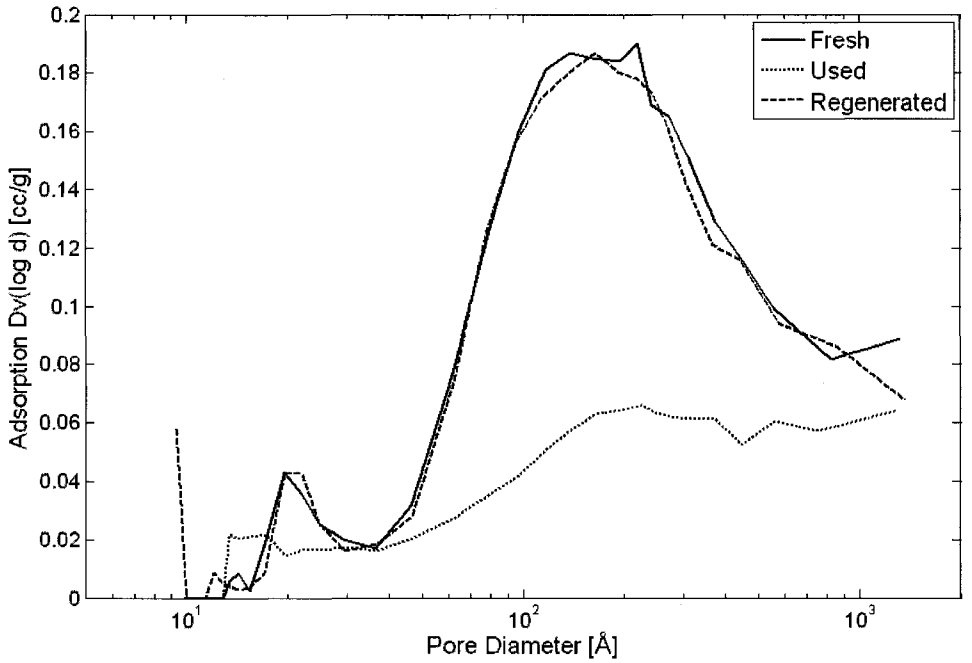

Figure 5-5: Pore size distribution of fresh, coked and regenerated catalyst.

Figure 5-6 demonstrates the coking pattern along the reactor: very quickly the colour changes from beige to gray (less than 10 minutes) and three distinct regions become evident as shown in Figure 5-6c: The middle of the bed is darkest gray; the entrance region (upper box) is slightly brighter; and, in the exit region of the bed (lower box), there is a gradient of colour from dark to light gray going down the reactor. These observations may be rationalized as follows: At the entrance, MeOH and DME reach equilibrium and C-C bond formation occurs to a limited extent. In the middle section, olefin production dominates together with methylbenzenes, the reactive intermediates of the MTO and MTG reactions (Arstad and Kolboe, 2001; Svelle et al, 2006). Chen et al. (2000) found that the oxygenate to olefin reaction was the main source of coke. In the last section, coking continues but only to a limited extent and most likely due to

secondary cracking reactions as all oxygenates would have been consumed. Coking by hydrocarbon decomposition at high temperatures due to significant temperature increase from the exothermic reaction could be ruled out since temperature measurements indicated the bed was isothermal.

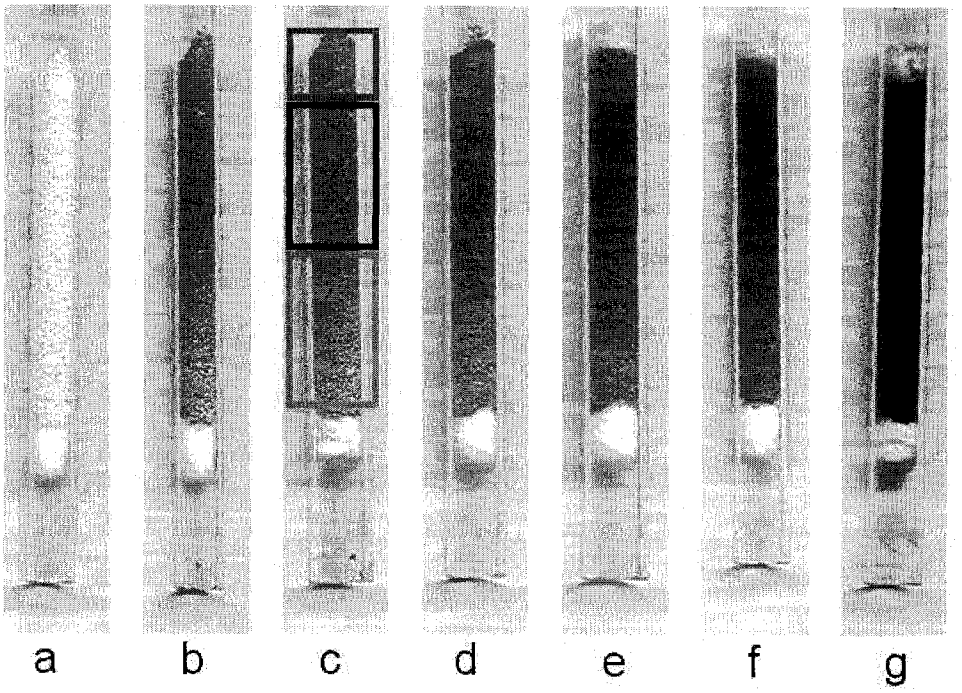

Figure 5-6: Catalyst coking at t = 0, 10, 20, 50, 110, 170, 1310 minutes in the 6 mm reactor, 10% MeOH in nitrogen, T=500°C, WHSV 0.43 g(MeOH)/gcat/h (gas flows from the top down through the bed).

The coking pattern shown In Figure 5-6 is representative of the product distribution given in Figure 5-2b. The product distribution was almost constant during the first 3 hours corresponding to the coking pattern in Figure 5-6b-f. The product distribution appears to be independent of the coke deposition. Methanol breakthrough is observed a short time after Figure 5-6f, which indicates that the strong acid sites are inaccessible.

5.2.5 Conclusions

Experiments conducted at high space velocities in the regime of partial to essentially full methanol and dimethyl ether conversion suggest that methane is formed directly from methanol and/or dimethyl ether. The largely non-aromatic C_{5+} intermediates predominate up until 100% MeOH/DME conversion. At this point, propylene yield is highest due to the cleavage of the C_{5+} fraction. Increasing the feed flow rate lowered the olefin production even at complete oxygenate conversion. The formation of ethylene closely parallels the aromatics, suggesting that it is by splitting off from xylene and trimethylbenzene intermediates in accordance with the labeling studies made by Svelle et al. (2006). Thus, ethylene is *not* a product of secondary cracking reactions.

In the region of full oxygenate conversion, catalyst deactivation depended on contact time: doubling the feed rate (from a WHSV of 0.22 h^{-1} to 0.43 h^{-1}) decreased the deactivation time by a factor of ten. As a result, the methanol capacity of the catalyst increased significantly as the feed rate was reduced.

The product distribution and catalyst methanol capacity (kg of MeOH converted per kg of catalyst) are highly dependent on the feed composition. At reduced MeOH partial pressure (10% methanol in nitrogen), the olefin production was higher compared to pure methanol feed. At the same time, the methanol capacity of the catalyst was decreased significantly. Clearly, increasing the methanol partial pressure increases the catalyst methanol capacity, while increasing the methanol feed by increasing the space velocity

decreases the methanol capacity. This is in contrast to the finding of Chen at al. 2000 for the SAPO-34 catalyst where they concluded that the coke deposition was based on the amount of methanol converted and temperature but not on WHSV.

Based on photographs of catalyst taken at intervals during an experiment, coking rates are low at the reactor entrance where the MeOH/DME reaches equilibrium. The main coking is due to the oxygenate to olefin and intermediates reaction. Following the main reaction zone, coking rates are low as only secondary cracking reactions occur and because the water level has reached its maximum.

5.2.6 References

Aguayo, A. T., Gayubo, A. G., Vivanco, R., Alonso, A., Bilbao, J., (2005). Initiation step and reactive intermediates in the transformation of methanol into olefins over SAPO-18 catalyst. Industrial & Engineering Chemistry Research, 44 (19), 7279-7286.

Arstad, B., Kolboe, S., (2001). The Reactivity of Molecules Trapped within the SAPO-34 Cavities in the Methanol-to-Hydrocarbons Reaction. Journal of the American Chemical Society, 123, 8137-8138.

Benito, P. L., Gayubo, A. G., Aguayo, A. T., Castilla, M., Bilbao, J., (1996). Concentration-dependent kinetic model for catalyst deactivation in the MTG process, Industrial & Engineering Chemistry Research, 35, 81-89.

Chang, C. D., Silvestri, A. J., (1977). The conversion of methanol and other O compounds to hydrocarbons over zeolite catalysts. Journal of Catalysis, 47, 249-259.

Chang, C. D., (1983). Hydrocarbons from methanol. Catalysis Reviews – Science and Engineering, 25, 1-118.

Chang, C. D., (1984). Methanol Conversion to Light Olefins. Catalysis Reviews - Science and Engineering, 26 (3&4), 323-345.

Chen, D., Rebo, H. P., Grønvold, A., Moljord, K., Holmen, A., (2000). Methanol conversion to light olefins over SAPO-34: Kinetic modeling of coke formation. Microporous and Mesoporous Materials, 35-36 121-135.

Chen, J. Q., Bozzano, A., Glover, B., Fuglerud, T., Kvisle, S., (2005). Recent advancements in ethylene and propylene production using the UOP/Hydro MTO process. Catalysis Today, 106, 103-107.

Dehertog, W. J. H., Froment, G. F., (1991). Production of light alkenes from methanol on ZSM-5 catalysis. Applied Catalysis, 71, 153-165.

Dessau, R.M., (1986). On the H-ZSM-5 catalyzed formation of ethylene from methanol or higher olefins. Journal of Catalysis, 99, 111-116.

Froment, G. F., Dehertog, W. J. H., Marchi, A. J., (1992). Zeolite catalysis in the conversion of methanol into olefins. Catalysis 9, 1-64.

Gayubo, A. G., Aguayo, A. T., Atutxa, A., Prieto, R., Bilbao, J., (2004). Role of Reaction-Medium Water on the Acidity Deterioration of a HZSM-5 Zeolite. Industrial & Engineering Chemistry Research, 43, 5042-5048.

Keil, F. J., (1999). Methanol-to-Hydrocarbons: Process Technology. Microporous And Mesoporous Materials, 29, 49-66.

Mihail, R., Straja, S., Maria, G., Musca, G., Pop, G., (1983). Kinetic Model for Methanol Conversion to Hydrocarbons. Chemical Engineering Science, 38, 1581-1591.

Park, T-Y., Froment, G. F., (2001a). Kinetic Modeling of the Methanol to Olefins Process. 1. Model Formulation. Industrial & Engineering Chemistry Research, 40, 4172-4186.

Park, T-Y., Froment, G. F., (2001b). Kinetic Modeling of the Methanol to Olefins Process. 2. Experimental Results, Model Discrimination, and Parameter stimation. Industrial & Engineering Chemistry Research, 40, 4187-4196.

Stöcker, M., (1999). Methanol-to-hydrocarbons: catalytic materials and their Behaviour. Microporous and Mesoporous Materials, 29, 3-48.

Svelle, S., Joensen, F., Nerlov, J., Olsbye, U., Lillerud, K.P., Kolboe, S. Bjørgen, M., (2006). Conversion of methanol in to hydrocarbons over zeolite H-ZSM-5: Ethene formation is mechanistically separated from the formation of higher alkenes. Journal of the American Chemical Society. 128 (46), 14770-14771.

Chapter 6
Trends in the MTO reaction by MS

6.1 Introduction

This chapter will shortly discuss the mass spectrometry (MS) as a viable measurement technique to follow trends in the MTO reaction as well as show trends in the reaction as function of temperature in a fluidized bed reactor. Due to the wide product distribution, product analysis by GC is time consuming and thus identifying optimal catalyst compositions, reactor control and kinetic analysis is essential to accelerate the development of the technology. MS is coupled together with GC measurements to be able detect rapid changes in the reaction kinetics while at the same time allowing for a quantitative analysis in periods of steady state. The focus of this work is twofold: (1) investigate the feasibility of MS to determine key product distribution changes and (2) improve the understanding of the MTO reaction mechanism over a ZSM-5 catalyst

6.2 Experimental

The catalyst for the study of the MTO reaction is a phosphorous modified ZSM-5 zeolite (Si/Al ratio of 140) with a mean diameter of 108 μm. Experiments were conducted in a 46 mm inner diameter fluidized bed and the reaction temperature was varied between 250-550°C with a WHSV between 0.2 – 0.8h^{-1}. The feed consisted of pure methanol, methanol/water (molar ratio 1:1) and methanol/Ar (molar ratio 1:1) mixtures to assess the effect of methanol partial pressure and water. Analysis of the product distribution

were made with a Varian CP3800 GC (FID) and online measurements by a Hiden MS QIC-20 were used to follow the trends in the reaction.

6.3 Results and discussion

Using MS to follow the product distribution of the MTO reaction poses several challenges due to the high level of overlap between the hydrocarbons. The majority of the components have therefore been lumped together with only a few separated individual species. The components that can be separated are water, argon, methane, methanol and DME. All other hydrocarbons overlap each other to such an extent that separation is only viable for component classes as olefin and paraffins.

Compared to the GC, the MS has the advantage that these products or product lumps can be followed in real time compared to the GC where it can take up to an hour to analyze a single sample. To obtain a better understanding of the MTO reaction, an experiment was carried out where the temperature was increased in steps of 50°C from 250°C to 550°C. Figure 6-1 A and B show the conversion of methanol and DME from 250°C to 550°C. It is clear that almost complete conversion is obtained above 450°C. Figure 6-1 C and D shows the production of olefins and methane. Reaction from MeOH and DME to hydrocarbons starts between 300 and 350°C and has a maximum around 500°C. At temperatures above 450°C the methane production increases significantly, especially from 500 to 550°C and at the same time a drop in olefin production is observed. The drop in DME and the increase in olefins in the step from 300 – 350°C before it levels off

are due to an overshoot by a few degrees in the temperature control. Generally, the trends are easy to follow on the MS and could be a valuable technique when following the conversion of MeOH/DME during a reaction/regeneration cycle where it could be a fast way to determine when regeneration is needed. This is most likely more suitable for the SAPO system where the deactivation is fast and time consuming GC measurements will be too slow to be practical. Especially for circulating fluidized beds the MS could help controlling regeneration to obtain optimum operation conditions.

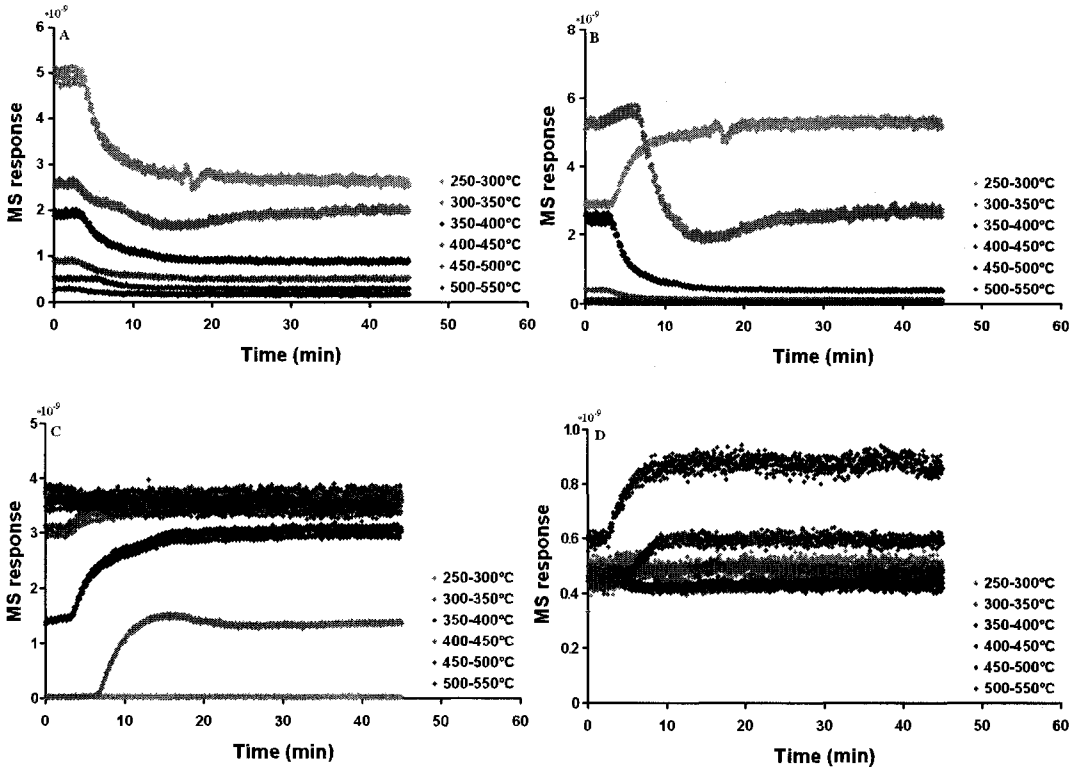

Figure 6-1: MS traces during the MTO reaction with temperature increments of 50°C from 250°C to 550°C. A) Methanol, B) DME, C) Hydrocarbons and D) Methane.

Experiments with different feed compositions and WHSV in the temperature range 450 – 550°C showed clear trends in the product distribution (Figure 6-2). The lower olefins - ethene and propene - increases with temperature as the higher olefins are broken down.

The methane concentration also starts to increase significantly from 500 – 550°C. The influence of feed composition on product distribution decreases with temperature with less spread in the individual components concentrations. This could indicate that the reaction progresses further towards an equilibrium at the highest temperature and that the equilibrium of the hydrocarbons is relatively independent of the feed concentration e.g. water, argon and partial pressure.

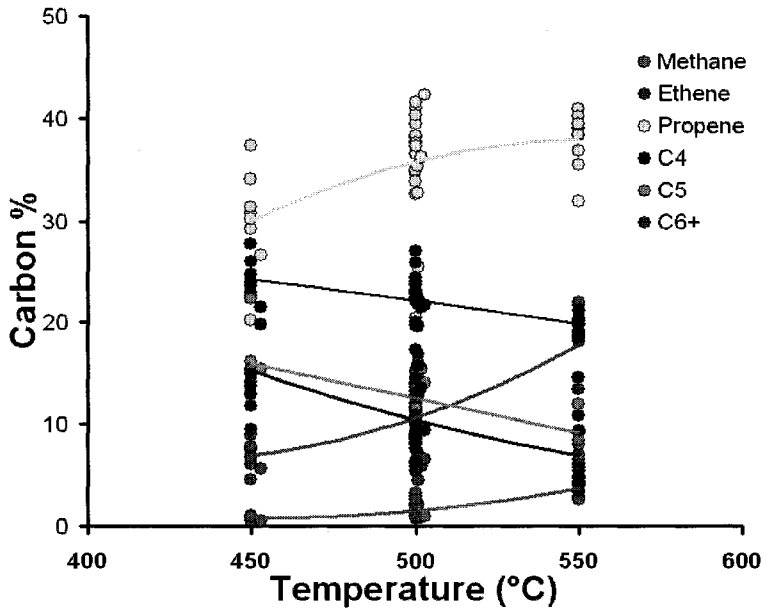

Figure 6-2: Product distribution from the MTO in the temperature interval 450 – 550°C with several different feed compositions

Comparing the concentrations of ethylene to the other hydrocarbons some trends is shown in Figure 6-3. At ethene concentrations below 5%, oxygenate conversions is below 95% and the trends in these data can not be directly compared to the concentrations above 5%. As the ethene concentration increases, the concentration of the higher hydrocarbons decrease with the largest hydrocarbons decreasing the most, this

trend is mostly coupled to the reaction temperature. Propene seems to be relatively independent of ethene and no definite trend can be observed. The scattering in the propene and, to a degree, the C_4 fraction relates to the changes in feed composition and WHSV. The high amount of experimental data gives a good insight into the MTO reaction and form a basis for modelling the reaction.

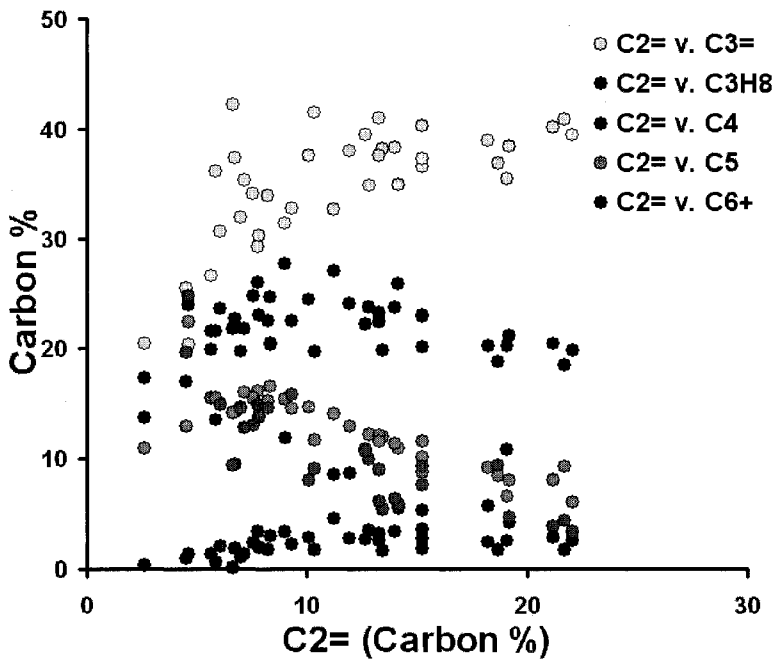

Figure 6-3: Comparison between ethene and other hydrocarbon concentration for the MTO reaction

6.4 Conclusion

The MS have been shown to be able a valuable instrument to follow key components in the MTO reaction with respect to oxygenate conversion and the undesired by-product methane in real time. The MS can be a good analysis tool for the control of the regeneration of the MTO reaction. It does, however, have limited use in following the

main products due to the overlap in the fragments. MTO experiments in the temperature range 450 – 550°C have shown some clear trends in the product distribution both with respect to temperature dependency and relation between the individual components that will help in the determination of a general reaction mechanism for the reaction.

Chapter 7
Kinetic modelling of MTO reaction over ZSM-5 in fluid bed*

7.1 Presentation of the article

The following article present the work related to the methanol to olefins reaction in fluidized bed. The objective of the article is to investigate the MTO reaction kinetic and develop a kinetic model.

Experimental data for the MTO reaction with different feed compositions of methanol either pure or co-feed with argon or water is presented. Based on these experimental data and experiments with 1-hexene feed a kinetic model is proposed based on the hydrocarbon pool mechanism and implemented into a fluid bed model. The fluid bed model is based on a two-phase model with a bubble and emulsion phase. The model is shown to be able to model the system fairly well.

*This article was submitted to I&EC Research

7.2 Kinetic modelling of MTO reaction over ZSM-5 in fluid bed

Mads Kaarsholm*, Finn Joensen†, Roberta Cenni†, Jamal Chaouki, Gregory S. Patience

Department of chemical engineering, École Polytechnique de Montréal, Canada

†Haldor Topsøe A/S, Denmark

7.2.1 Abstract

Reaction of methanol to olefins has been studied in a small scale fluid bed reactor over a phosphorus modified ZSM-5 containing catalyst. Increasing the temperature from 400°C – 550°C showed significantly changes in the product distribution with increased light fractions while changes were not as pronounced when changing feed rate and compositions. Feeding 1-hexene resulted in approximately the same product distribution as with methanol suggesting that the reaction path of the olefins is coupled to equilibrium reactions. A model based on the hydrocarbon pool mechanism is proposed where the olefins are produced through equilibrium reactions with a larger hydrocarbon species in the catalyst pores. The model predicts well the product distribution of the olefinic species in the investigated temperature interval. Further experimental work is required to adequately characterise the paraffin and C_{6+} fractions.

* Corresponding auther. Tel: + 45 45 27 22 55
E-mail address: mkaa@topsoe.dk

7.2.2 Introduction

The Methanol To Olefin (MTO) reaction over acid zeolites was first discovered in the late 1970's by researchers at Mobil when trying to convert methanol over ZSM-5 to others oxygenated compounds[1]. Large effort have since been taken to optimize the reaction with respect to both olefin and gasoline production. Stöcker[2] gave an excellent review of the different catalyst with respect to pore size, zeolite types and effects of zeolite modifications with different metals.

ZSM-5 and SAPO-34 are among the most intensively studied catalysts for methanol conversion. The main difference between the two catalysts is the pore and cage structure: SAPO-34 has narrow pores with a diameter of 3.8Å and large cages, larger aromatic compounds are therefore allowed to form inside the cages but the narrow pores inhibits aromatic intermediates from exiting the cages. ZSM-5 has larger pores with diameters of 5.1 - 5.6Å where larger molecules like aromatics can escape. The SAPO-34 zeolite therefore has a narrow product distribution of C_1-C_5 hydrocarbons while the ZSM-5 zeolite gives products in the range of C_1-C_{10}. Due to the accumulation of large aromatic species inside the cages of SAPO-34 the catalyst deactivates much faster than the ZSM-5[2].

Studies of the MTO reaction carried out in fixed bed reactors[3-6] have drawbacks of radial and axial gradients and a moving coking front[7]. A fluidized bed would be more ideal reactor for exothermic reactions with catalyst deactivation due to uniform temperature and possibility of continuous regeneration. Further, coking will be uniform due to solid circulation. Several investigations of the MTO reaction in fluidized bed have also been

presented with both SAPO-34 and ZSM-5 zeolites[8-11] showing good selectivity. Constant catalyst activity and product distribution can also be obtained due the continuous regeneration.

The kinetics of the MTO reaction have been the focus of many studies over the years. Stöcker[2] summarizes the work on the pathway for the first C-C bond which has been disputed for years. Keil[10] gives a review of the kinetic modelling of the reaction which has mainly been in terms of lumped models. Detailed models have also been developed[12-14]. Recently the group of Bilbao at Universidad del Pais Vasco have collected extensive amount of experimental data and modelled the MTO/MTG reaction kinetics and deactivation on both ZSM-5 and SAPO catalysts[5-6,8,15-17]. This work is reasonable successful at characterising the deactivation both as function of time on stream and regeneration. The modelling of the product distribution has mainly been focused on lumped fractions ignoring for the individual components. However, the individual olefinc species have been considered for kinetic studies over SAPO-34, and a model consistent with the hydrocarbon pool mechanism was proposed[17]. Part and Froment[18] developed a kinetic model based on elementary steps of carbenium ion chemistry in which ethylene and propylene are the main products from methanol and DME and with equilibrium reactions between C_4 to C_8 olefins. Schoenfelder et al.[9] developed a kinetic model for MTO over ZSM-5 that predicts the separate olefins ethylene, propylene and butylenes while lumping the paraffins and higher olefins. The propylene and butylenes are formed by reaction with lower olefins and methanol. The model predicts the experimental data well, but higher hydrocarbons than butylenes were

not quantified in the experimental work and, therefore, been incorporated with the aromatics fraction. Previous work on kinetic models generally neglect cracking of olefins or exclude propylene and ethylene cracking/oligorimerisatrion reactions – though Bos et al[19] included direct reactions from both butylene and propylene to ethylene. Buchanan et al.[20] performed experiments of olefin cracking over ZSM-5 at 510°C with $C_{5=}$ – $C_{8=}$ olefins and showed that $C_{5=}$ cracks to ethylene, propylene and some butylenes while the higher olefins predominantly cracks to $C_{3=}$ - $C_{5=}$ olefins. These reactions have been shown to be relatively fast at this temperature and it appears necessary to include them in the reaction pool in order to model MTO correctly. Zhou at al.[21] reacted ethylene, propylene and n-butylene over SAPO-34 at 450°C in a small scale fixed bed reactor with WHSV ranging from 1 to 424 h^{-1}. They showed that the resulting product distribution was close to equilibrium and proposed a kinetic model where all olefins are in equilibrium with a carbenium ion lump. The model was able to reproduce their results fairly well.

In this work experimental data from the MTO reaction over a phosphorus-modified ZSM-5 catalyst conducted in a small scale fluid bed will be presented. Based on available literature studies and 1-hexene experiments, a kinetic model is proposed. The model is based on the hydrocarbon pool mechanism where the olefins are formed through reversible reactions with a large hydrocarbon species. The fluid bed is modelled as a two phase system with a bubble and an emulsion phase with reaction only in the emulsion phase.

7.2.3 Experimental

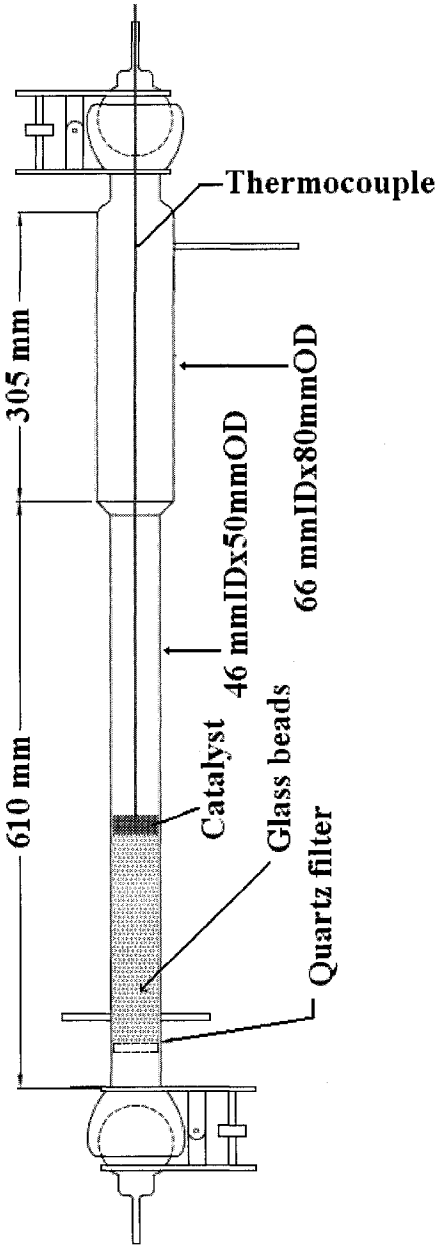

Figure 7-1: Drawing of the glass fluid bed reactor – glass beads are used to elevate the catalyst for catalyst amounts below 100g

7.2.3.1 Equipment

MTO experiments were carried out in a 4.6 cm inner diameter glass fluid bed (Figure 7-1) with a 6.6 cm inner diameter disengagement zone. The gas was distributed through

a quartz frit. The reactor was heated by two electrical band heaters: one in the reaction zone and one in the disengagement zone. Both were controlled based on thermocouples mounted on the exterior surface of the quartz reactor. A thermocouple, inserted in the middle of the reaction zone recorded the temperature. Liquid feed are delivered via a dual piston pump with feed steps of 0.01 ml/min and gas was fed from one of two lines both controlled by Brooks mass flow controllers with a maximum flow rate of 2NL/min. The reactor feed composition may be varied by a Valco 8-port valve. The feed was preheated in a sand bath to 300°C before entering the fluid bed. All flows and reactor temperatures were controlled by a computer. The exit gas was analysed by a Hiden MS QIC-20 and a Varian CP3800 GC. A diagram of the system is shown in Figure 7-2.

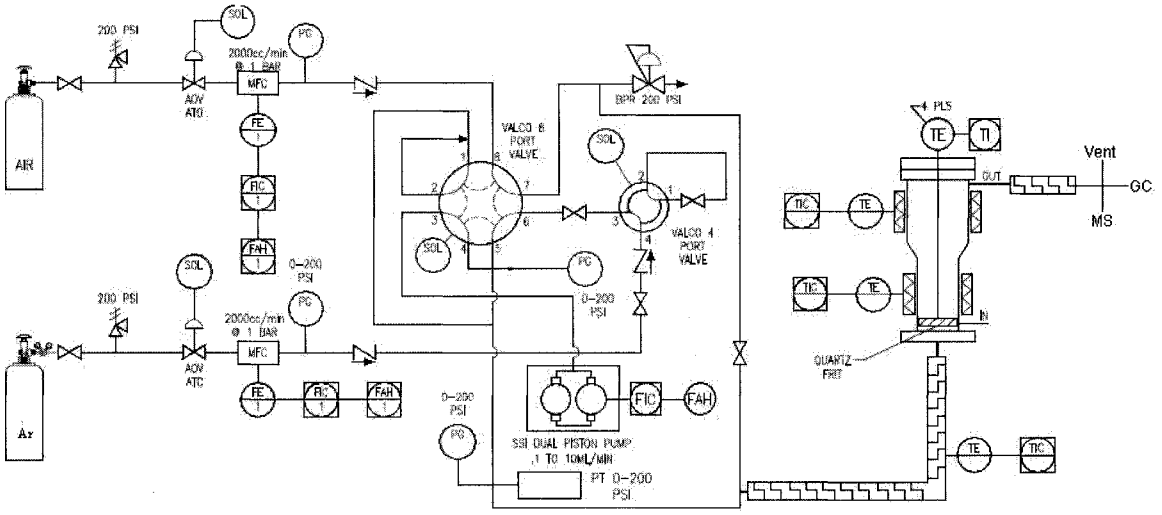

Figure 7-2: Schematic diagram of the experimental setup

7.2.3.2 Catalyst

The catalyst was made of 10% CBV28014 (Zeolyst) imbedded in a Si/Al matrix consisting of Catapal B, Levasil 100s/30% and kaolin which was spray dried and

calcined in air at 550°C for 4 h. The catalyst was contacted with an aqueous $(NH_3)_2HPO_4$ solution and then dried and calcined. The resulting catalyst contained 1.5% phosphorus and had an average particle size of 108 μm. The phosphorous-modification has been done to decrease methane formation. The introduction of Catapal, Levasil and kaolin increase methane formation and impregnation for the fluid bed catalyst significantly decrease the methane formation from these components.

The particle size distribution was measured on a Horiba LA-950. The minimum fluidization velocity at ambient temperature and pressure was 0.00507 m/s in a 3" transparent fluid bed where the tapped particle density and density at minimum fluidization, were also measured. The catalyst properties are listed in Table 7-1.

Table 7-1: Particle properties of the catalyst

d_p < 45	0.4	200 < d_p > 229	2.9
45 < d_p < 68	4.7	229 < d_p < 262	1.6
68 < d_p < 89	16.6	262 < d_p < 350	1.3
89 < d_p < 102	15.5	d_p	108 μm
102 < d_p < 117	16.7	u_{mf}	0.005 m/s
117 < d_p < 133	15.3	ρ_p	1270 kg/m^3
133 < d_p < 153	11.9	ρ_{tapped}	855 kg/m^3
153 < d_p < 175	8.1	ρ_{mf}	744 kg/m^3
175 < d_p < 200	5.0	ε_{mf}	0.405

7.2.3.3 Experimental conditions

The fluid bed was loaded with 20 to 330g of catalyst. The heating elements were positioned 4 centimetres above the distributor and the temperature control of the catalytic bed was therefore not optimal for inventories less than 100g. With larger inventories the temperature just above the distributor was measured to ensure that the temperature gradient over the bed was low (between 3-7°C). For experiments conducted

with below 100g of catalyst glass beads were used to elevate the bed. The gas velocity was at all times below u_{mf} of the glass beads thereby ensuring the catalyst remained above the beads. The feed consisted of pure methanol and mixtures of methanol with water or argon. The total flow rates range from 0.5 – 3.6 NL/min corresponding to superficial gas velocities between 1.3 – 10 cm/s at operating conditions. All experiments were conducted between 400 – 550°C.

7.2.4 Experimental data

Prior to studying the MTO kinetics, the stability of the catalyst with regard to the product distribution was tested in order to establish the influence of coking on activity. An experiment carried out at WHSV of $2.4h^{-1}$ with pure methanol at 550°C showed that the product distribution was stable for the first 15 hours in the fluid bed. Other experiments were performed at 450, 500 and 550°C with a WHSV of $0.4h^{-1}$ with pure methanol feed for 23 hours. The catalyst tested at 550°C was regenerated in air for 14 hours and the experiment was repeated. The product distribution before and after regeneration was similar indicating that irreversible deactivation was minimal. Samples of the catalyst were taken from the experiments and the carbon content analysed by TGA (Thermogravimetric analysis) measurements the maximum carbon was 4.8 wt % after 23 hours at 550°C. The results are given in Table 7-2. The selectivity to carbon is also higher at 550°C where approximately 1.5% of the feed is converted to carbon. All experiments reported hereafter were conducted over a period of 4-5 hours where the

effect of reversible/irreversible deactivation was negligible. Three GC traces were taken for each experiment.

Table 7-2: Carbon deposition on the MTO catalyst

Temperature	TOS (h)	Wt % carbon	selectivity to Carbon %
550	4	0.77	1.38
550	8	1.47	1.33
550	22	4.80	1.67
500	4	0.04	0.07
500	8	0.55	0.49
500	22	1.84	0.61
450	4	0.46	0.82
450	8	1.56	1.41
450	23	1.34	0.42
550*	4	0.74	1.32
550*	8	1.47	1.33
550*	22.5	4.40	1.46

The experimental data are given in Table 7-3. In experiment No. 20, 100 ml/min H_2 were added to the feed gas to investigate the effect of H_2 on the reaction. No change in the product distribution was observed with the addition of hydrogen indicating that hydrogen does not influence the reaction mechanism by hydrogenation of the olefins.

Table 7-3: Experimental results from the fluid bed experiments – product distribution is given in carbon % *100ml H_2 was co-feed with methanol and argon

Exp no.	Temp.	MeOH (l) ml/min	Ar (g) ml/min	Water (l) ml/min	Cat. g	Methane	Ethene	Ethane	Propene	Propane	DME	MeOH	C_4	C_5	C_{6+}
1	402	1.84	139.5	0	220	0.43	8.36	0.15	20.35	2.96	3.69	2.49	24.65	16.49	20.43
2	450	1.84	139.5	0	220	0.81	7.75	0.24	29.28	3.36	0.62	0.89	26.03	16.13	14.89
3	500	1.84	139.5	0	220	2.15	12.84	0.67	34.85	3.47	0.00	0.30	23.70	12.16	9.87
4	546	1.84	139.5	0	220	3.93	19.09	1.14	35.49	2.62	0.00	0.10	20.22	6.55	10.87
5	550	0.92	558	0	220	4.22	18.20	0.94	39.02	2.46	0.00	0.09	20.16	9.13	5.78
6	450	0.92	558	0	220	1.04	7.54	0.19	34.11	2.37	0.21	1.40	24.71	15.45	12.99
7	451	3.68	139.5	0	220	0.80	6.09	0.17	30.74	2.04	3.65	3.06	23.58	14.99	14.88
8	450	0.92	0	0.92	220	0.96	6.75	0.17	37.37	1.90	1.36	5.09	22.64	14.24	9.53
9	553	1.84	0	1.84	220	6.12	13.42	0.73	38.27	1.63	0.78	1.87	19.78	11.98	5.42
10	552	1.84	0	0	330	2.91	19.22	1.22	38.45	4.21	0.00	0.07	21.16	8.05	4.71
11	549	1.84	0	1.84	330	2.60	21.71	0.51	40.88	1.76	0.19	0.20	18.48	9.24	4.43
12	550	1.84	1144	0	330	2.85	21.20	0.51	40.17	2.91	0.00	0.04	20.37	8.04	3.91
13	450	1.84	1144	0	330	0.80	9.02	0.16	31.43	3.43	0.09	0.15	27.73	15.35	11.85
14	499	1.84	0	0	330	1.34	11.21	0.46	32.71	4.63	0.01	0.13	27.01	13.97	8.52
15	499	1.84	1144	0	330	1.23	11.96	0.30	38.05	2.78	0.02	0.16	24.04	12.86	8.62
16	502	1.84	0	0	220	2.00	14.14	0.71	34.93	5.52	0.00	0.04	25.92	10.88	5.86
17	500	1.84	1144	0	220	1.17	12.64	0.23	39.51	2.66	0.00	0.15	22.16	10.87	10.60
18	501	0.92	558	0	220	1.62	15.22	0.56	36.57	3.57	0.00	0.11	22.88	10.15	9.32
19	500	0.92	0	0.92	220	1.43	13.26	0.37	41.07	2.62	0.18	0.45	22.40	12.03	6.20
20*	500	0.92	558	0	220	1.53	13.28	0.41	37.66	3.17	0.00	0.31	23.18	11.53	8.94
21	500	0.92	558	0	220	1.58	14	0.54	38.35	3.44	0	0.63	23.7	11.39	6.35
22	554	0.92	0	0	220	4.89	22.06	1.71	39.50	2.59	0.00	0.01	19.76	6.04	3.44
24	501	0.92	558	0	110	2.95	15.22	0.34	37.27	1.83	0.42	2.72	20.07	11.55	7.63
25	500	0.92	0	0	110	3.23	15.25	0.58	40.29	2.78	0.00	0.75	22.98	8.73	5.40
26	500	1.68	2288	0	20	0.72	2.63	0.06	20.41	0.31	8.29	25.65	13.69	10.90	17.36
27	453	2.50	0	0	50	0.54	5.64	0.06	26.60	1.35	2.10	6.76	21.53	15.47	19.88
28	501	2.50	0	0	50	0.91	7.14	0.11	35.40	1.34	0.70	3.82	21.78	16.00	12.78
29	550	2.50	0	0	50	3.29	6.98	0.26	31.95	1.06	2.13	5.46	19.68	14.62	14.56
31	500	1.68	0	0	50	0.97	8.21	0.14	33.89	1.78	0.48	2.38	22.46	15.16	14.54
32	501	0.84	0	0	50	0.93	9.33	0.19	32.74	2.32	0.26	1.40	22.49	14.55	15.78
34	502	1.68	2288	0	50	0.84	5.85	0.07	36.23	0.66	2.78	3.11	21.50	15.42	13.54
35	450	0.92	558	0	110	0.95	7.82	0.14	30.29	1.91	0.09	8.24	23.01	13.74	13.81
36	550	0.92	558	0	110	2.56	18.69	0.40	36.89	1.75	0.00	3.13	18.80	8.43	9.34

Feeding 1-hexene instead of methanol to the catalyst results in a product distribution similar to the one obtained from methanol feed, indicating that cracking and oligomerization are an important part of the reaction scheme. This is also in agreement with the literature, where investigations on the reaction of $C_{3=}$ – $C_{8=}$ and hexane over ZSM-5 have shown a product spectrums of C_2 – C_{10} together with parafins and aromatic[20,22-24]. Recently Zhou et al.[21] have shown that feeding ethylene, propylene or n-butylene over SAPO-34 gives approximately the same product distribution which is close to the thermodynamic equilibrium. As SAPO-34 and ZSM-5 are both acidic catalysts the reaction mechanism of the light olefins interconversion is likely to be similar and a similar pattern should be expected for ZSM-5.

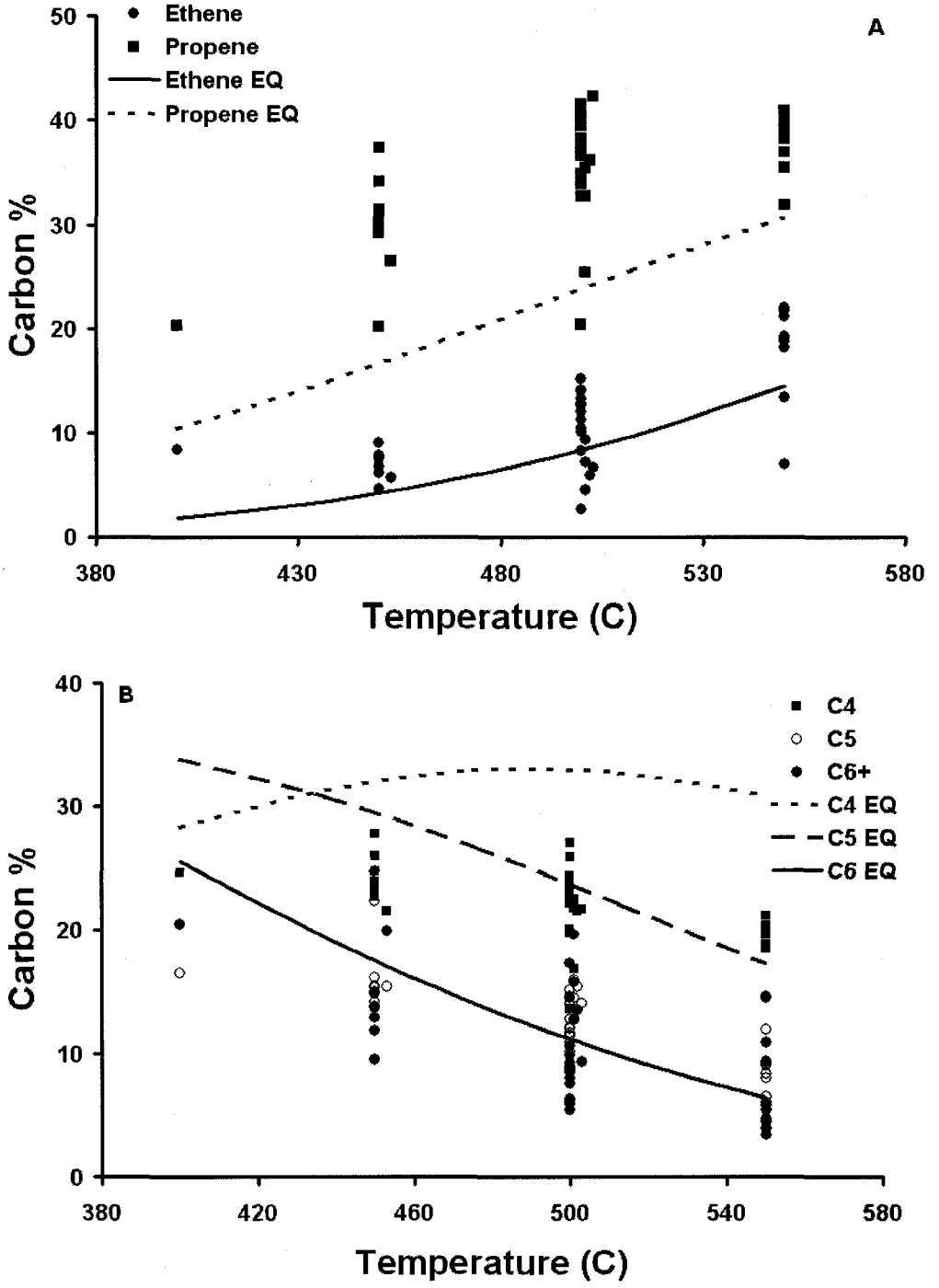

Figure 7-3: Comparison between experimental data and equilibrium composition of the C2 – C6 olefins in the temperature range 400 – 550°C a) ethylene and propylene b)C_4, C_5,C_6

Due to the results obtained in the 1-hexene experiment, the work of Norval et al.[25-26] who have studied the equilibrium of the MTG process over ZSM-5 and the recent work of Zhou et al.[21] it is of interest to establish whether or not the olefins reach equilibrium concentrations. The equilibrium distribution between C_2 – C_6 olefins have been calculated with HCS Chemistry 5 in the temperature range 400 – 550°C where all isomers of the olefins have been considered in the calculations. Figure 7-3 shows that the product distribution and the equilibrium concentration. The experimental data is far from equilibrium concentrations, especially propylene which is higher than the equilibrium concentration, while the C_4 and C_5 are lower. On the other hand, the trends between the equilibrium calculations and experimental data are in agreement.

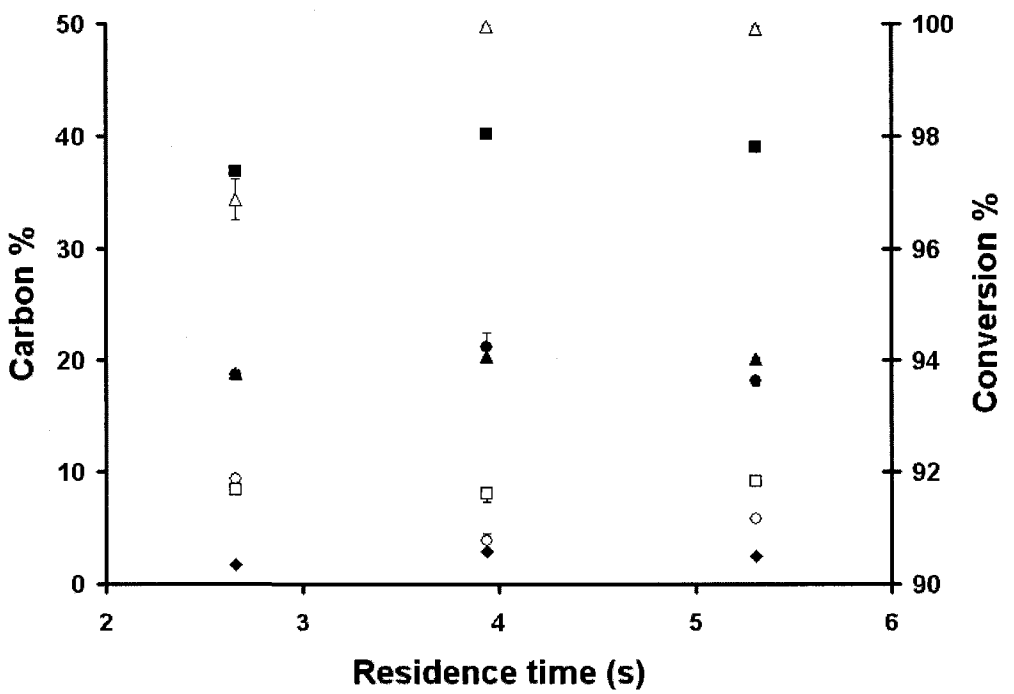

Figure 7-4: Product distribution vs. residence time with methanol/Argon feed (molar ratio 1:1) over ZSM-5 at 550°C. Δ: conversion , ●: ethylene,■: propylene, ◆: propane, ▲: C_4, □: C_5, ○: C_{6+}

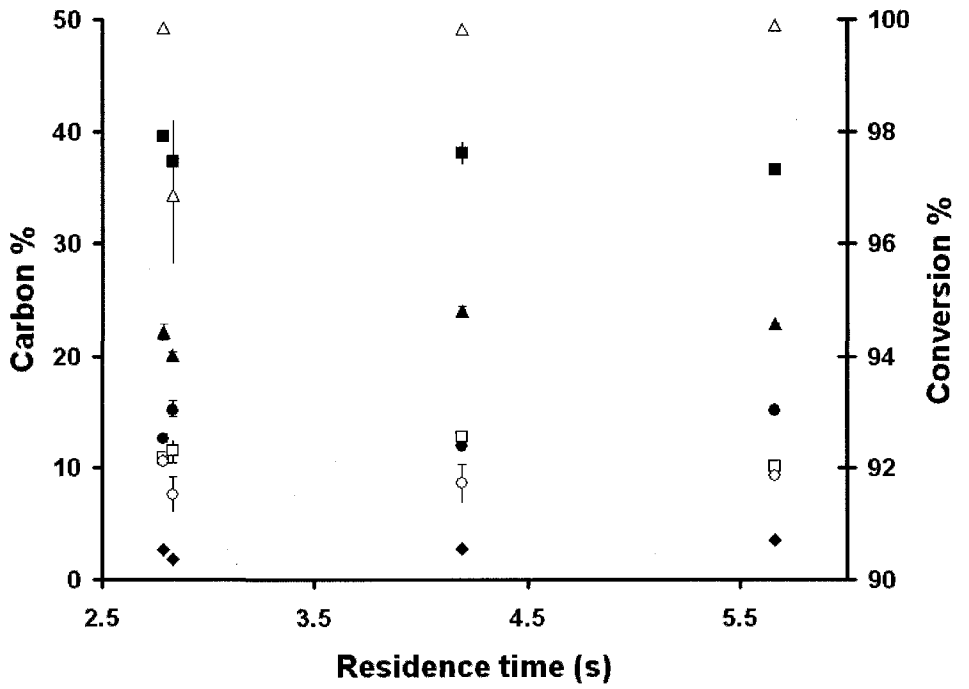

Figure 7-5: Product distribution vs. residence time with methanol/Argon feed (molar ratio 1:1) over ZSM-5 at 500°C. Δ: conversion , ●: ethylene,■: propylene, ◆: propane, ▲: C_4, □: C_5, ○: C_{6+}

Figure 7-4 – 7-6 show the product distribution as function of time with an equimol methanol/argon feed at residence times between 2.5 and 6 seconds. The product distribution is relatively constant and full conversion is obtained after 4 seconds regardless of temperature. The product distribution at each temperature is relatively insensitive to the residence time in the interval investigated. Larger changes are evident with changes in temperature: higher temperatures result in an increase in the ethylene and propylene and a decrease in the higher fractions. The change is largest for ethylene and the C_{6+} fractions. Figure 7-7 shows the product distribution as function of residence time with pure methanol feed. At short residence times, the concentration of higher hydrocarbons increases suggesting that they are intermediates. This was also found in a

previous fixed bed study where an increased C_{5+} fraction was observed as the catalyst began to deactivate indicating that they are intermediates[7].

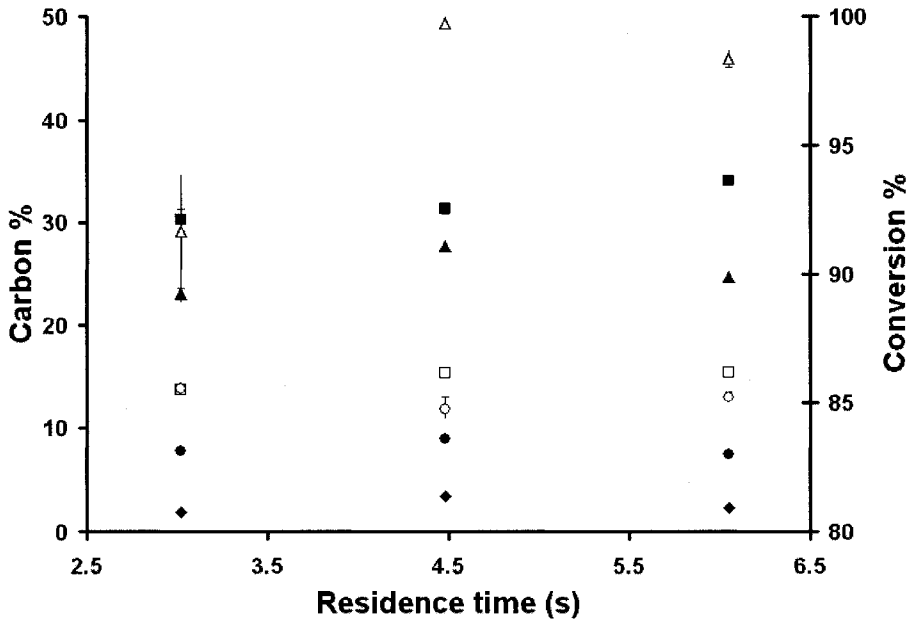

Figure 7-6: Product distribution vs. residence time with methanol/Argon feed (molar ratio 1:1) over ZSM-5 at 450°C. Δ: conversion , ●: ethylene,■: propylene, ◆: propane, ▲: C_4, □: C_5, ○: C_{6+}

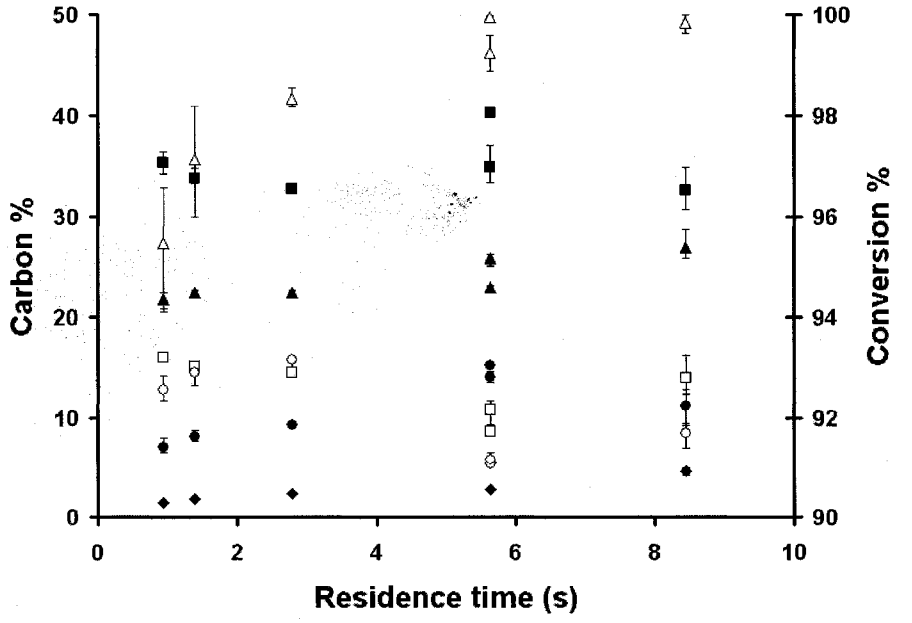

Figure 7-7: Product distribution vs. residence time with pure methanol feed over ZSM-5 at 500°C. Δ: conversion , ●: ethylene,■: propylene, ◆: propane, ▲: C_4, □: C_5, ○: C_{6+}

7.2.5 Fluid bed model

The fluid bed was modelled assuming gas rises predominately in the bubble and the reaction takes place in the catalyst, in the emulsion phase, with interphaes mass transfer between the two. This two phase model is well documented in the literature[27]. The model was used recently by Werther and Hartge[28] to characterize an industrial fluidized bed reactors and by Abba et al.[29] to describe fluidization from bubbling conditions to fast fluidization. For modelling of the fluid bed the following assumptions have been made:

- Gas flow only in the axial direction - dispersion in the radial direction is not considered (with the exception of interphase mass transfer)
- No catalyst in the bubble phase
- The activity of the catalyst is considered constant e.g. no deactivation due to the short reaction time compared to the deactivation time of the catalyst

The mass balance around the bubble and emulsion phases for the model can be written as:
Bubble phase:

$$\frac{\partial(\delta u_b C_{b,i})}{\partial h} = -\delta K_{be}(C_{b,i} - C_{e,i}) + \Gamma \frac{Y_{e,i}}{1 - Y_{e,C_x^+}} \tag{7-1}$$

Emulsion phase:

$$\frac{\partial((1-\delta)u_{mb} C_{e,i})}{\partial h} = \delta K_{be}(C_{b,i} - C_{e,i}) - \Gamma \frac{Y_{e,i}}{1 - Y_{e,C_x^n}} + W(-r_i) \tag{7-2}$$

Where Γ is the gas expansion due to reaction, which considered to go to the bubble phase by formation of bubbles in the emulsion phase. The implemented equations are

given below and a schematic drawing is shown in Figure 7-8. The equations were discretized using a block element approach with the number of blocks as a parameter the implemented equations are given in Equation 7-3 and 7-4.

$$0 = -F_{b,n} y_{b,i,n} + F_{b,n-1} y_{b,i,n-1} - \frac{\delta}{1-\delta} V_e K_{be} \left(C_{b,i,n} - C_{e,i,n}\right) + \sum_i^N \left(W_n(-r_i)\right) \cdot \frac{y_{e,i,n}}{1 - y_{e,C_x^+,n}} \tag{7-3}$$

$$0 = -F_{e,n} y_{e,i,n} + F_{e,n-1} y_{b,i,n-1} + \frac{\delta}{1-\delta} V_e K_{be} \left(C_{b,i,n} - C_{e,i,n}\right) - \sum_i^N \left(W_n(-r_i)\right) \cdot \frac{y_{e,i,n}}{1 - y_{e,C_x^+,n}} + W_n(-r_i) \tag{7-4}$$

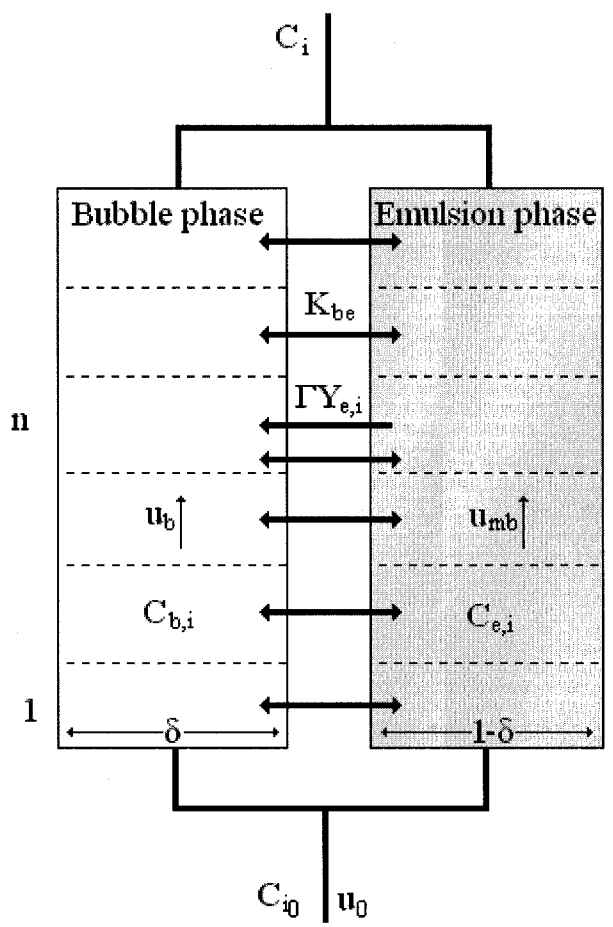

Figure 7-8: Schematic drawing of the fluid bed model.

Optimization of parameters has been done with the use of the simplex method and the error calculations have been evaluated from Equation 7-5

$$R_i^2 = 1 - \frac{\sum_n^N x_{i,n,\exp}\left(x_{i,n,cal} - x_{i,n,\exp}\right)^2}{\sum_n^N \left(x_{i,n,\exp} - \bar{x}_{i,\exp}\right)^2} \tag{7-5}$$

The hydrodynamic correlations used to in the fluid bed calculations are given in Table 7-4. The mass transfer coefficient correlations used in this work is the one from Sit and Grace[30]. The bubble diameter has been calculated form the correlation of Mori and Wen[31]. The used catalyst is Geldart A particles and the minimum bubbling velocity is therefore used in the correlations for the gas in the emulsion phase. The molecular diffusion coefficient is not known and has been estimated to be 0.4 cm^2/s, based on the average binary diffusion coefficient between mixtures of methanol, DME and water. Since a porous plate distributor and relatively low gas velocities are used in the work the initial bubble size is small, below 5 mm in the first centimetre of the bed. The mass transfer coefficient in the first part of the bed is therefore high and no limitations on the mass transfer are expected. General values of the mass transfer coefficient are in the range of 3 – 15 s^{-1} at the exit of the bed with the lowest value at the highest gas velocity and catalyst inventory.

Table 7-4: Hydrodynamic correlations

Variable	Correlation	Ref
Mass transfer coefficient	$k_{be} = \frac{u_{mb}}{3} + \left(\frac{4D\varepsilon_{mf}\bar{u}_b}{\pi \bar{d}_b}\right)^{1/2}$, $K_{be} = \frac{6k_{be}}{d_b}$	Sit and Grace[30]
Bubble diameter	$d_b = d_{bm} - (d_{bm} - d_{b0})\exp\left(\frac{-0.3h}{D_t}\right)$ (cm) $d_{b0} = 0.00376(u_0 - u_{mb})^2$, $d_{bm} = 0.652(A_t(u_0 - u_{mb}))^{0.4}$	Mori and Wen[31]
Bubble velocity	$u_b = u_0 - u_{mb} + 0.711(gd_b)^{1/2}$	
Minimum fluidization velocity	$u_{mf} = \frac{\mu}{d_p \rho_g}\left[\left[(33.7)^2 + 0.0408\left(\frac{d_p^3 \rho_g (\rho_s - \rho_g) g}{\mu^2}\right)\right]^{1/2} - 33.7\right]$	Wen and Yu[32]
Minimum bubbling	$\frac{u_{mb}}{u_{mf}} = \frac{2300\rho_g^{0.126}\mu^{0.523}\exp(0.716F)}{d_p^{0.8} g^{0.934}(\rho_p - \rho_g)^{0.934}}$	Abrahamsen and Geldart[33]
Bubble fraction	$\delta = \frac{u_0 - u_{mb}}{u_b - u_{mb}}$	

7.2.6 Kinetic model

Several kinetic models have been proposed for the MTO reaction, mostly over ZSM-5 and SAPO zeolites[5,8-9,14,17-19,34-36]. The main difference in the models based on ZSM-5 and SAPO is the addition of C_6^+ compounds in the models with the ZSM-5 zeolite. Further it has been shown through ^{13}C experiments that the catalytically active reaction intermediates in ZSM-5 and SAPO-34 are somewhat different[37,38]. Transient $^{12}C/^{13}C$ methanol conversion studies on ZSM-5 showed that, upon switching from $^{12}CH3OH$ to $^{13}CH3OH$, the ^{13}C content of ethylene closely follows that of the aromatics and that the higher olefins to a considerable extent are formed from methylation and interconversion.

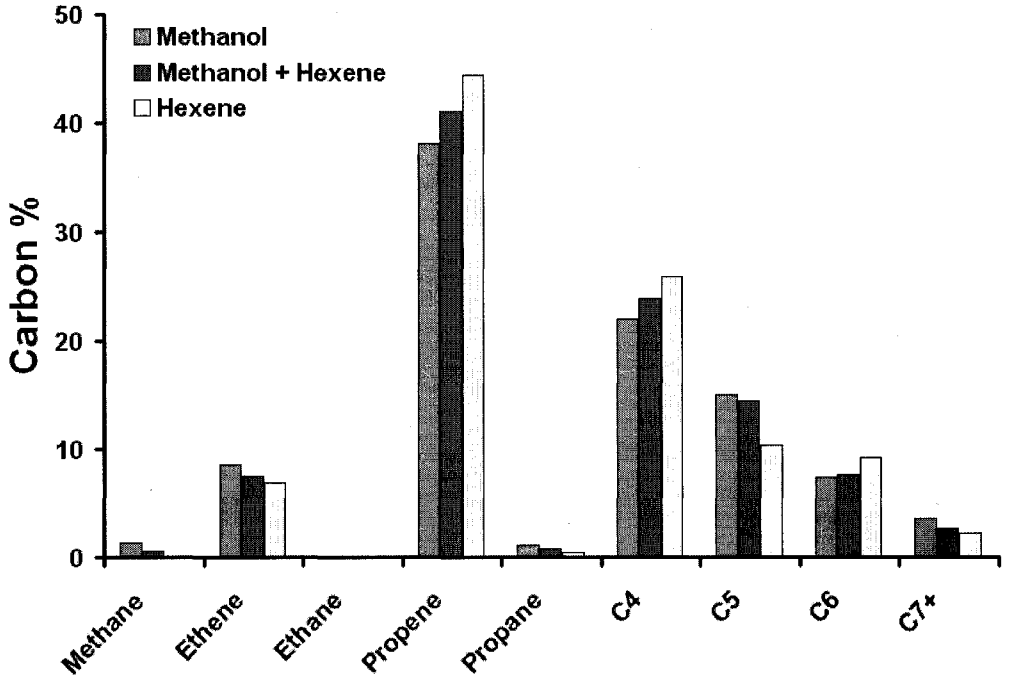

Figure 7-9: Product distribution of reaction over ZSM-5 with three different feed compositions and a total inlet flow rate of 1.57 L/min at 500°C 1) Methanol/Argon molar ratio 1:2 2) Methanol/1-hexene/Argon molar ratio 9:1:20 and 3) 1-hexene/Argon molar ratio 1:2

The experiments with 1-hexene in argon feed over ZSM-5, previously described, have shown that the product distribution is quite similar to the product distribution with pure methanol feed. Figure 7-9 shows the product distribution of experiments made with methanol and 1-hexene diluted in Argon feed over ZSM-5 catalyst with constant inlet flow rate. The product distributions are similar, although there are some changes in the individual olefin fractions. Feeding 1-hexene yields slightly more propylene, butylenes and hexenes compared to feeding methanol and less of the other olefins. Methane is formed from methanol/DME and not from the olefin reactions which also have been found from fixed bed experiments[25]. Since no methane is formed, formation of pentenes most likely happens from cracking of higher olefins formed by oligomerization and not

from direct cracking of 1-hexene. Propane and aromatic compounds are also observed in the exit gas with 1-hexene but to a lesser degree than with methanol.

Based on the product distribution of the experiments with methanol and 1-hexene feed the product distribution looks like it is highly dependent on the cracking and oligomerization reactions and the exact route from methanol to hydrocarbons might therefore not be crucial to the product distribution. A route from higher olefins to ethylene and propylene should also be included in the kinetics, which in most cases is not present in the current available models.

The kinetics of the MTO reaction are complicated, involving oxygenates, paraffins, olefins and aromatics, with the main components being the light olefins ethylene and propylene. The kinetic model is developed to enable the prediction of the main fractions of the MTO process. Ethylene and propylene are taken as individual components while the olefins and paraffins in the C_4 and C_5 fractions are lumped together.

The kinetic scheme that has been used to model the reaction is based on fast reaction between methanol and DME to give an equilibrium composition. Methanol and DME react to form a hydrocarbon pool component (C_x^+), which in this work has been taken as decene. C_x^+ is considered to react to each of the C_2-C_6 olefins through reversible reactions. The C_x^+ is treated as a component related to the catalyst and therefore only present in the emulsion phase.

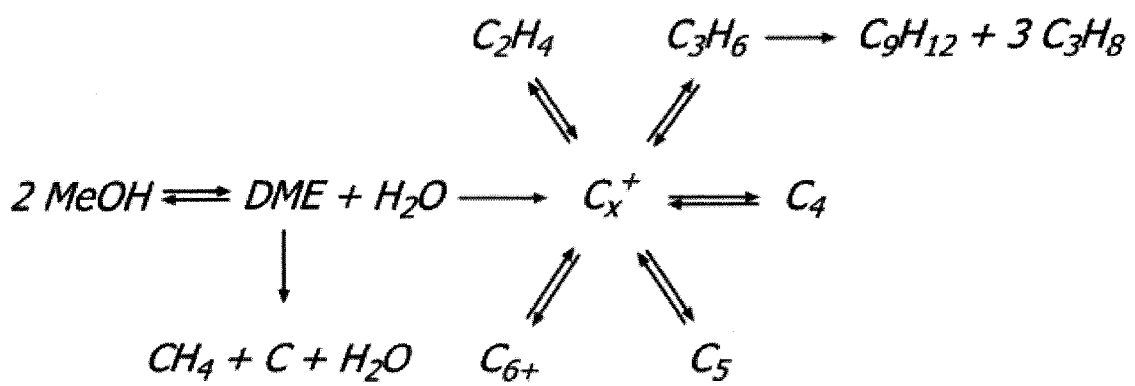

Figure 7-10: Schematic drawing of the kinetic model

Reactions for the formation of aromatics have been taken into account and are assumed to form from propylene and the excess hydrogen goes to the formation of paraffins. The aromatic compound in this work is taken as trimethylbenzene and the paraffin as propane. Methane is assumed to be formed directly from methanol and the extra carbon present in the reaction from methanol to methane is assumed to go to carbon formation since CO and CO_2 was not measured in amounts that could justify reaction to these components. All reactions with the exception of the MeOH/DME equilibrium have been regarded as first order reactions and the influence of water have also been taken into account the reactions are listed in Table 7-5 a schematic drawing is shown in Figure 7-10.

The influence of water in the kinetics is taken into account in terms of equation 7-6; the constants in K_w have been found by optimization. In the calculation Z is in the range 0.8 – 1, the effect large but it does improve the predictions especially when water is co-feed.

$$Z = \frac{1}{(1 + K_W C_W)} \text{ where } K_w = 3.6 \exp\left[\frac{-12.1}{R}\left(\frac{1}{T} - \frac{1}{T_0}\right)\right] \tag{7-6}$$

The temperature dependency of the reactions is taken into account with the Arrhenius equation with a reference temperature of 500°C.

$$k = k^* \exp\left[\frac{-E_a}{R}\left(\frac{1}{T} - \frac{1}{T^*}\right)\right] \tag{7-7}$$

Table 7-5: Kinetic model with optimized parameters for k_0 and activation energy k* is calculate with a reference temperature of 500°C

No	Reaction	Reaction rate	k_0	k^* ($m^3/(kg \cdot s)$)	Ea (kcal/mol)
1	$2CH_3OH \leftrightarrow C_2H_5OH$	Considered in Equilibrium			
2	$10CH_3OH \rightarrow C_x^+ + 10H_2O$	$-r_2 = k_2 C_{MeOH} Z$	1.7	$2.83 \cdot 10^{-2}$	6.28
3	$5C_2H_5OH \rightarrow C_x^+ + 5H_2O$	$-r_3 = k_3 C_{DME} Z$	9	$4.43 \cdot 10^{-4}$	15.2
4	$C_x^+ \rightarrow 5C_2H_4$	$-r_4 = k_4 C_{C_x^+} Z$	$2.70 \cdot 10^5$	0.508	20.2
5	$5C_2H_4 \rightarrow C_x^+$	$-r_5 = k_5 C_{C_2H_4} Z$	14.6	$1.63 \cdot 10^{-5}$	21.0
6	$C_x^+ \rightarrow \frac{10}{3} C_3H_6$	$-r_6 = k_6 C_{C_x^+} Z$	$2.76 \cdot 10^3$	1.56	11.46
7	$\frac{10}{3} C_3H_6 \rightarrow C_x^+$	$-r_7 = k_7 C_{C_3H_6} Z$	65.0	$2.05 \cdot 10^{-4}$	19.41
8	$C_x^+ \rightarrow 2.5C_4H_8$	$-r_8 = k_8 C_{C_x^+} Z$	87.1	0.940	6.94
9	$2.5C_4H_8 \rightarrow C_x^+$	$-r_9 = k_9 C_{C_4H_8} Z$	0.23	$2.31 \cdot 10^{-5}$	14.12
10	$C_x^+ \rightarrow 2C_5H_{10}$	$-r_{10} = k_{10} C_{C_x^+} Z$	0.73	0.467	0.69
11	$2C_5H_{10} \rightarrow C_x^+$	$-r_{11} = k_{11} C_{C_5H_{10}} Z$	$1.33 \cdot 10^{-4}$	$1.03 \cdot 10^{-5}$	3.92
12	$C_x^+ \rightarrow \frac{5}{3} C_6H_{12}$	$-r_{12} = k_{12} C_{C_x^+} Z$	2.52	0.893	1.59
13	$\frac{5}{3} C_6H_{12} \rightarrow C_x^+$	$-r_{13} = k_{13} C_{C_6H_{12}} Z$	13.5	$2.44 \cdot 10^{-3}$	5.23
14	$6C_3H_6 \rightarrow C_9H_{12} + 3C_3H_8$	$-r_{14} = k_{14} C_{C_3H_6} Z$	$1.11 \cdot 10^{-4}$	$4.23 \cdot 10^{-5}$	1.48
15	$2CH3OH \rightarrow CH_4 + C + 2H_2O$	$-r_{15} = k_{15} C_{MeOH} Z$	3.46	$1.11 \cdot 10^{-2}$	8.80

7.2.7 Modelling results

The parameters in the model were estimated by minimizing Equation 7-5 with simplex. The k^* and E_a values were optimized simultaneous with a reference temperature of 500°C. Since the C_{6+} fraction was measured as a lump fraction and the aromatic have

not been measured specifically the C_{6+} and aromatic fractions in the model account for the total measured C_{6+} fraction. The methanol reaction to DME is considered to be in equilibrium due to high reaction rate at the reaction temperature. The results are presented in Table 7-5. The rate constants from decene to olefins at 500°C are generally 4-5 orders of magnitude higher than the reverse reaction. Furthermore, the reaction from methanol to decene is approximately 10 times faster than from hexene to decene. Calculations of the 1-hexene experiments with the obtained kinetics shows only 11% 1-hexene conversion versus the 89% conversion observed during the experiment. It is evident that the model does not accurately describe the cracking of the higher olefinic species and further investigation into this part of the kinetic model is needed for a more accurate description.

The activation energy values of the C_x^+ to olefin reactions decreases with an increase in olefin mass. This agrees with experimental findings where increasing temperatures leads to higher concentrations of the lower olefins. The values of the activation energies are higher than the values reported by Gayubo et al.[17] which were in the range of 55 – 70 kj/mol for ethylene and propylene and 20-25 kj/mol for the higher olefins. Their work was based on SAPO catalyst and the difference in the active sites on the catalyst compared to the ZSM-5 might influence the activation energies to some extent.

Looking at the difference in the forward and backward reactions from the hydrocarbon pool species to the olefin, it is clear that the reverse reaction is much slower. Zhou et al.[21] have reported reaction rates for similar reactions in a SAPO catalyst at 450°C and they reported that the reaction rates were all of the same order of magnitude. The large

difference in reaction rates could be due to a large fraction of higher components in the SAPO catalyst remain in the pores compared to the ZSM-5.

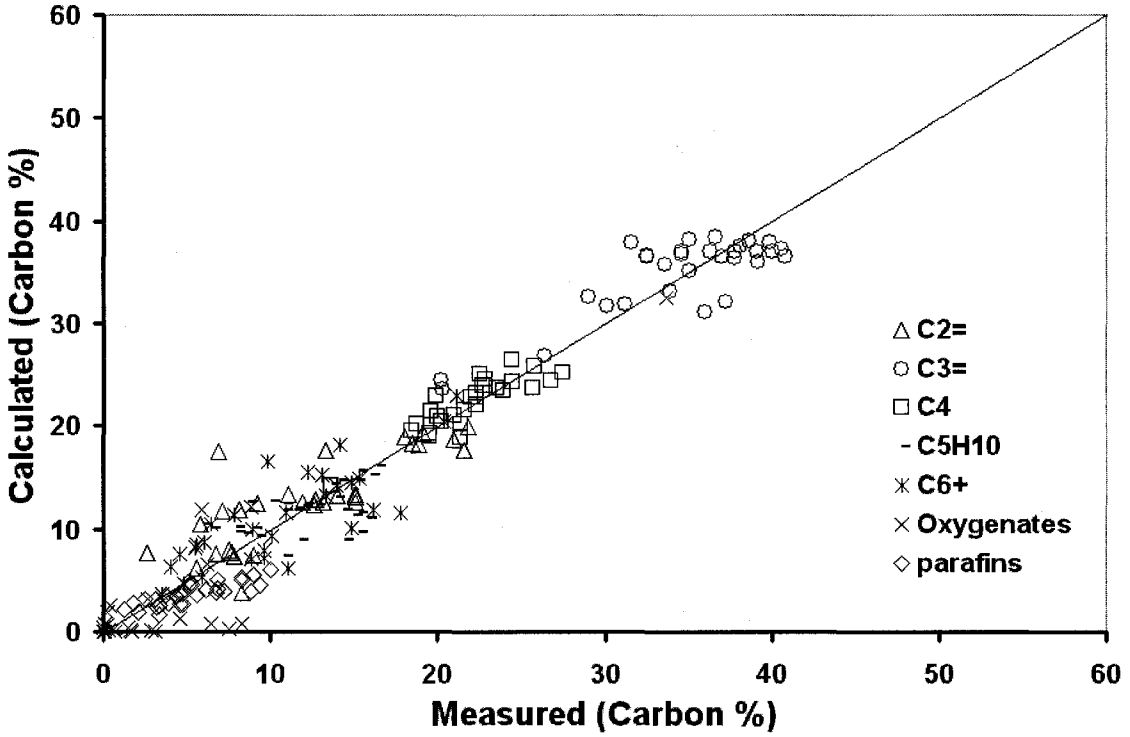

Figure 7-11: Comparison of the calculated product distribution to the measured data.

The calculated and experimental data are compared in Figure 7-11. The model capture the overall trends quite well but requires improvements to simulate the species concentrations. The model is poor in representing the trends for the C_{6+}, paraffin fractions and oxygenate conversion.

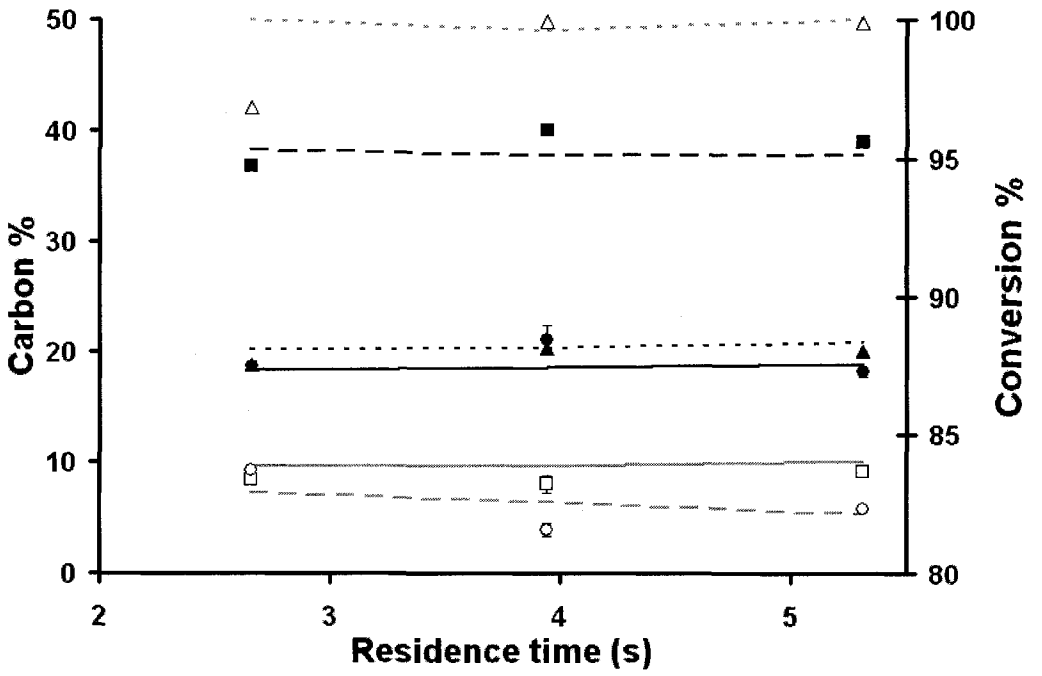

Figure 7-12: Measured (points) and calculated (lines) data at 550°C with methanol/argon (ratio 1:1) feed as function of residence time in the fluid bed. Δ(····): conversion: ●(—): ethylene,■(---): propylene, ▲(····): C_4, □(—): C_5, ○(---): C_{6+}.

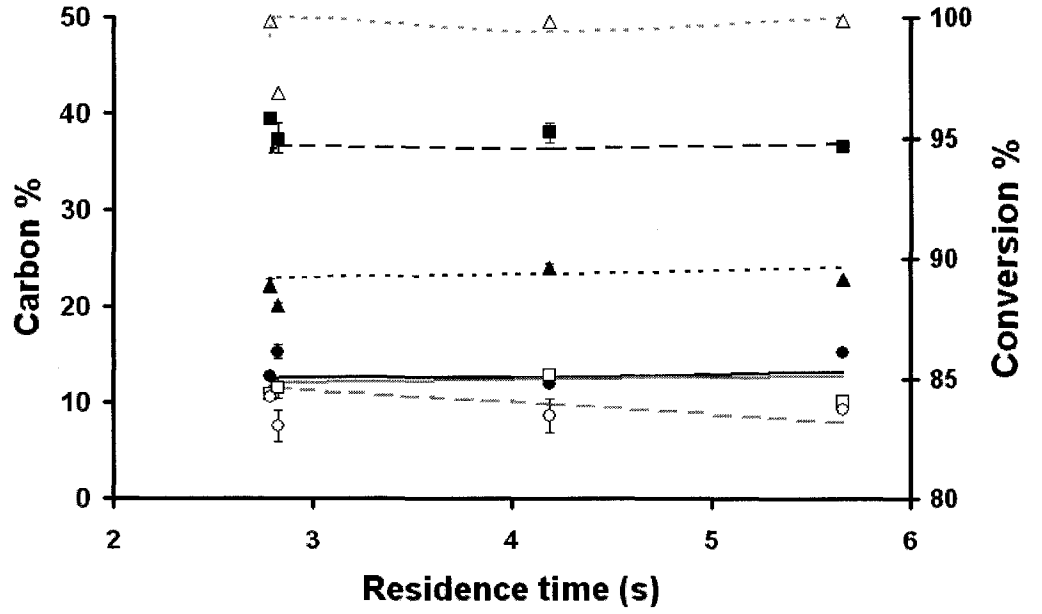

Figure 7-13: Measured (points) and calculated (lines) data at 500°C with methanol/argon feed (ratio 1:1) as function of residence time in the fluid bed. Δ(····): conversion: ●(—): ethylene, ■(---): propylene, ▲(····): C_4, □(—): C_5, ○(---): C_{6+}.

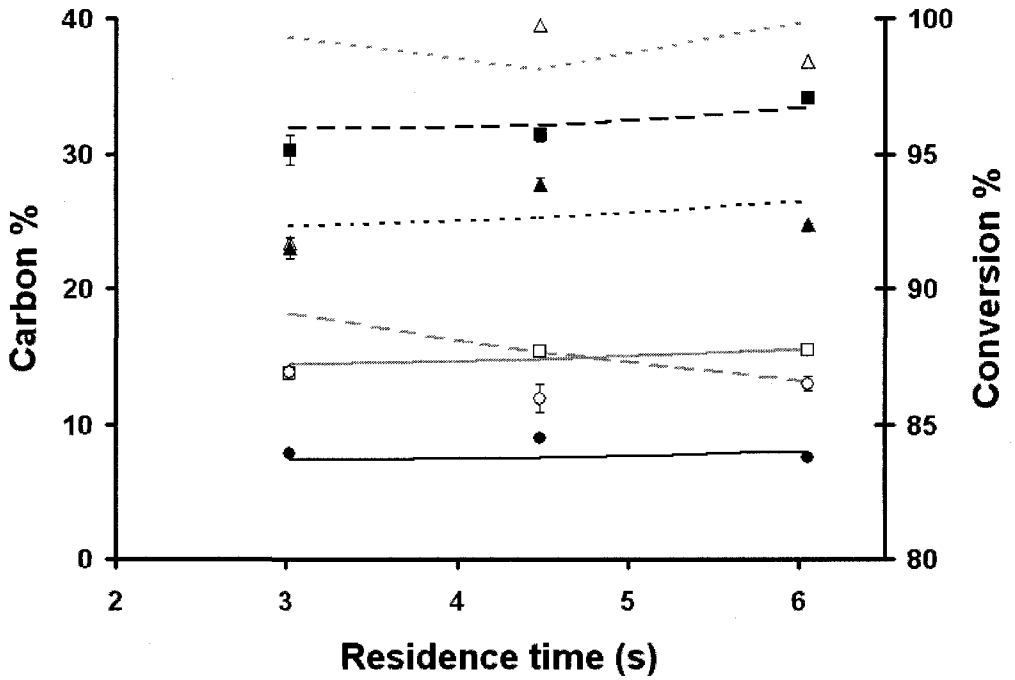

Figure 7-14: Measured (points) and calculated (lines) data at 450°C with methanol/argon feed (ratio 1:1) as function of residence time in the fluid bed. Δ(····): conversion: ●(—): ethylene,■(---): propylene, ▲(····): C_4, □(—): C_5, ○(---): C_{6+}.

Figure 7-12 – Figure 7-14 compare the experimental data and the calculations with methanol/argon feed at three different temperatures. Overall, the calculations of the olefins are in agreement with the experimental data with the exception of the C_{6+} fraction. This could be because the C_{6+} fraction lumps both aromatics and large olefins. The mechanism for these fractions most certainly are different and therefore require separate kinetics. However, they only represent a small fraction of the overall product. Figure 7-15 shows the calculated and measured data at 500°C with a feed consisting of methanol. The same trends as for the methanol/argon feed are observed. Overall, the model is able to fit the experimental data fairly well from 450°C to 550°C especially with respect to the main olefin species.

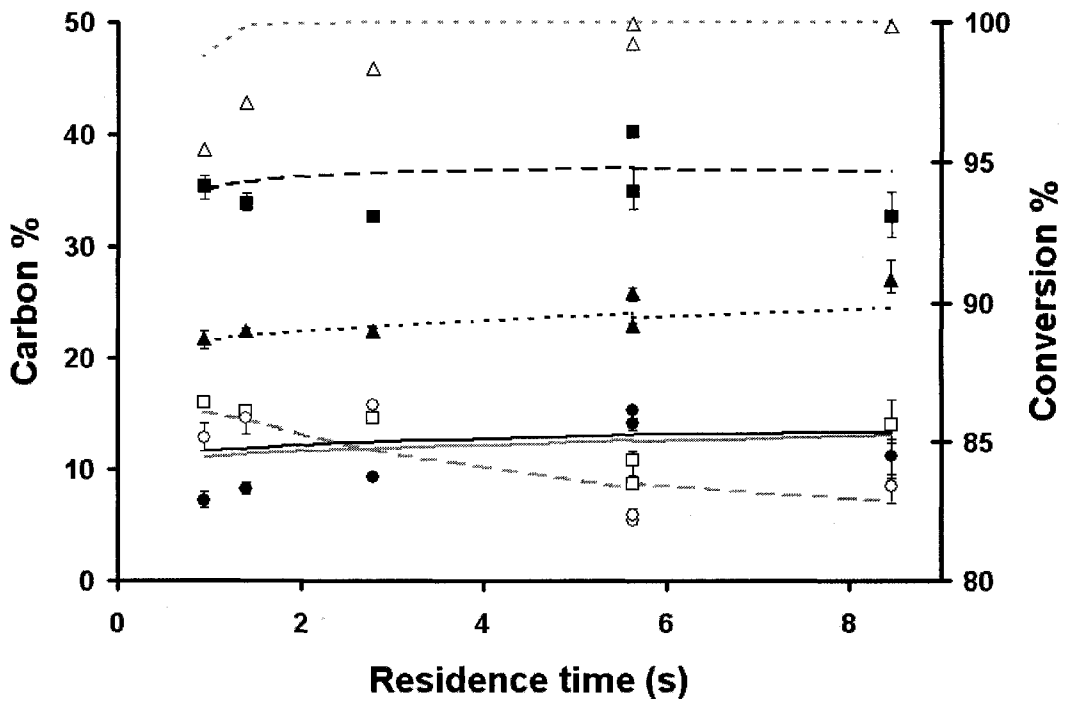

Figure 7-15: Measured (points) and calculated (lines) data at 500°C with methanol feed ratio 1:1 as function of residence time in the fluid bed. Δ(····): conversion: ●(—): ethylene,■(---): propylene, ▲(····): C_4, □(—): C_5, ○(---): C_{6+}.

7.2.8 Conclusion

Experimental data for the MTO reaction in fluid bed show that methanol and 1-hexene feed yield approximately the same product distribution. Methane formation is almost non-existent with 1-hexene feed compared to methanol feed indicating that methane is predominately formed from oxygenates. When oxygenates are converted to hydrocarbons, they follow the same reaction mechanism as with 1-hexene feed and the olefin composition approaches an equilibrium composition. Equilibrium calculations, however, show that much less light olefins and more higher olefins should be produced. This could be due to the narrow pores in the ZSM-5 which could allow easier passage

for the light olefins out of the catalyst thus shifting the product distribution towards lighter products.

A model for the MTO reaction over ZSM-5 is proposed. The model is based on the hydrocarbon pool mechanism and consists of 15 reactions where all olefins are formed through equilibrium reactions with a large hydrocarbon species. The model predicts the experimental data fairly well for the olefins but require improvements with respect to the paraffin's and C_{6+} fractions.

7.2.9 Nomenclature

A_t = Cross-sectional area of the fluid bed (m^2)

C = Molar concentration ($kmol/m^3$)

C_x^+ = Hydrocarbon pool species (Decene)

D = Molar diffusion coefficient (m^2/s)

D_t = Reactor diameter (m)

dp = Particle diameter (m)

d_b = Bubble diameter (m)

d_{b0} = Initial bubble diameter at the distributor (m)

d_{bm} = Maximum bubble diameter (m)

E_a = Activation energy (kJ/mol)

F = Fine fraction

F = Flow rate (kmol/s)

g = gravity (m/s^2)

h = Height in bed (m)

K_{eq} = Equilibrium constant

k_i = Reaction rate constant ($m^6/kmol \cdot s$)

K_{be} = Bubble to emulsion mass transfer coefficient (s^{-1})

k_{be} = Bubble to emulsion mass transfer coefficient (m/s)

N = Total number of components in the system

r_i = Reaction rate of component i ($kmol/kg \cdot s$)

R = Ideal gas constant ($kcal/mol \cdot K$)

T = Temperature (K)

u_{mf} = Minimum fluidization velocity (m/s)

u_{mb} = Minimum bubbling velocity (m/s)

u_b = Bubble velocity (m/s)

u_0 = Superficial gas velocity (m/s)

V_e = Volume of emulsion (m^3)

W = Catalyst weight (kg)

y = Mole fraction

Greek symbols

Γ = Gas expansion due to reaction

δ = Bubble phase volumetric fraction

ε_{mf} = Void fraction at minimum fluidization

ε_{cat} = Void fraction of the catalyst

μ = Gas viscosity (kg/m·s)

ρ_p = Particle density (kg/m^3)

ρ_b = Bulk density (kg/m^3)

ρ_{tapped} = Tapped density (kg/m^3)

ρ_{mf} = Minimum fluidization density (kg/m^3)

ρ_g = Gas density (kg/m^3)

Subscripts

e = Emulsion Phase

b = Bubble Phase

i = Component index

n = CSTR in series

exp = experimental data

cal = calculated value

7.2.10 References

(1) Chang, C. D.; Silvestri, A. J. The conversion of methanol and other O-compounds to hydrocarbons over zeolite catalysts. *Journal of Catalysis.* **1977**, 47, 249

(2) Stöcker, M. Methanol-to-hydrocarbons: catalytic materials and their Behaviour. *Microporous and Mesoporous Materials.* **1999**, 29, 3

(3) Chang, C. D.; Chu, C. T-W. Methanol conversion to Olefins over ZSM-5. II.Olefin Distribution. *Journal of Catalysis.* **1984**, 86, 297

(4) Park, T-Y.; Froment, G. F. Kinetic Modeling of the Methanol to Olefins Process. 2. Experimental Results, Model Discrimination, and Parameter Estimation. *Ind. Eng. Chem. Res.* **2001**, 40, 4187

(5) Gayubo, A. G.; Anuayo, A. T.; Olazar, M.; Vivanco, R.; Bilbao, J. Kinetics of the irreversible deactivation of the HZSM-5 catalyst in the MTO process. *Chem. Eng. Sci.* **2003**, 58, 5239

(6) Mier, D. Aguayo, A. T. Atutxa, A. Gayubo, A. G. Bilbao, J. Kinetic study of the simultaneous cracking of paraffins and methanol on HZSM-5 zeolite catalyst. *International Journal of Chemical Reactor Engineering*, **2007**, 5, A60

(7) Kaarsholm, M.; Joensen, F.; Nerlov, J.; Cenni, R.; Chaouki, J.; Patience, G. S. Phosphorus modified ZSM-5: Deactivation and product distribution for MTO. *Chem.. Eng. Sci.* **2007**, 62, 5527

(8) Gayubo, A. G.; Aguayo A. T.; Alonso, A.; Bilbao J. Kinetic Modeling of the Methanol-

to-Olefins Process on a Silicoaluminophosphate (SAPO-18) Catalyst by Considering Deactivation and the Formation of Individual Olefins. *Ind. Eng. Chem. Res.* **2007**, *46,* 1981

(9) Schoenfelder, H.; Hinderer, J.; Werther, J.; Keil, F. J. Methanol to olefins – predictions of the performance of a circulating fluidized-bed reactor on the basis of kinetic experiments in a fixed-bed reactor. *Chem. Eng. Sci.* **1994**, 49, 5377

(10) Keil, F. J. Methanol-to-hydrocarbons: process technology. *Microporous And Mesoporous Materials.* **1999**, 29, 49

(11) Chen, J. Q.; Bozzano, A.; Glover, B.; Fuglerud, T.; Kvisle, J. Recent advancements in ethylene and propylene production using the UOP/Hydro MTO process. *Catalysis Today*. **2005**, 106, 103

(12) Mihail, R.; Straja, S.; Maria, G.; Musca, G.; Pop, G. Kinetic Model for Methanol Conversion to Hydrocarbons. *Chem. Eng. Sci.* **1983**, 38. 1581

(13) Park, T-Y.; Froment, G. F. Kinetic Modeling of the Methanol to Olefins Process. 1. Model Formulation. *Ind. Eng. Chem. Res.* **2001**, 40, 4172

(14) Park, T-Y.; Froment, G. F. Kinetic Modeling of the Methanol to Olefins Process. 2. Experimental Results, Model Discrimination, and Parameter Estimation. *Ind. Eng. Chem. Res.* **2001**, 40, 4187

(15) Gayubo, A. G.; Aguayo, A. T.; Castilla, M.; Olazar, M.; Bilbao, J. Catalyst reactivation kinetics for methanol transformation into hydrocarbons. Expressions for designing reaction-regeneration cycles in isothermal and adiabatic fixed bed reactor. *Chem. Eng. Sci.* **2001**, 56, 5059

(16) Gayubo, A. G.; Aguayo, A. T.; Castilla, M.; Moran, A. L.; Bilbao, J. Role of water in the kinetic modelling of methanol transformation into hydrocarbons on HZSM-5 zeolite. *Chemical Engineering Communications*. **2004**, 191, 944

(17) Gayubo, A. G.; Aguayo, A. T.; Sánchez del Campo. A. E.; Tarrio, A. M.; Bilbao, J. Kinetic modelling of methanol transformation into olefins on a SAPO-34 catalyst. *Ind. Eng. Chem. Res.* **2000**, 39, 292

(18) Park, T-Y.; Froment, G. F. Analysis of fundamental reaction rates in the methanol-to-olefins process on ZSM-5 as a basis for reactor design and operation. *Ind. Eng. Chem. Res.* **2004**, 43, 682

(19) Bos, R. A. N.; Tromp, P. J. J.; Akse, H. N. Conversion of methanol to lower olefins. Kinetic modelling, reactor simulation, and selection. *Ind. Eng. Chem. Res.* **1995**, 34, 3808

(20) Buchanan, J. S.; Santiesteban, J. G.; Haag, W. O. Mechanistic considerations in acid-catalyzed

cracking of olefins. *Journal of Catalysis*. **1996**, 158, 279

(21) Zhou, H.; Wang, Y.; Wei, F.; Wang, D.; Wang, Z. Kinetics of the reactions of the light alkenes over SAPO-34. *Applied Catalysis A: General*. **2008**, 348, 135

(22) Tabak, S. A.; Krambeck, F. J.; Garwood, W. E. Conversion of propylene and butylene over ZSM-5 catalyst. *AIChE Journal.* **1986**, 32(9), 9 1526

(23) Lukyanov, D. B.; Shtral, V. I.; Khadzhiev, S. N. A Kinetic model for the hexane cracking reaction over H-ZSM-5. *Journal of Catalysis.* **1994**, 146, 87

(24) Norval, G. W.; Phillips, M. J.; Virk, K. S.; Simons, R. V. Olefin conversion over zeolite H-ZSM-5. *Canadian Journal of Chemical Engineering.* **1987**, 67, 521

(25) Norval, G. W.; Phillips, M. J.; Missen, R. W.; Smith, W. R. Identification and application of partial chemical equilibria in reactor modeling. *AIChE Journal.* **1992**, 38, 1288

(26) Norval, G. W.; Phillips, M. J.; Missen, R. W.; Smith, W. R. Calculated Equilibria for the alkene and alcohol aromatization processes. Applied Catalysis. **1989**, 54, 37

(27) Kunii, D.; Levenspiel, O. Fluidization Engineering. Butterworth-Heinemann series in chemical engineering, Newton, MA (1991).

(28) Werther, J.; Hartge, E.-U. Modeling of industrial fluidized-bed reactors. *Ind. Eng. Chem. Res.* **2004**, 43, 5593

(29) Abba, I. A.; Grace, J. R.; Bi, H. T.; Thompson, M. L. Spanning the flow regimes: Generic Fluidized-bed reactor model. *AIChE Journal.* **2003**, 49, 1838

(30) Sit, S. P.; Grace, J. R. Effect of bubble interaction on interphase mass transfer in gas fluidized beds. *Chem. Eng. Sci.* **1981**, 36, 327

(31) Mori, S.; Wen, Y. Estimation of bubble diameter in gaseous fluidized beds. AIChE Journal **1975**, 21(1), 109

(32) Wen, C.Y.; Yu Y. H. Mechanics of fluidization. *Chemical Engineering Progress Symposium Series.* **1966**, 62, 100

(33) Abrahamsen, A. R.; Geldart, D. Behaviour of gas-fluidized beds of fine powders Part 1. Homogeneous expansion. *Powder Technology.* **1980**, 26, 35

(34) Alwahabi, S. M.; Froment, G. F. Conceptual reactor design for the methanol-to-olefins process on SAPO-34. *Ind. Eng. Chem. Res.* **2004**, 43, 5112

(35) Iordache, O. M.; Maria, G. C.; Pop, G. L. Lumping analysis for the methanol conversion to olefins kinetic model. *Ind. Eng. Chem. Res.* **1988**, 27, 2218

(36) Soundararajan, S.; Dalai, A. K.; Berruti, F. Modeling of methanol to olefins (MTO) process in a circulation fluidized bed reactor. *Fuel.* **2001**, 80, 1187

(37) Bjørgen, M.; Svelle, S.; Joensen, F.; Nerlov, J.; Kolboe, S.; Bonino, F.; Palumbo, L.; Bordiga, S.; Olsbye, U. Conversion of methanol to hydrocarbons over zeolite H-ZSM-5; On the origin of the olefinic species. *Journal of Catalysis*. **2007**, 249 195

(38) Svelle,S.; Joensen, F.; Nerlov, J.: Olsbye,U.; Lillerud, K-P.; Kolboe, S.; Bjørgen, M. Conversion of Methanol into Hydrocarbons over Zeolite H-ZSM-5: Ethene Formation Is Mechanistically Separated from the Formation of Higher Alkenes. *J. Am. Chem. Soc*. 2006, 128, 14770

Chapter 8
General discussion

As described in Chapter 2 considerable effort have been devoted to identifying reaction pathways and developing kinetic models capable of describing the complex reaction but so far there remain significant shortcomings. The two main zeolite types used in the MTO reaction ZSM-5 and SAPO follow distinct reaction pathways, deactivation time and product. On could argue that a SAPO based catalyst would be more suitable for the work describe herein since it is most suitable for fluidized bed operation, however, there are several reasons to examine the ZSM-5 system. The coking rate for ZSM-5 is much slower, which makes it easier to study the steady state operation since the catalyst does not have to be continuously regenerated or changed. The broader product distribution of the ZSM-5 zeolite was also considered to be of interest. Furthermore, since both fixed bed and fluidized bed studies were completed in this study the ZSM-5 was chosen to be the best choice of zeolite.

The spray dried catalyst used in the study is an experimental catalyst that has yet to be optimized for the MTO reaction. The introduction of kaolin, levasil and especially catapal B resulted in an increased methane production compared to what was observed for the pure zeolite. The methane production rate was reduced by doping it with phosphorous but the level of methane is still above what is found for the pure zeolite. The shape of the catalyst differs from a normal fluid bed catalyst by having a relatively

large fraction which has blow-holes, as can be seen in Figure A-2. It has, however, been considered as a spherical catalyst during calculations.

In the fixed bed experiments we concluded that methane was predominately produced from methanol and/or DME. This was later confirmed during the fluid bed experiments where it was shown during experiments with 1-hexene as feed that methane only form in a limited amount from the cracking/oligorimazation reactions. Methane formation is, to a large degree, formed from the support material in the spray dried catalyst and not on the zeolite and the amount of methane in a commercial catalyst would be expected to be lower. The fact that methane is more related to the support material than the zoelite also supports the idea that methane formation is not directly coupled to the methanol to olefin reaction.

The experiment with 1-hexene showed that ethylene was produced at relatively high concentrations, which would not have been expected from the fixed bed experiments and the latest literature (Bjørgen et al. 2007) on the subject, who concluded that ethylene is predominately formed from xylene and trimethylbenzene and not from secondary cracking reactions. Some aromatics were present in the products from 1-hexene feed but since methanol is not present to support the methylazation of the benzene ring, formation of ethylene from xylene and trimethylbenzene as the primary source is unlikely in this case.

Feeding methanol and 1-hexene resulted in almost the same product distribution and it was assumed it was because the product distribution reached chemical equilibrium, has also been proposed by others (Norval et al, 1989; Zhou et al, 2008). However equilibrium calculations showed that the experimental results had more light olefins compared to the equilibrium. It could be argued, that equilibrium is established inside the catalyst and the small molecules would have an advantage getting out of the small pores of the zeolite, hence shifting the product distribution to the lighter fractions.

Three different fluidized bed setups were used for the MTO reaction a 3" fluidized bed in stainless steel equipped with either a sintered metal distributor or a perforated plate distributor and a 4.1 cm inner diameter fluidized bed in stainless steel with a sintered metal distributor in addition to the quartz reactor. It was found that methanol decomposition on the sintered metal distributor gradually increased the inlet pressure to the point where the reactor had to be shut down. Changing the distributor for the 3" fluidized bed reactor resulted in operation problems where perturbations in the inlet pressure could cause backflow of catalyst into the windbox and feeding line. This was especially problematic during feed changes between methanol feed and inert gas during startup and shutdown. For a description of the two fluidized bed reactors and the problems occurred refer to Appendix B.

8.1 Elevation of the catalyst with glass beads

Due to a gap between the distributor and the heating zone the catalyst had to be elevated when a small amount of catalyst was used, otherwise the reaction temperature could not

be reached. Elevating the catalyst was facilitated by adding sand/glass beads with a larger particle diameter and higher density on top of the distributor and then placing the catalyst on top. This configuration was tested in a 3" transparent cold flow fluid bed. Sand with an average diameter of 250μm and a density of 2650 kg/m^3 was placed in the bottom with catalyst on top. The catalyst was fluidized on top of the sand from the minimum fluidization and up to the minimum fluidization of the sand. At this point the sand began to fluidize which caused the two kinds of particles to mix. Reducing the gas velocity below the minimum fluidization of the sand particles caused the sand and catalyst to separate with catalyst moving to the top of the bed. The majority of the separation was done after approximately 5 min and reached a steady level after 30 min. The separation was never complete since a bit of catalyst could be observed close to the bottom of the reactor and at the wall although it was not much. This can be attributed to the fact that there was an overlap in the particle size distribution even though the large density difference between the particles should help the separation. Only the principle was tested to verify that it could be used. To avoid the problem with overlapping in the particle size glass beads with an average size of 500μm was used for the experiments in the fluid bed. The particle size distribution of the catalyst, sand and glass beads is depicted in Figure 8-1. The overlap between the sand and catalyst is evident and changing from sand to glass beads reduced the overlap significantly.

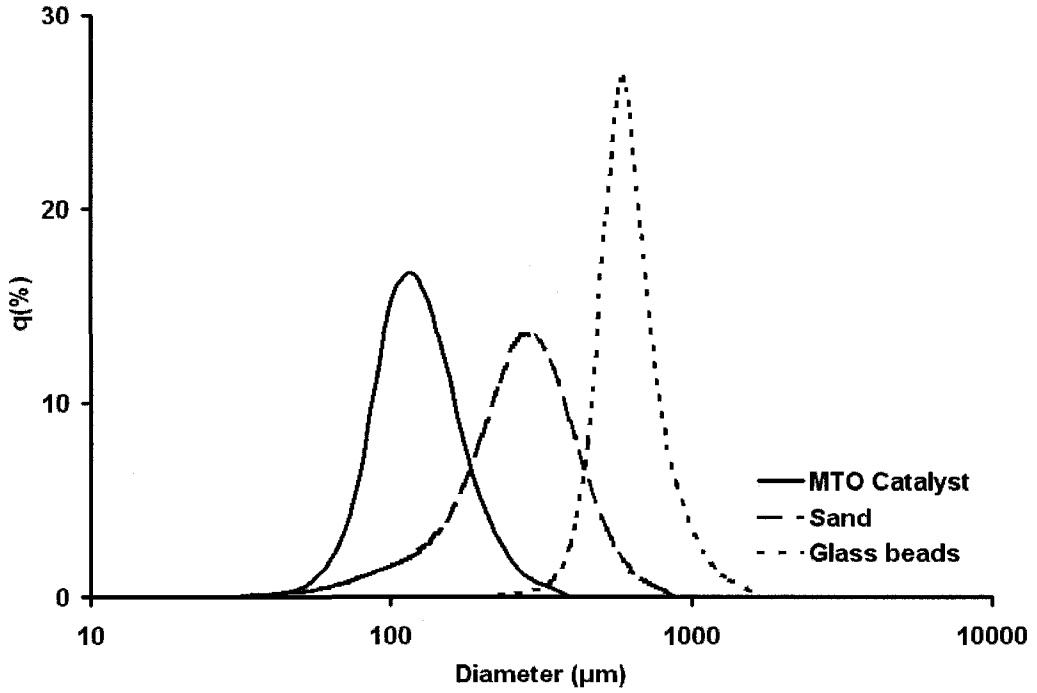

Figure 8-1: Particle size distribution of the MTO catalyst, sand and glass beads used – measured was preformed n a Horiba LA-950

8.2 Kinetic and Modelling of the MTO reaction

As described in Chapter 2 much work has been done on the modelling of the MTO reaction over both SAPO and ZSM-5 catalysts. Only a limited number of models include the lower olefins as separate species, while still being relatively simple. All the models based on SAPO only include hydrocarbons up to C_5 and the majority of models based on ZSM-5 lumps the olefins together. The model of Schoenfelder et al. (1994) include both separate light olefins and higher carbons and it was therefore used to model our experimental data. The model is also based on a ZSM-5 catalyst but with a higher Si/Al ratio than the zeolite used in this work. The model was implemented in the two phase

model described in Chapter 7 and since the model parameters are based on another catalyst the parameters was re-estimated to fit the fluid bed data. Figure 8-2 depicted the model prediction vs. the experimental data. Agreement between the experimental data and model is poor which may be due to the experimental data used in the development of the model had very low amounts of hydrocarbons higher than C_4, which is not the case with the catalyst in this study.

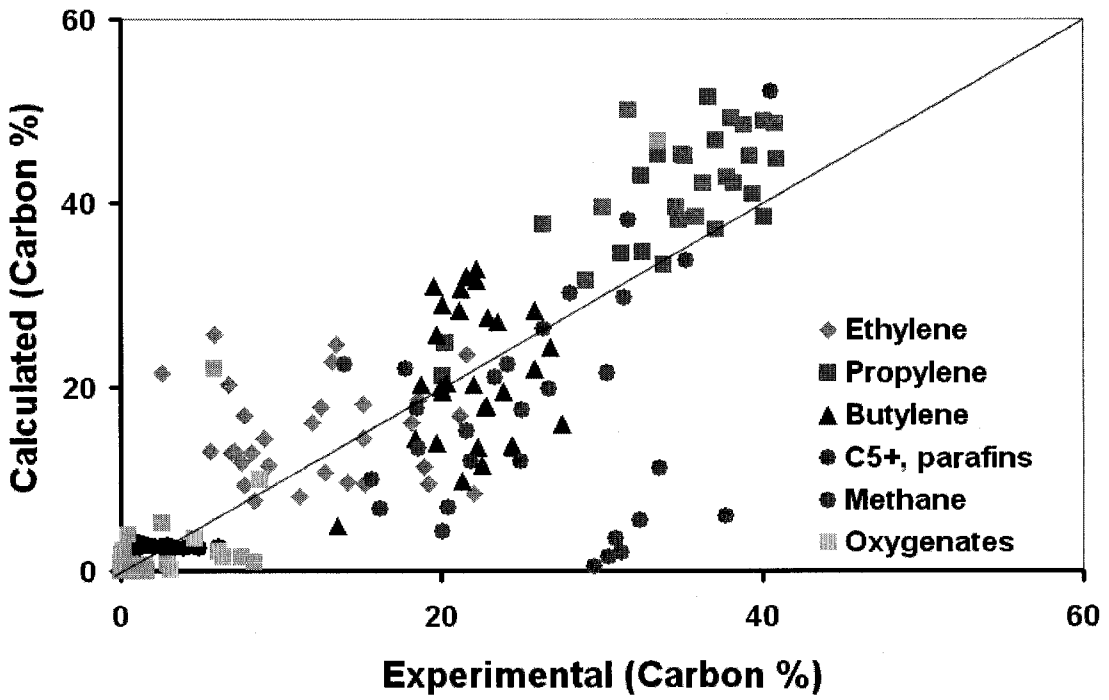

Figure 8-2: Calculated values with the use of the model of Schoenfelder et al. (1994) versus the obtained experimental data from fluidized bed.

The model of Park and Froment (2004) include the cracking and oligorimazation reactions, which allows 1-hexene to form other olefins but not ethylene and propylene. A hydrocarbon pool mechanism with a high molecular weight hydrocarbon as the carbon pool component was found to model the MTO reaction well. A similar scheme

has recently been used by Zhou et al (2008) to characterize the MTO reaction over SAPO-34. Some of the main differences between the two models are the fact that over ZSM-5 hydrocarbons larger than C_5 have to be included both as olefins and aromatics. Further, it was found that methane is formed mainly from the methanol and/or DME and not from the hydrocarbon pool. The main purpose of the model is to be able to characterize the light olefin fractions, to obtain this goal while still maintaining a limited amount of reactions, lumped fractions for the paraffins and C_{6+} have been used. The model is also in line with work in olefin interconversion where Tsunoda and Sekiguchi (2008) recently have published a reaction scheme for the OMEGA process with butane as feed stock in which butane through reversible reactions react to all C_2 to C_8 olefins.

In Chapter 4, both a two phase model as well as a n-CSTR in series model were used to characterize the MeOH to DME reaction in a fluidized bed. The n-CSTR was superior. For the MTO reaction in a fluidized bed, the two phase model was chosen because the bed height was generally higher than in the experiments with methanol dehydration and because the gas velocity spanned a larger range. Further, the two phase model did not perform significantly worse than the n-CSTR model for the methanol dehydration. Using the n-CSTR model for the MTO reaction instead of the two phase model would not change the results significantly.

Optimum production of propylene was found to be at residence times slightly higher than what is needed to obtain full conversion of oxygenates. This is evident from the

investigations in fixed beds in Chapter 5. The proposed kinetic model follows the same trend with a decrease in the hexene concentration and increase in propylene at residence times over that of full conversion. Optimum propylene yield from the model is 38.5% on carbon basis at 550°C. The model slightly under predicts the maximum propylene production from the fluid bed experiments which have a maximum value of 41%.

Chapter 9
Conclusion and recommendations

9.1 General conclusions

The main objective of the work has been to develop a kinetic model for the methanol to light olefins reaction which includes each of the light fractions of ethylene, propylene and C_4. A fluidized bed was identified to be the most suitable reactor type for the investigation. To be able to develop the kinetic model, the study was divided into three sections 1) evaluate the methanol dehydration kinetics in a fluidized bed. 2) investigate the reaction mechanism and deactivation of the MTO reaction in a fixed bed and 3) kinetic study of the MTO reaction in a fluidized bed reactor.

The dehydration of methanol to DME was studied in a 4.6 cm fluidized bed reactor at low gas velocities. A kinetic expression for the methanol to DME reaction has been proposed and the kinetic parameters were estimated with both a two phase fluid bed model and an n-CSTR's in series reactor model. The kinetic model coupled with the n-CSTR model was shown to fit the experiments better compared to the two phase fluid bed model. The new model was superior to the literature model of Barĉiĉ and Levec (1992). The fluidized bed was shown to be a good reactor type for the kinetic modelling of the methanol to DME reaction due to the isothermal conditions and the conversions that could be obtained at relatively low gas velocities. Low gas velocities are needed to operate at conditions where the n-CSTR in series model can be used which puts some limitations on the conversion range obtainable at a given temperature. Varying the

catalyst inventory could increase the conversion range. Using the fluidized bed to investigate the kinetics was shown to be feasible and reactions where hotspots or temperature gradients are of concern, like the MTO reaction, could benefit from this reactor technology.

Fixed bed experiments of the MTO reaction suggested that methane was formed directly from methanol and/or dimethyl ether. At partial conversion largely non-aromatic C_{5+} intermediates dominated the product distribution. At residence time a bit longer that what would result in 100% conversion of the oxygenates propylene yield is highest, which is attributed to cleavage of the C_{5+} fraction. The formation of ethylene closely parallels the aromatics, suggesting that it is by splitting off from xylene and trimethylbenzene intermediates, in accordance with the labeling studies made by Svelle et al. (2006), and not a product of secondary cracking reaction.

The product distribution and methanol capacity of the catalyst are highly dependent on the feed composition with higher olefin production at lower partial pressure of methanol feed. At the same time, methanol capacity is reduced.

Catalyst deactivation is highly dependent on the residence time doubling the feed rate (from a WHSV of 0.22 h^{-1} to 0.43 h^{-1}) decreased the deactivation time by a factor of ten. The methanol capacity is therefore also dependent on the feed rate.

Decreasing the partial pressure and increasing the space velocity of methanol feed both decrease the methanol capacity of the catalyst by increasing the deactivation. This is in contrast to the findings of Chen at al. 2000 for the SAPO-34 catalyst where they

concluded that coke deposition was based on the amount of methanol converted and temperature but not on WHSV.

Catalyst coking was examined based on photographs of catalyst taken at intervals during an experiment. Three distinct zones were identified: At the entrance the coking rate is low which is attributed to the methanol dehydration reaction, the main coking zone due to oxygenate to olefin and intermediates reaction follows shortly after the entrance zone. Following the main reaction zone, coking rates are low as only secondary cracking reactions takes place and full oxygenate conversion have been reached.

The experimental study of the reaction paths of the MTO reaction conducted in a fluidized bed showed that methanol and 1-hexene feed yielded approximately the same product distribution. This result confirms that cracking and oligorimerisatrion reactions are an important part of the reaction network. Methane formation from the 1-hexene reaction was almost non-existent confirming the findings from the fixed bed experiments that methane is predominately formed from oxygenates. Ethylene production from the 1-hexene experiment was not significantly lower than from methanol and cracking of higher olefins to ethylene is therefore a part of the proposed reaction kinetics – this is in contrast to the findings of the fixed bed where it was concluded that ethylene predominantly is formed from splitting of polymethylated benzenes. When oxygenates are converted to hydrocarbons, they follow the same reaction mechanism as with 1-hexene feed and the olefin composition approaches an equilibrium composition. Equilibrium calculations, however, show that much less light olefins and more higher

olefins should be produced. Restrictions from the narrow pores in the ZSM-5 which could allow easier passage for the light olefins might shift the product distribution towards lighter products, if one considers equilibrium inside the zeolite.

A reaction kinetic model is proposed for the MTO reaction over ZSM-5 which includes 15 reactions. All olefins are considered to be formed through reversible reactions with a large hydrocarbon species. The model characterizes the experimental data fairly well for all the light olefins, which was the main objective but requires improvements with respect to the paraffins and C_{6+} fractions.

9.2 Recommendation

9.2.1 Kinetics in fluidized bed

Kinetic measurements in a small scale fluidized bed have shown good results in this work. Expanding the work to include an in-depth analysis of the effect of the hydrodynamic at low gas velocities with exothermic reactions where the reaction kinetics are well known would be desirable. Determination of basis operation interval where the isothermal conditions are maintained and changes in the bed hydrodynamic are minimal would be highly attractive for future studies of exothermic reaction.

9.2.2 MTO reaction kinetic

While the proposed model are able to predict the product distribution of the light olefins improvements of the paraffin and C_{6+} fractions are still needed. From the fixed bed study it was shown that the aromatic and heavy olefins follows separate reaction pathways.

Modeling of the 1-hexene experiments was unsuccessful and splitting the aromatic fraction from the C_{6+} would be desired.

9.2.3 Equilibrium inside the catalyst?

The experimental data from the MTO reaction in fluidized bed suggested that the reaction is close to equilibrium. Calculations of the equilibrium showed that the experimental data followed the same trends of the equilibrium but the fraction of the light olefins was much larger than the equilibrium this was especially the case for the propylene. Considering equilibrium concentration inside the cages of the zeolite it would be interesting to determine if transport restrictions out of the zeolite pore system could account for the observed difference between the experimentally obtained product distribution and the equilibrium.

References

Abba, I. A., Grace, J. R., Bi, H. T., & Thompson, M. L. (2003). Spanning the flow regimes: Generic Fluidized-bed reactor model. *AIChE Journal*, 49, 1838-1848.

Abrahamsen, A. R., & Geldart, D. (1980). Behaviour of gas-fluidized beds of fine powders Part 1. Homogeneous expansion. *Powder Technology*, 26, 35-46.

Aguayo, A. T., Gayubo, A. G., Vivanco, R., Alonso, A., & Bilbao, J. (2005). Initiation step and reactive intermediates in the transformation of methanol into olefins over SAPO-18 catalyst. *Industrial & Engineering Chemistry Research,* 44 (19), 7279-7286.

Alwahabi, S. M., & Froment, G. F. (2004). Conceptual reactor design for the methanol-to-olefins process on SAPO-34. *Industrial & Engineering Chemistry Research,* 43, 5112-5122

Andersen, J. (2003). Mto: meeting the needs for ethylene and propylene production, Paris. ERTC Petrochemical Conference.

Anthony, R. G. (1981). A kinetic model for methanol conversion to hydrocarbons. *Chemical Engineering Science,* 36, 789.

Arstad, B., & Kolboe, S., (2001). The Reactivity of Molecules Trapped within the SAPO-34 Cavities in the Methanol-to-Hydrocarbons Reaction. *Journal of the American Chemical Society*, 123, 8137-8138.

Berĉiĉ, G., & Levec, J. (1992). Intrinsic and Global Reaction Rate of Methanol

Dehydration over γ-Al_2O_3 Pellets. *Industrial & Engineering Chemistry Research,* 31, 1035-1040.

Beech, J. H., Nicoletti, M. P., Lattner, J. R., Alexion, D. G., & Paik, P. K. (2004). Method and system for regeneration catalyst from a plutilaty of hydrocarbon conversion apparatuses. Exxonmobil chemical company. US 20040064007A1

Benito, P. L., Gayubo, A. G., Aguayo, A. T., Castilla, M., & Bilbao, J. (1996). Concentration-dependent kinetic model for catalyst deactivation in the MTG process. *Industrial & Engineering Chemistry Research,* 35, 81-89.

Berger, R. J, Ramírez, J. P., Kapteijn, F., & Moulijn, J. A. (2002). Catalyst performance testing: bed dilution revisited. *Chemical Engineering Science,* 57, 4912-4932.

Bjørgen, M., Olsbye, U., Svelle, S., & Kolboe, S. (2004). Conversion of methanol to hydrocarbons: the reactions of the hepta-methylbenzenium cation over zeolite H-beta. *Catalysis Letters*, 93, 37-40.

Bjørgen, M., Svelle, S., Joensen, F., Nerlov, J., Kolboe, S., Bonino, F., Palumbo, L., Bordiga, S., & Olsbye, U. (2007) Conversion of methanol to hydrocarbons over zeolite H-ZSM-5; On the origin of the olefinic species. *Journal of Catalysis*, 249, 195-207

Bos, R. A. N., Tromp, P. J. J., & Akse H. N. (1995). Conversion of methanol to lower olefins. Kinetic modelling, reactor simulation, and selection. *Industrial & Engineering Chemistry Research,* 34, 3808-3816.

Buchanan, J. S., Santiesteban, J. G., & Haag, W. O. (1996). Mechanistic considerations in acid-catalyzed cracking of olefins. *Journal of Catalysis*, 158, 279-287

Campbell, S. M., Bibby, D. M., Coddington, J. M., & Howe, R. F. (1996). Dealumination of HZSM-5 Zeolites. *Journal of Catalysis*, 161, 350-358.

Chang, C. D., & Silvestri, A. J. (1977). The conversion of methanol and other O-compounds to hydrocarbons over zeolite catalysts. *Journal of Catalysis,* 47, 249-259.

Chang, C. D. (1980). A kinetic model for methanol conversion to hydrocarbons. *Chemical Engineering Science,* 35, 619-622.

Chang, C. D. (1983). Hydrocarbons form methanol. *Catalysis Review Science and Engineering,* 25, 1-118.

Chang, C. D. (1984). Methanol Conversion to Light Olefins. *Catalysis Review Science and Engineering,* 26 (3&4), 323-345.

Chang, C. D., Chu, C. T-W., & Socha, R. F. (1984). Methanol conversion to Olefins over ZSM-5. I. Effect of temperature and zeolite SiO_2/Al_2O_3. *Journal of Catalysis,* 86, 289-296.

Chang, C. D., Hellring, S. D., & Pearson, J. A. (1989). On the existence and role of free radicals in methanol conversion to hydrocarbons over HZSM-5. *Journal of Catalysis*, 115, 282-285.

Chen, D., Rebo, H. P., Grønvold, A., Moljord, K., & Holmen, A., (2000). Methanol conversion to light olefins over SAPO-34: Kinetic modeling of coke formation. *Microporous and Mesoporous Materials*, 35-36, 121-135.

Chen, J. Q., Bozzano, A., Glover, B., Fuglerud, T., & Kvisle, S. (2005). Recent

advancements in ethylene and propylene production using the UOP/Hydro MTO process. *Catalysis Today*, 106, 103-107.

Chen, N.Y., & Reagan, W.J., (1979). Evidence of autocatalysis in methanol to Hydrocarbon reactions over zeolite catalysts. *Journal of catalysis*, 59, 123-129.

Christensen, D., Vervloet, D., Nijenhuis, J., van Wachem, B.G.M., van Ommen J.R., & Coppens, M.-O. (2008). Insights in distributed secondary gas injection in a bubbling fluidized bed via discrete particle simulations. *Powder Technology*, 183, 454-466.

Chisholm, P. N., Coute, N. P., Lattner, J. R., Xu, T., Smith, J. S., & Kuechler, K. H. (2003). Convertingoxygenates to olefins over a catalyst comprising acidic molecular sieve of controlled carbon atom to acid site ratio. Exxonmobil chemical company, US 20030125598A1

Chu, C. T-W., & Chang, C. D. (1984). Methanol conversion to Olefins over ZSM-5. II.Olefin Distribution. *Journal of Catalysis,* 86, 297-300.

Clarke, J. K. A., Darcy, R., Hegarty, B. F., O'Donoghue, E., Amir-Ebrahimi, V., & Rooney, J. J. (1986). Free radicals in dimethyl ether on H-ZSM-5 zeolite. A novel dimension of heterogeneous catalysis. *Journal of the Chemical Society, Chemical Communications,* 425-426.

Coute, N. P., Kuechler, K. H., Chisholm, P. N., Vaughn, S. N., Lattner, J. R., & Kuechler, W. L. (2004). Process for making olefins. Exxonmobil chemical company, US 6,673,978B2

Dahl, I. M., & Kolboe, S. (1993). On the reaction mechanism for propene formation in the MTo reaction over SAPO-34. *Catalysis Letters,* 20, 329-336.

Dahl, I. M., & Kolboe, S. (1994). On the reaction mechanism for hydrocarbon formation from methanol over SAPO-34. *Journal of Caralysis*, 149, 458-464.

Dehertog, W. J. H., & Froment, G. F., (1991). Production of light alkenes from methanol on ZSM-5 catalysis. *Applied Catalysis*, 71, 153-165.

Dessau, R.M. (1986). On the H-ZSM-5 catalyzed formation of ethylene from methanol or higher olefins. *Journal of Catalysis*, 99, 111-116.

Dewaele, O., Geers, V. L., Froment, G. F., & Marin, G. B. (1999). The conversion of methanol to olefins: A transient kinetic study. *Chemical Engineering Science*, 54, 4385-4395.

Fogler, H. S. (2005). Elements of chemical reaction engineering. Prentice Hall, 4th edition

Froment, G. F., Dehertog, W. J. H., & Marchi, A. J. (1992). Zeolite catalysis in the conversion of methanol into olefins. *Catalysis* 9, 1-64.

Gayubo, A. G., Benito, P. L., Aguayo, A. T., Aguirre, I., & Bilbao, J. (1996). Analysis of kinetic models of the methanol-to-gasoline (MTG) process in an integral reactor. *Chemical Engineering Journal,* 63, 45-51.

Gayubo, A. G., Aguayo, A. T., Sánchez del Campo. A. E., Tarrio, A. M., & Bilbao, J. (2000). Kinetic modelling of methanol transformation into olefins on a SAPO-34 catalyst. *Industrial & Engineering Chemistry Research.* 39, 292-300

Gayubo, A. G., Ortega, J. M., Aguayo, A. T., Arandes, J. M., & Bilbao, J. (2000). MTG fluidized bed reactor-regenerator unit with catalyst circulation: process simulation and operation of an experimental setup. *Chemical Engineering Science*, 55, 3223-3235.

Gayubo, A. G., Aguayo, A. T., Castilla, M., Olazar, M., & Bilbao, J. (2001). Catalyst reactivation kinetics for methanol transformation into hydrocarbons. Expressions for designing reaction-regeneration cycles in isothermal and adiabatic fixed bed reactor. *Chemical Engineering Science*, 56, 5059-5071.

Gayubo, A. G., Anuayo, A. T., Olazar, M., Vivanco, R., & Bilbao, J. (2003). Kinetics of the irreversible deactivation of the HZSM-5 catalyst in the MTO process. *Chemical Engineering Science*, 58, 5239-5249.

Gayubo, A. G., Aguayo, A. T., Atutxa, A., Prieto, R., & Bilbao, J. (2004a). Role of Reaction-Medium Water on the acidity deterioration of a HZSM-5 Zeolite. *Industrial & Engineering Chemistry Research,* 43, 5042-5048.

Gayubo, A. G., Aguayo, A. T., Castilla, M., Moran, A. L., & Bilbao, J. (2004b). Role of water in the kinetic modelling of methanol transformation into hydrocarbons on HZSM-5 zeolite. *Chemical Engineering Communications*, 191, 944-967.

Gayubo, A. G., Aguayo A. T., Alonso, A., & Bilbao J. (2007). Kinetic Modeling of the Methanol-to-Olefins Process on a Silicoaluminophosphate (SAPO-18) Catalyst by Considering Deactivation and the Formation of Individual Olefins.. *Industrial & Engineering Chemistry Research. 46,* 1981-1989.

Gray, C., & Webster, G. (2001). A Study of Dimethyl Ether (DME) as an Alternative Fuel for Diesel Engine Applications. Transport Canada Publication No.: TP 13788E, May 2001

Haw, J. F., Song, W., Marcus, D. M., & Nicholas, J. B. (2003). The mechanism of methanol to hydrocarbon catalysis. *Accounts of Chemical Research,* 36, 317-326.

Hetsroni, G., (1982). "Handbook of Multiphase Systems" Hemisphere-McGraw Hill.

Horio, M., & Wen, C. Y. (1977). An assessment of fluidized-bed modelling. *AIChE symposium series*, 73, 9-21.

Houdek, J., & Andersen, J. (2005). On-purpose propylene - technology development. Kuala Lumpur, ARTC 8th annual meeting.

International Zeolite Association, (2006). www.iza-online.org

Iordache, O. M., Maria, G. C., & Pop, G. L. (1988). Lumping analysis for the methanol conversion to olefins kinetic model. *Industrial & Engineering Chemistry Research,* 27, 2218-2224

Kaarsholm, M., Joensen, F., Nerlov, J., Cenni, R., Chaouki, J., & Patience, G. S. (2007). Phosphorous modified ZSM-5: Deactivation and product distribution for MTO *Chemical Engineering Science*, 62, 5527-5532.

Keil, F. J. (1999). Methanol-to-hydrocarbons: process technology. *Microporous And Mesoporous Materials*, 29, 49-66.

Kokotailo, G. T., Lawton, S. L., Olson, D. H., & Meier, W. M. (1978). Structue of Synthetic zeolite ZSM-5. *Nature*, 272, 437-438.

Kunii, D. & Levenspiel, O. (1991). Fluidization Engineering. Butterworth-Heinemann series in chemical engineering, Newton, MA

Kunii, D. and Levenspiel, O. (1968). Bubbling bed model. Model for the flow of gas through a fluidized bed. *I&EC Fundamentals,* 7(3), 446-452.

Lattner, J. R., Smith, J. S., & Davuluri, R. P. (2005). Circulating fluid bed reactor system. Exxonmobil chemical company, US 20050087477A1

Lorences, M. J., Laviolette, J.-P., Patience, G. S., Alonso M., & Díez, F. V. (2006). Fluid bed gas RTD: Effect of fines and internals. *Power Technology,* 168, 1-9.

Lorences, M. J., Patience, G. S., Díez, F. V., & Coca, J. (2003). Butane oxidation to maleic anhydride: kinetic modeling and byproducts. *Industrial & Engineering Chemistry Research,* 42, 6730-6742.

Lu, W.-Z., Teng, L.-H., & Xiao, W.D. (2004). Simulation and experiment study of dimethyl ether synthesis from syngas in a fluidized-bed reactor. *Chemical Engineering Science*, 59, 5455-5464.

Lukyanov, D. B., Shtral, V. I., & Khadzhiev, S. N. (1994). A Kinetic model for the hexane cracking reaction over H-ZSM-5. *Journal of Catalysis,* 146, 87-92

Lurgi (2005). Lurgi successful in the middle east and in south east asia. Press release March 7, www.Lurgi.de

Lurgi (2008). New Project Development Agreement for integrated polypropylene complex. Press release September 9, www.Lurgi.com

Maria, G., & Muntean, O. (1987). Model reduction and kinetic parameters identification for the methanol conversion to olefins. *Chemical Engineering Science*, 42, 1451-1460.

May, W. G. (1959). Fluidized-bed reactor studies. *Chemical Engineering Progress*, 55(12), 49-56.

Mier, D., Aguayo, A. T., Atutxa, A., Gayubo, A. G., & Bilbao, J. (2007). Kinetic study of the simultaneous cracking of paraffins and methanol on HZSM-5 zeolite catalyst. *International Journal of Chemical Reactor Engineering*, 5, A60

Mihail, R., Straja, S., Maria, G., Musca, G., & Pop, G. (1983a). Kinetic Model for Methanol Conversion to Olefins. *Industrial and engineering chemistry process design and development,* 22, 532-538.

Mihail, R., Straja, S., Maria, G., Musca, G., & Pop, G. (1983b). Kinetic Model for Methanol Conversion to Hydrocarbons. *Chemical Engineering Science,* 38, 1581-1591.

Mollavali, M., Yaripour, F., Atashi, H., & Sahebdelfar, S. (2008). Intrinsic Kinetic Study of Dimethyl Ether Synthesis from Methanol on γ-Al_2O_3 Catalysts. . *Industrial & Engineering Chemistry Research,* 47, 2365-3273.

Möller, K. P., Böhringer, W., Schnitzler, A. E., van Steen, E., & O'Connor, C. T. (1999). The use of a jet loop reactor to study the effect of crystal size and the co-feeding of olefins and water on the conversion of methanol over HZSM-5. *Microporous and Mesoporous Materials*, 29, 127-144

Mori, S. & Wen, Y. (1975). Estimation of bubble diameter in gaseous fluidized beds. *AIChE Journal,* 21(1), 109-115.

Novella, E. C., Alonso, M. A., Zamorano, M. A. U., & Granados D. P. S. (1988). Conversion del metanol en hidrocarburos C_1-C_{10} sobre zeolita tipo ZSM-5 : Modelo cinetico simplificado. *Anales De Quimica,* 85, 292-297.

Norval, G. W., Phillips, M. J., Virk, K. S., & Simons, R. V. (1987). Olefin conversion over zeolite H-ZSM-5. *Canadian Journal of Chemical Engineering,* 67, 521-523

Norval, G. W., Phillips, M. J., Missen, R. W., & Smith, W. R.(1989) Calculated Equilibria for the alkene and alcohol aromatization processes. *Applied Catalysis*, 54, 37-52

Norval, G. W., Phillips, M. J., Missen, R. W., & Smith, W. R. (1992). Identification and application of partial chemical equilibria in reactor modeling. *AIChE Journal*, 38, 1288-1293

Ondrey, G. (2005). Methanol-to Propylene process slated for its commercial debut. *Chementator*, www.che.com. April, 5

Ortega, J. M., Gayubo, A. G., Anuayo, A. T., Olazar, M., & Bilbao, J. (1998). MTG process in a fluidized bed with catalyst circulation: operation and simulation of an experimental unit. *Industrial & Engineering Chemistry Research,* 37, 4222-4230.

Park, T-Y., & Froment, G. F. (2001a). Kinetic Modeling of the Methanol to Olefins

Process. 1. Model Formulation. *Industrial & Engineering Chemistry Research,* 40, 4172-4186.

Park, T-Y., & Froment, G. F. (2001b). Kinetic Modeling of the Methanol to Olefins Process. 2. Experimental Results, Model Discrimination, and Parameter Estimation. *Industrial & Engineering Chemistry Research,* 40, 4187-4196.

Park, T-Y., & Froment, G. F. (2004). Analysis of fundamental reaction rates in the methanol-to-olefins process on ZSM-5 as a basis for reactor design and operation. *Industrial & Engineering Chemistry Research.* 43, 682 -689

Radmanesh, R., Chaouki, J., & Guy, C. (2006). Biomass Gasification in a Bubbling Fluidized Bed Reactor: Experiments and Modeling. *AIChE Journal*, 52(12), 4258-4272.

Sapre, A. V. (1997). Catalyst deactivation kinetics from variable space-velocity Experiments. *Chemical Engineering Science*, 52, 4615-4623.

Schipper P. H., & Krambeck, F. J. (1986). A reactor design simulation with reversible and irreversible catalyst deactivation *Chemical Engineering Science,* 41, 1013-1019.

Schoenfelder, H., Hinderer, J., Werther, J., & Keil, F. J. (1994). Methanol to olefins – predictions of the performance of a circulating fluidized-bed reactor on the basis of kinetic experiments in a fixed-bed reactor. *Chemical Engineering Science*, 49, 5377-5390.

Sedran, U., Mahay, A., & De Lasa, H. L. (1990). Modelling methanol conversion to hydrocarbons: alternative kinetic models. *Chemical Engineering Journal*, 45, 33-42.

Semelsberger, T. A., Borup, R. L., & Greene, H. L. (2006). Dimethyl ether (DME) as an alternative fuel. *Journal of Power Sources,* 156, 497-511.

Shaikh, A. A. & Batran, H. (2007). On bubble-side transport limitations in catalytic fluid-bed reactors. *Chemical Engineering Research and Design,* 85, 1215-1218.

Sit, S. P., & Grace, J. R. (1981). Effect of bubble interaction on interphase mass transfer in gas fluidized beds. *Chemical Engineering Science*, 36, 327-335.

Soundararajan, S., Dalai, A. K., & Berruti, F. (2001). Modeling of methanol to olefins (MTO) process in a circulation fluidized bed reactor. *Fuel*, 80, 1187-1197

Stöcker, M. (1999). Methanol-to-hydrocarbons: catalytic materials and their Behaviour. *Microporous and Mesoporous Materials*, 29, 3-48.

Stöcker, M. (2003). Methanol to olefins - present scenario and future perspectives. SINTEF Materials and Chemistry Oslo.

Svelle, S., Bjørgen, B., Kolboe, S., Kuck, D., Letzel, M., Olsbye, U., Sekiguchi, O., & Uggerud, E. (2006). Intermediates in the methanol-to-hydrocarbons (MTH) reaction: a gasphase study of the unimolecular reactivity of multiply methylated benzenium cations. *Catalysis Letters*, 109, 25-35.

Svelle, S., Joensen, F., Nerlov, J., Olsbye, U., Lillerud, K.P., Kolboe, S., &

Bjørgen, M., (2006). Conversion of methanol in to hydrocarbons over zeolite H-ZSM-5: Ethene formation is mechanistically separated from the formation of higher alkenes. *Journal of the American Chemical Society*. 128 (46), 14770-14771.

Tabak, S. A., Krambeck, F. J., Garwood, W. E. (1986). Conversion of propylene and butylene over ZSM-5 catalyst. *AIChE Journal,* 32(9), 1526-1531

Tabak, S. A., & Yurchak, S. (1990). Conversion of methanol over ZSM-5 to fuels and Chemicals. *Catalysis Today*, 6, 307-327.

Tsunoda, T., & Sekiguchi, M. (2008) The omega process for propylene production by olefin interconversion. *Catalysis Surveys from Asia*, 12, 1-5

UOP (2008). UOP Technology Licensed to EuroChem to Convert Methanol to Olefins in New Nigerian Petrochemicals Plant. Press release January 30, www.upo.com

Van Deemter, J. J. (1961). Mixing and contacting in gas-fluidized beds. *Chemical Engineering Science,* 13(3), 143-154.

Wen, C.Y., & Yu, Y. H. (1966). Mechanics of fluidization. *Chemical Engineering Progress Symposium Series*, 62, 100-111.

Werther, J., & Hartge, E.-U. (2004). Modeling of industrial fluidized-bed reactors. *Industrial & Engineering Chemistry Research,* 43, 5593-5604.

Wu, X., & Anthony, R. G. (2001). Effect of feed composition on methanol conversion light olefins over SAPO-34. *Applied Catalysis A: General*, 218, 241-250.

Zhou, H., Wang, Y., Wei, F., Wang, D., & Wang, W. (2008) Kinetics of the reactions of the light alkenes over SAPO-34. *Applied Catalysis A: General*, 348, 135-141

Appendix A

Catalyst preparation

The catalyst was prepared for the fluid bed by dissolving Catapal B in a weak solution of nitric acid with stirring until a gel forms. After, Levasil S100/30% was added during stirring together with water to control viscosity. After a couple of hours, kaoline and the zeolite (CBV 28014 from Zeolyst, Si/Al =140) is introduced to the mixture. The slurry is stirred to make it homogenous before spray drying. The dry matter content before it is spray dried is 27 - 29% and with a pH-value of 4.0. The inlet pressure to the spray drier is between 6 and 8 bar, and the inlet temperature 280°C with an outlet temperature of 110°C. After spray drying the catalyst was calcined at 550°C for four hours

To test the catalyst in a fixed bed it was made into tablets, crushed and sieved to a particle size of 500 – 700 μm before testing in a 8 mm inner diameter fixed bed at 500°C with a WHSV of 23.5 $g_{MeOH}/g_{cat}\cdot h$. The catalyst produced a high amount of methane. To reduce the methane production the catalyst was doped with phosphorous by wetting the catalyst with an aqueous solution of $(NH_3)_2HPO_4$. The catalyst was then dried and calcined (at 550°C for four hours). The phosphorous loading tested was 0.5, 0.75, 1.0, 1.5 and 5 wt%. An additional test was done where $(NH_3)_2HPO_4$ was introduced into the slurry mixture before it was spray dried (0.5 wt%). The catalysts were tested in the fixed bed reactor and the methane formation decreased with phosphorous loading and a

positive effect on the catalyst lifetime was also observed. The results for the methane production are given in Figure A-1. The catalyst with 5 wt% phosphorous deactivated very rapidly and results are therefore not shown. It was found that a phosphorous loading of the catalyst of 1.5 wt% was optimal for the catalysts tested. The catalyst particle size range is between 40 and 250 μm with a mean diameter of 108 μm. The particles are shown in Figure A-2, it is seen that the majority of the particles have a mushroom-like shape and are not spherical as would have been desired for fluidized bed operation.

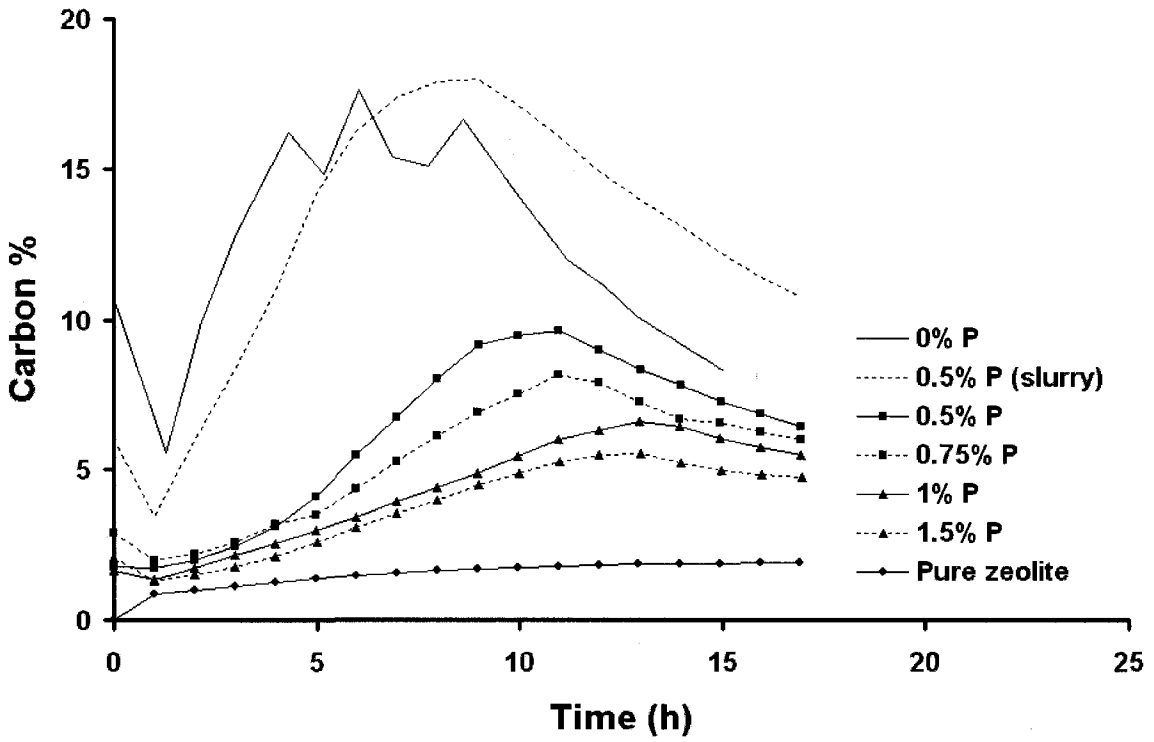

Figure A-1: Methane formation with time at different phosphor loadings of the fluid bed catalyst. Temperature 500°C and WHSV 23.5 $g_{MeOH}/g_{cat}\cdot h$

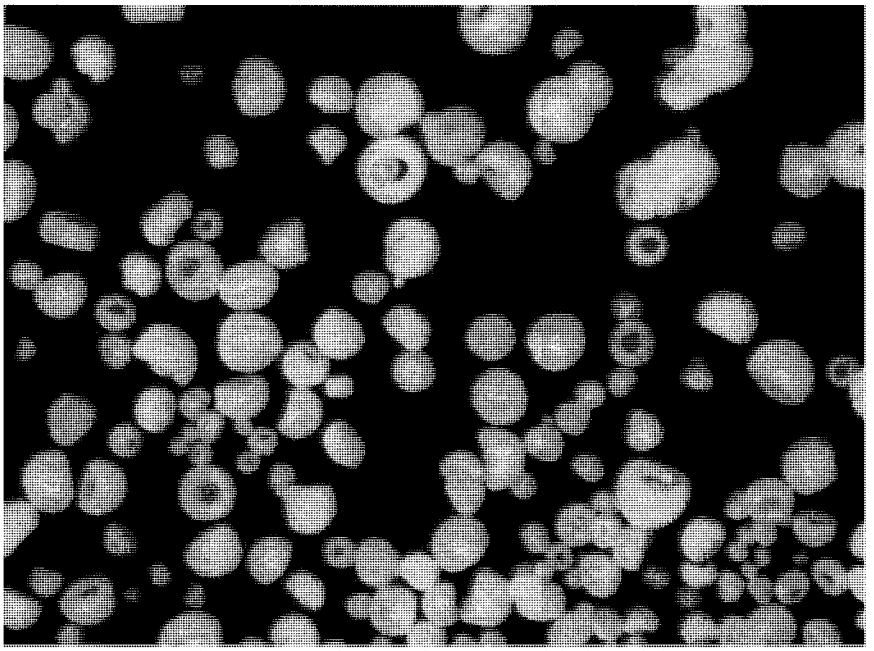

Figure A-2: Picture of the spray dried particles

Appendix B

Fluidized bed reactors used

A significant amount of work in several different fluidized bed reactor setups has been conducted. This Appendix will summarize problems that occurred with the different reactors and the reason for conducting the MTO reaction in the 4.6 cm inner diameter quartz fluidized bed reactor.

Three different reactors have been used a 3" inner diameter fluidized bed reactor setup in stainless steel, a 4.1 cm inner diameter fluidized bed in stainless steel and a 4.6 cm inner diameter fluidized bed in quartz. In the following a short description of the two setups – that had to be abandoned mainly due to methanol decomposition problems in the feeding section – will be given.

3" inner diameter fluidized bed

A fluid bed reactor system with a 3" inner diameter fluid bed in stainless steel was constructed including a feed section for both liquid and gas feed, a quench section to collect higher hydrocarbons and water and a gas analysis line to a GC. A diagram of the entire system is given in Figure B-2. A control system was setup for the reactor to monitor and control the reaction with shutdown procedures if pressure or temperature limits were exceeded. A drawing of the fluid bed is given in Figure B-1 and the dimensions of the different sections are listed in Table B-1. The reactor is heated in three

zones – the windbox, bed section and the freeboard – with each zone heated by a separate heater.

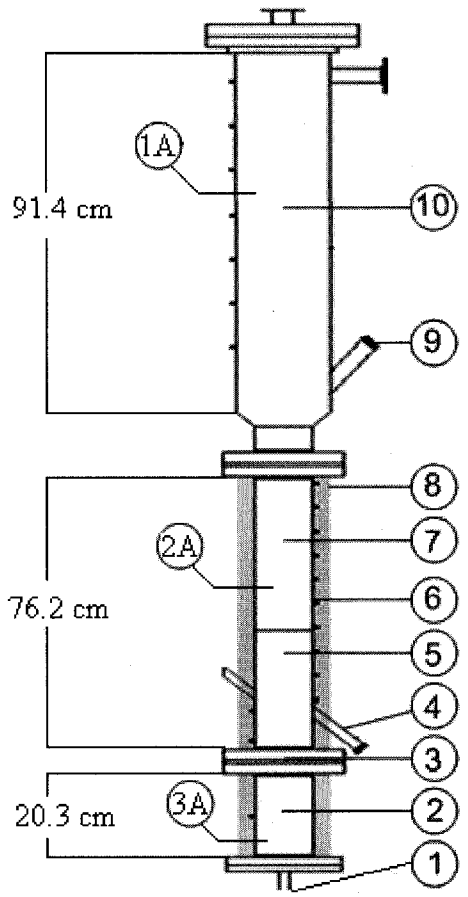

Figure B-1: Drawing of the 3" inner diameter fluid bed Legend: 1) feed inlet, 2) windbox, 3) distribution grid 4) solid outlet, 5) fluid bed region, 6) sampling/measuring ports, 7) freeboard, 8) electrical heating, 9) solid inlet, 10) disengagement zone

Table B-1: Dimensions of the 7.79 cm inner diameter reactor.

#	Type	Nominal diameter (cm)	Schedule	Material	Wall thickness (cm)	Inner diameter (cm)	Outside diameter (cm)
1A	Pipe	15,24	40	SS316L	0.71	15.41	16.83
2A	Pipe	7,62	40	SS310	0.55	7.79	8.89
3A	Pipe	7,62	40	SS310	0.55	7.79	8.89

The fluid bed was initially equipped with a sintered metal distributor and MTO experiments showed promising results with a stable product distribution but the inlet pressure was increasing with time until it was shutdown either manually or by the control system. The pressure drop was reduced during regeneration and it was found to be caused by coking of the sintered metal distributor. The initial experiments were done by preheating the windbox to about 300°C. To reduce coking the inlet temperature to the fluid bed was reduced to a minimum by reducing the windbox temperature to 110-130°C. The coking on the sintered metal distributor was not reduced significantly mainly because it was heated by the catalyst at the reaction temperature of 500°C. Since it was not possible to use the sintered metal distributor it was changed to a perforated plate distributor with 3/64" holes. Changing the distributor eliminated the pressure build-up in the feeding section. Another problem occurred, since the catalyst particles are much smaller than the distributor holes weeping of the particles became a problem. Weeping of particles was not a problem during normal operation since the feed gas kept the catalyst from entering the windbox. It became a significant problem if perturbations occurred in the feed flow and during start-up and shutdown where a valve switch between gas and liquid feed is needed. It was found that a small change in the inlet pressure caused the pressure above the catalyst bed to be higher than the inlet pressure as a result catalyst was pushed into the windbox and further down into the feeding section. The regular shutdowns each time catalyst was pushed into the windbox and the cleaning needed of the feeding section made it impractical to conduct the MTO reaction in this reactor and it was therefore abandoned.

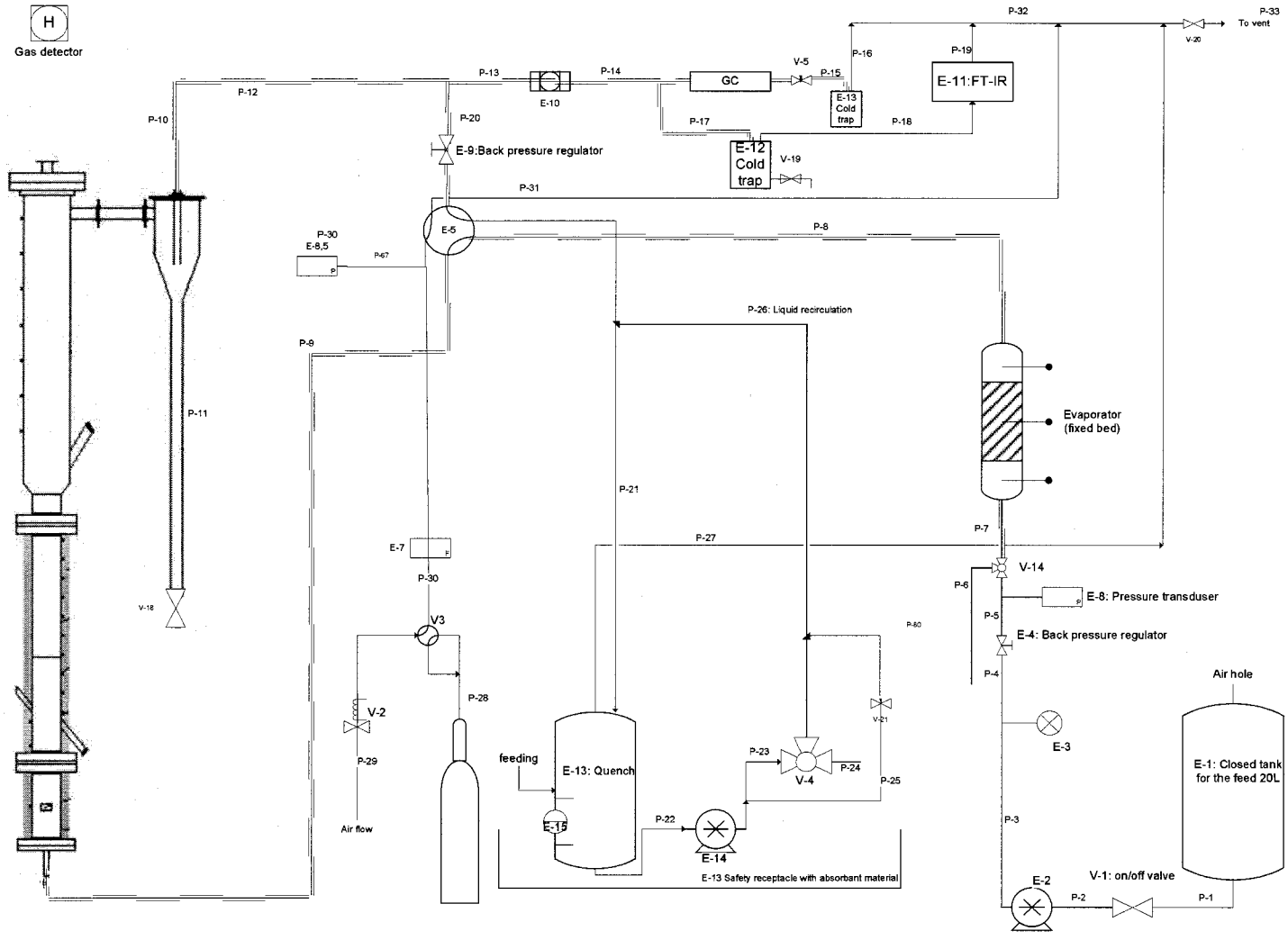

Figure B-2: Schematic diagram of the 3" fluidized bed setup

4.1 cm inner diameter stainless steel fluidized bed reactor

At the same time as the 3" fluidized bed setup was ready for experimental work a newly acquired 4.1 cm inner diameter stainless steel fluidized bed setup became available and experimental work in this reactor was also conducted. A quartz fluidized bed with two external electrical heaters was also supplied with this setup. A schematic drawing of the stainless steel fluidized bed setup is given in Figure B-3 for schematic diagrams of the entire setup refer to Figure 4-2 where the only change is the fluidized bed setup. The fluidized bed is immersed in a fluidized bed sand bath which heat the bed and feed section of the reactor to the given reaction temperature. The gas distributor is made of sintered metal. The coking problem in the feeding section of this setup was even more pronounced than in the 3" fluidized bed with coking not only on the sintered metal distributor but also in the windbox and the feed line to the windbox. After several hours of MTO experiments in the reactor the feed line became blocked by coke and large lumps of coke was flushed out of the windbox during the subsequent cleaning. Due to the high decomposition rate of methanol in the stainless steel fluidized bed reactors it was decided to conduct the experiments in the quartz reactor where these problems were not encountered. A description of the quartz reactor is given in Chapter 4.2.3.

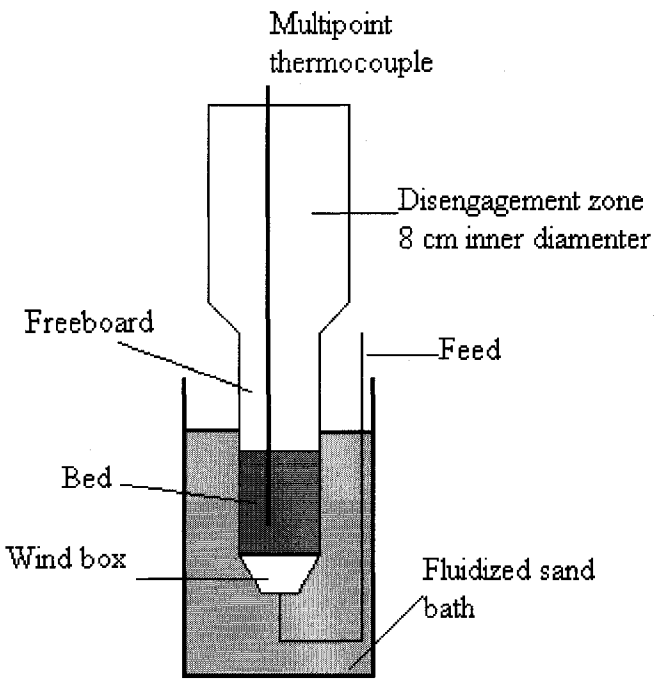

Figure B-3: 4.1cm inner diameter fluidized bed reactor